TÉCNICO LISBOA

Improvement of ship hulls for comfort in passenger vessels

João Pedro Gil Rosa

Thesis to obtain the Master of Science Degree in

Naval Architecture and Ocean Engineering

Advisor/Supervisor: Dr. Shan Wang

Examination Committee

Chairperson: Dr. Carlos Guedes Soares
Advisor: Dr. Shan Wang
Members of the Committee: Dr. Sergey Sutulo

October 2019

Acknowledgments

First, I would like to thank professors Carlos Guedes Soares and Shan Wang for introducing me to this amazing research topic. As well as for their continuous support and guidance throughout each step of this dissertation.

To professors José Manuel Gordo and Tiago Santos for providing the two parent ships used for the various hull transformations.

To professor Roberto Vettor for continuous help with strip theory and wave statistics. As to his support on various other sections of this dissertation.

To Dr. Cláudia Lucas Gaspar for providing the wave data in the coast of Algarve.

To Mr. Emre Uzunoglu for providing a providing a Matlab script to generate the correct type of input files for the seakeeping program.

To Mr. Hossam Abdelwahab for providing experimental results of the containership S-175.

To professor Maria Emília Rosa for the continuous support during my academic years.

To all my dear friends, I would like to thank for their continuous friendship, that gave me support both in and out of the academic context, during the past few months.

Finally, I want to thank to my family, my parents and sister for their unconditional support throughout my academic career.

Abstract

The objective of the work is to improve hulls from passenger vessels for comfort. The Overall Motion Sickness Index (OMSI), defined as the mean MSI value on the main deck, is used as the main parameter to be minimized, in order to obtain improved hulls for comfort. Two different passenger ships are submitted to various hull transformations in order to investigate their influence on passenger's comfort. These are categorized into two groups: geometric and hull from transformations. The transformations are performed using MaxSurf Modeler developed by Bentley systems, based on the Lackenby Method. Each new hull is submitted to a seakeeping analysis that accounts for various heading angles and a specific operating scenario, described by the JONSWAP Spectrum. An in-house strip theory code CENTEC-SK, developed at CENTEC in Instituto Superior Técnico, is used to predict heave, roll and pitch motions at various headings. This program is selected based on a comparison between a commercially available software and experimental results from S-175 containership, collected by International Towing Tank Conference (ITTC). The improved hulls, selected based on the study of OMSI, are compared to their parent hulls regarding their RAOs plots. A similar comparison is performed regarding the absolute vertical accelerations, at strategic locations on the main deck. In order to assess the influence of comfort-oriented hull transformations, on other parameters of the seakeeping performance of a ship, the hull resistance is compared between each hull transformation. Finally, the improved hull forms are compared to their parent hulls regarding their operability index based on comfort criteria.

Keywords: Passenger ship, Comfort, Motion sickness, Strip theory, Seakeeping analysis, Operability index

Resumo

Esta dissertação visa melhorar cascos de navios de passageiros para melhorar o conforto em viagem. O Overall Motion Sickness Index (OMSI), definido como a média de valores de MSI ao longo do convés principal, é utilizado como parâmetro a ser minimizado, a fim de obter cascos melhorados para o conforto dos passageiros. Dois tipos de navios de passageiros são submetidos a variadas transformações de casco, a fim de investigar a influencia das mesmas sobre o nível de conforto dos passageiros. Estas transformações são categorizadas em dois grupos: transformações geométricas e transformações de forma de casco. Tais transformações são obtidas a partir do programa MaxSurf Modeler desenvolvido por Bentley Systems, por base no método de Lackenby. Cada novo casco é submetido a uma análise das movimentações do navio, que tem em conta vários ângulos de ataque e os estados de mar encontrados pelo navio, descritos pelo espectro de JONSWAP. CENTEC-SK que é um código baseado na teoria das faixas, desenvolvido pelo CENTEC no Instituto Superior Técnico, é utilizado para calcular as movimentações de navio. Este programa é selecionado com base numa comparação feita entre um programa comercial equivalente, com resultados reais obtidos experimentalmente para o navio de porta-contentores S-175. Os cascos melhorados e selecionados com base no estudo de OMSI são comparados com os respetivos navios parentes relativamente às movimentações de navio. As acelerações verticais absolutas são igualmente comparadas em localizações estratégicas do convés. Por forma a perceber o impacto de transformações de casco viradas para o conforto dos passageiros, é feito um estudo de resistência a todas transformações efetuadas. Por fim, aos cascos considerados como melhorados é feito um estudo de operabilidade e comparado com os respetivos navios parentes.

Keywords: Navio de passageiros, Conforto, Teoria das faixas, Comportamento em ondas, Índice de operabilidade

Contents

List of Tables

List of Figures

Nomenclature

Hull Coefficients

C_B	Block coefficient
C_M	Midship section coefficient
C_P	Prismatic coefficient
C_{WP}	Waterplane coefficient

Ship Motions

z	Absolute vertical acceleration at remote location
β	Wave heading (Same as μ)
ω_0	Circular wave frequency
ω_e	Circular encounter frequency
ξ_a	Wave amplitude
ξ_j	Amplitude of harmonic motion
ξ_z	Absolute vertical displacement at remote location
f_e	Encounter frequency
F_n	Froude number
V	Ship speed

Physics Constants

ρ	Density of salt water
g	Gravitational constant

Reference Frame

x', y', z'	Reference frame for remote locations along the deck
x, y, z	Inertial reference frame of the ship

Ship Dimensions

Δ	Ship displacement
B_{OA}	Breath overall

B_{WL}	Breath at waterline
D	Depth
GM	Metacentric Height
KB	Vertical center of buoyancy
L_{OA}	Length overall
L_{PP}	Length between perpendiculars
L_{WL}	Length of waterline
LCB	Longitudinal center of buoyancy
LCG	Longitudinal center of gravity
T	Draft/Design waterline (same as D_{WL})
VCG	Vertical center of gravity (same as KG)
$H_{1/3}$	Significant wave height (Same as H_s)
m_{iz}	Spectral moments (i = 0,2,4)
RMS_{az}	RMS vertical acceleration responses
RMS_{vz}	RMS vertical velocity responses
RMS_z	RMS vertical displacement responses
S_ξ	Idealized wave spectrum
S_{az}	Ship vertical acceleration upon S_ξ
S_z	Ship vertical displacement responses upon S_ξ
T_p	Peak period

Acronyms

CFD Computational Fluid Dynamics.

ITTC International Towing Tank Conference.

LFE Lateral Force Estimator.

MII Motion Induced Interruptions.

MSI Motion Sickness Index.

RAO Response Amplitude Operator.

RMS Root Mean Square.

VI Vomit Incidence.

Glossary

Set *n* Name give to the different types of hull transformations, where n represents the number of that same transformation..

Chapter 1

Introduction

1.1 Motivation

For naval architects it is crucial to consider the performance of a ship, at an early design stage. One of its parameters is the seakeeping performance, which has been widely used since the development of practical strip theories. From these theories different tools can be used to check and improve a certain ship operability, regarding its motions as an example.

The seakeeping qualities depend not only on the expected seaway, but also on the ship's mission, that is, the type of service and topology. Particularly in passenger or cargo vessels the wellness and comfort on board, crew and passenger's safety are the primary elements to be improved. These qualities become even more important for passengers' ships, when considering the collateral effect of seakeeping, the seasickness. These ship motions increase the amount of energy required form the crew. In addition, it increases the level of fatigue and drowsiness on passengers, particularly in long journeys. Becoming a defining factor for certain passengers, on ships or ferries, who can opt between different types of transportation. In terms of comfort, the seasickness produced by the ship's motion also affects the earnings obtained on board, since nauseate passengers are less likely to show interest on the extra services, such as shops and restaurants, etc. When it comes to safety, seasickness and motions also have harmful effects, particularly in emergency situations. In such conditions both crew and costumers have worsened performances.

Even though seakeeping qualities are not the only leading aspect on the design process, it is reasonable to work on possible improvements, despite certain fixed parameters. Commonly the optimization procedures for seakeeping, consider that an optimum hull is the one where absolute vertical acceleration in regular head waves due to combined pitch, heave and roll motions are minimized. These methods however do not account for sea spectra and operating scenarios, in order to reduce computational efforts. In the case of passenger ships a sickness index should be considered too. One of these indexes is the Overall Motions Sickness Incidence (OMSI), based on the mean Motion Sickness Incidence (MSI) value on the main deck. This way it is possible to create an optimization procedure accounting for the response of the ship in multiple locations, operating scenarios and sea spectra. It is particularly interesting for the study of passenger vessels, since there are multiple locations of concern. There is an interest in seeing how the OMSI performs in the improvement of different passenger vessels, operating in their respective operating scenario.

1.2 Topics overview and objectives

This dissertation will focus on two particular passenger ships, giving solutions that improve the comfort of their passenger. Such solutions are based on the results, from a seakeeping analysis of different types of hull variations performed to the parent ships. Most of the hull transformations considered require some flexibility to changes on the main project, being suited on a preliminary design stage. Also, these transformations should be easily implemented and based on simple methods that do not require a detailed input, but still with consistent results.

The two parent ship hulls are transformed using both form coefficients and geometrical variations. The Lackenby Method [29] is used to perform the transformations based of form coefficients, namely C_B, LCB and C_M. On the other hand geometrical relationships are used to change the length at waterline L_{WL} and the breath at waterline B_{WL}. Both type of transformations are implemented using *MAXSURF* Modeler [6].

The implementation of the seakeeping analysis is done using strip theory based programs, adequate to the type of vessels in study. Two different programs were proposed and compared to available experimental results: an in-house code from Fonseca and Guedes Soares [17](named *CENTEC-SK*), and a commercially available software called *MAXSURF* Motions by Bentley Systems [7]. Based on the seakeeping analysis the Overall Motions Sickness Index (OMSI) is calculated using *MATLAB*. This index is used as a parameter to compare each ship hull variation, considering as improved the hull variations with the smallest values of OMSI. These results are then confirmed by comparing the ship RAOs and absolute vertical accelerations on strategic locations, to the same results from the parent ships. It is then followed by a simple ship hull resistance comparison using results obtained from *MAXSURF* Resistance [8]. Finally, an operability assessment based the operability index, is performed to the improved hull forms from each type of transformation, at their specific operation sight.

The calculation procedure is summarized in Figure 1.1. As shown in the figure each parent hull is submitted to a set of hull transformations using *MAXSURF* Modeler. These are then converted into an offset table in the form of a text file (.txt) using *Rhino*. Once the surface is in the format of a text file, it is possible to generate the input for the seakeeping program and directly run it using *Matlab*. Based on the results from the seakeeping program all following calculations (Wave Spectrum, MSI, OMSI) and plots (RAOs and Vertical Accelerations) are obtained using *Matlab*. The Operability Index is also calculated using *Matlab*, but only for certain hulls considered improved based on the OMSI analysis. The hull variations obtained in the beginning are also used directly on *MAXSURF* Resistance to predict the hull resistance of each new hull.

1.3 Structure of the dissertation

The dissertation is divided into seven different Chapters. Their content can be summarized in the form:

- **Chapter 1** is an introductory chapter, where the motivations and objectives for this project are presented. It is also explained the type of results obtained in the work and their respective process of calculation.
- **Chapter 2** is dedicated to the state of the art, regarding the previous work on the methods to predict seakeeping, seasickness studies and optimization methods based on a seakeeping analysis.

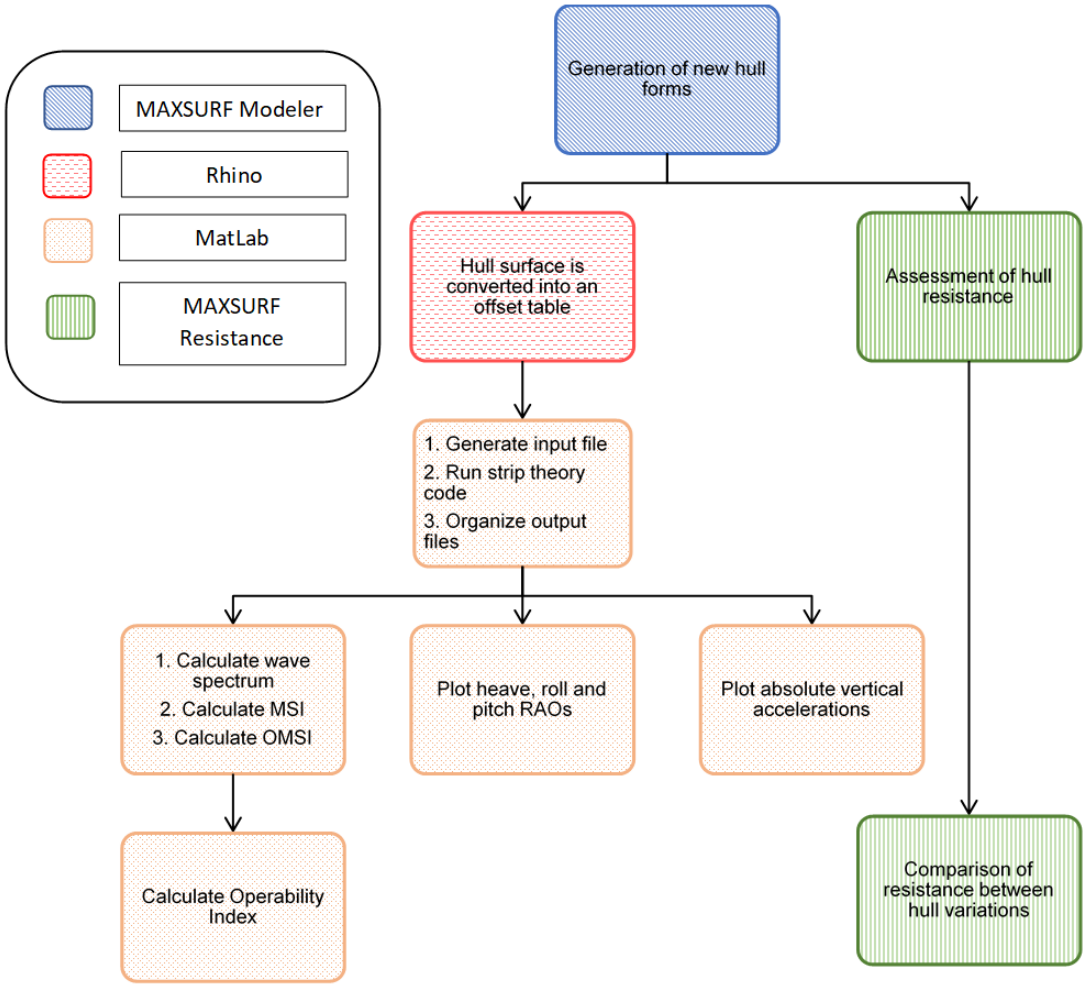

Figure 1.1: Flow chart for main results obtained for each hull variation

- **Chapter 3** is where the background theory, methods, assumptions and equations required to perform the seakeeping analysis of the two vessels are presented.
- **Chapter 4** is dedicated to the comparison between two seakeeping programs with experimental results to gauge the most suitable one to be used on this dissertation.
- **Chapter 5** includes detailed information on the parent ships, their operation scenarios and the type of transformations performed to each hull. It is also presented a study on the Motion Sickness Index distribution on the main deck of the two parent ships.
- **Chapter 6** presents the results of the seakeeping analysis performed to each hull transformations. These new hull are compared to their parent ships, regarding OMSI, RAOs, absolute vertical accelerations, ship hull resistance and operability index.
- **Chapter 7** contains the summary and final considerations on the work performed by the author.

Chapter 2

State of the art

2.1 Seakeeping Analysis

The performance prediction of a ship in calm and rough water is nowadays one of the main concerns of the naval architects. However, this has not always been the case, since predicting the ship motions and wave-induced loads is not an easy task and therefore barely considered in the design procedures. This paradigm finally changed after pioneering developments in seakeeping computations in the 1950's. This was encouraged by the increased awareness on the importance of reducing the ship motions and minimizing the wave induced loads, on the design of high-speed dry-cargo ships and tankers. St. Denis and Pierson [14] pioneered a new method on seakeeping analysis based on the application of the principle of superposition to the ship-motion problem. Hypothesizing that the responses of a ship to irregular waves can be considered as the summation of the responses to regular waves of all frequencies. A hypothesis that became a landmark in seakeeping research, leading to different developments in both theoretical and numerical methods of predicting ship wave responses. Many different facilities for ship-motion and wave-load tests were created. These included the remodeling of tanks, originally designed for resistance and propulsion tests, by equipping them with wavemakers to be used for head- and following-wave experiments. These transformations lead to one of the most significant and complete experiments conducted on sixteen different Series 60 hull forms by Vossers et al. [49] [50]. The motions, the power increase and the wave-induced loads were measured for each hull in head, following and oblique regular waves. It became of the most importance to the study of the hull-form effect on seakeeping characteristics. There were no similar results for hull forms not related with Series 60, with only published data for heave and pitch motion in head seas. This is mainly due to the characteristics of ship-motion and wave-load experiments, which are very time consuming and extremely expensive.

One of the approaches for the computation of fluid-structure interaction associated with fixed or floating structures in regular wave is potential flow theory which assumes inviscid, incompressible and irrotational flow. In linear potential flow theory, the solution to the fluid-structure interaction problem is solved, such that the linearized free surface boundary condition is satisfied as well as the body boundary condition on the surface of the hull. In addition, the waves caused by the presence of the body or its motion satisfy a radiation condition in the far field. One of the limitations of potential flow theory is the negligence of the effect of viscosity. This discrepancy is obvious when overestimating the roll motion at resonance.

Such factors stressed out the importance of the development of theoretical and numerical methods

for predicting wave responses. Korvin-Kroukovsky and Jacobs [27] developed an early proposal of the strip theory for heave and pitch motions in head waves. It became in fact, the first motion theory relevant for numerical computations, that was accurate enough for engineering applications. Followed by an extension in the following year by Jacobs [25] to include the wave-induced vertical shear forces and bending moments for a ship in regular head waves. Even though the experimental results compared to Korvin-Kroukovsky and Jacobs [27] strip theory were overall satisfactory, its forward-speed terms in the coefficients of the equations of motions did not satisfy the symmetry relationship proved by Timman and Newman [46]. New strip theories for heave and pitch motions in head waves were later developed to solve the symmetry problem, such as Söding [43] in Germany, Tasai and Takaki [44] in Japan. Both theories obtained positive results on the symmetry relationship proved by Timman and Newman [46]. Nonetheless the biggest breakthrough came from the work of Salvesen et al. [39], where a new strip theory was formulated. This new theory became one of the most cited strip theories and has been widely used in both academic and commercial computational programs, as is the case of *MAXSURF* Motions [7]. Strip theory by Salvesen et al. [39] could predict heave, pitch, sway, roll and yaw motions, assuming potential flows a linear and harmonic oscillatory motions and ship lateral symmetry. It could also predict wave-induced vertical and horizontal shear forces, bending moments and torsional moments for ships advancing at constant speed with arbitrary heading in waves. Based the on comparisons between computed values and experimental data the method showed satisfactory results. In particular for heave and pitch motions and vertical loads. However, the accuracy in predicting sway, yaw and roll motions in oblique waves was not demonstrated.

2.2 Seasickness

Seasickness is a well documented effect that has tormented many generations of sailors. In fact, the word ”nausea” which refers to the inclination to vomit, comes from the word ”naus”, that in the Greek language means ship. It then comes as no surprise, that in the last century this effect has been extensively studied. Stevens and Parsons [42] gave a highlight on the reports of seasickness at sea, over the years, which are also listed here:

- Hill [23] in 1936 estimated that over 90% of inexperienced passengers become seasick in very rough conditions and some 25% to 30% became seasick during the first two or three days in moderate seas.
- Chinn [11] in 1951 reported during the first two or three days of an Atlantic crossing in moderate seas 25% to 30% of passengers on liners became seasick.
- Handford et al [22] in 1954 found a 34% incidence rate of vomiting among troops on a military transport ship crossing the Atlantic.
- Bruner [9] in 1955 observed from a questionnaire survey of 699 men aboard destroyers involved in escort duty in the U.S. Navy that 39% were never sick, 39% were occasionally sick, 10% were often sick and 13% were almost always sick.
- Trumbull et al [47] in 1960 found the incidence of vomiting reported on military transport ships traveling across the Atlantic to vary from 8.5% to 22.1 % on three crossings.
- Pethybridge et al [37] in 1978 found that 67% and 73% of the crew of two British Royal Navy ships had been seasick during their career, 42% and 56% had been sick in the past 12 months. During sea trials over five days in rough weather, 38% and 47% of the crew on the two vessels were sick on at least one occasion.

- Pethybridge [36] in 1982 found that 10% to 30% of naval crew members suffered from seasickness during commonly experienced sea conditions and that this incidence rises to between 50% to 90% in the worst conditions.
- Attias et al [2] in 1987 reported that aboard a 300 ton vessel in Sea States 2 and 3, 53% of those not receiving seasickness medication were sick on the first two days and 23% were sick on the third day.

Collectively the studies above helped to better understand seasickness, regarding its influence on sailors/passengers and the conditions it may occur. In other words these studies helped to answer two questions: ”What causes seasickness” and ”How can it be predicted”.

To answer the first question both Dobie [15] and later Stevens and Parsons [42] presented examples of what causes of seasickness. Dobie [15] presented an analysis on how different elements of the ships such as whole-body motions and whole-body vibration influence seasickness and human performance at sea. Such work was followed by Stevens and Parsons [42] who explained the causes of seasickness on a physiology level and how it is related to specific types of motion and frequencies.

It was however more difficult to answer the second question. Even with all the records and understanding of the causes, one was trying to predict an outcome that is dependent on different variables. One of the most notorious examples was based on the studies sponsored by the US Navy in the early 1970s, to investigate the ship motions effects on humans. Here the first mathematical model for sickness, Motion Sickness Incidence (MSI), was developed by O'Hanlon and McCauley [34] and further refined in McCauley et al. [31]. For this study a series of experiments were carried out on over 500 subjects, while seated with their heads against a backrest, and eyes opened in an enclosed vertically oscillating cabin. During these experiments they were exposed to the effects of 25 combinations of 10 frequencies (from 0.083 to 0.700Hz) and various magnitudes (from 0.278 to 5.500 ms^{-2} RMS) up to two hours. It was found that the main sickness cause was the vertical motion component and the maximum sensitivity component was 0.167Hz. This mathematical model is used in this dissertation to calculate the values of MSI.

Other attempts to predict motion sickness were later carried by Lawther and Griffin [30]. They proposed a new index, namely the Vomit Incidence (VI), which is the motion sickness dose value (MSDV) times a constant varying in accordance to the exposed population characteristics (age, gender). This index was based on a study on a car ferries operating in the English Channel, analysing the consequent sickness among passengers. The data was gathered along 17 different voyages of about 6 hours, involving more than 4900 passengers. The results were identical to the ones obtained by O'Hanlon and McCauley [34], obtaining strong correlations between MSI and vertical accelerations, both in magnitude and duration of exposure. Complementary they showed that roll and pitch motions combined with heave, may produce more seasickness than what classical methods predicted, even if not provoking sickness by themselves.

Sea sickness does not occur only to passenger under vertical accelerations. During deck operation, sickness my also occur, particularly due to roll. Usually these type of considerations are solved by introducing a roll-angles criteria, for seakeeping assessments. A better alternative was proposed by Graham [19], which used the Motion Induced Interruptions (MII) to represent the number of loss-of-balance events that occur during an arbitrary deck operation. It was shown that the incidence of MIIs could be related to a concept of Lateral Force Estimator (LFE), which is a combination of the earth-

referenced lateral acceleration and the ship-referenced lateral acceleration due to roll motion. This greatly reduced computational efforts since the LFE value could be calculated in the frequency domain. The LFE concept is the assumption that the ship-referenced vertical acceleration is negligible. The LFE is only a valid estimator of MIIs under conditions in which the vertical acceleration is small. Therefore, it can be used as a complementary parameter to MSI, when performing seakeeping assessments.

2.3 Parametric Studies

With the possibility to incorporate the seakeeping analysis into performance studies, based on strip theory, many naval architects started using such results to assess the seakeeping qualities. They studied different types of hulls and optimized them, commonly based on hull variations. Such variations can be obtained by different methods, one of them being the Lackenby Method [29]. This method of Lackenby [29] changes the buoyancy center and the shape coefficients, without altering the other hull important quantities. The method preserves the length of the ship if there is no vertical transom. The method performs translations of stations that are proportional to their area, represented as ordinates. In the case of a ship with vertical transom or flat vertical panel in the bow, the method causes an undesired variation in the ship's length.

In the beginning of the 1980s, Bales [3] presented a method to optimize a destroyer-type hull form, in head seas and at various speeds. Based on analytical predictions, the author derived the optimum hull using regression formulas to correlated relevant performances to form parameters. This was one of the first approaches, that enabled the considerations of the seakeeping performance in the early stages of ship design, as opposed to simply evaluating the performance of the final design.

Following the same idea, Grigoropoulos and Loukakis [21] developed a numerical method for analytical seakeeping optimization. The optimization should depart from a parent hull form, which should meet the initial requirements from the "owner" and generally good seakeeping qualities. This parent hull was then subjected to a series of transformations based on geometrical parameters which affected the seakeeping characteristics. In this work the variant hull forms were derived based on Lackenby's Method [29], which was extended so that waterlines and sectional area curves of any shape can be accommodated and any of the six parameters $\{C_{WP}$, LCF, C_B, LCB, C_M, $KB(x)\}$ could be independently varied. On other methods the Response Amplitude Operator (RAO) are obtained to determine the response spectrum, to compare the curves between each hull form. The authors proposed to focus the optimization on the peak values of the RAO of a few ship responses, more specifically the absolute vertical accelerations and the relative vertical motion. This method reduced the computational time. An optimal result corresponded to the minimum value of a sum, based on the seakeeping performance expressed in weighted sum of the peak values of a prescribed set of ship responses in regular waves, for various ship speeds and headings. This method was applied to both merchant and naval ship and proved to be suitable to be incorporated in the preliminary design spiral. A complementary assessment of propulsive performance in waves was required, since such matters were not considered in the method.

Later on, Kukner and Sariöz [28] further studied the application of seakeeping analysis into early stages of the ship design. The development of a realistic seakeeping design criteria was applied to high speed hull forms. The proposed design methodology came to overcome the main difficulties associated to this process, which are:

1. A systematical generation of new hull forms is a difficult task.

2. Seakeeping performance assessment of each alternative development requires excessive computing time.

3. It is difficult to have a single merit of seakeeping performance to compare different alternative designs.

This methodology becomes particularly important since the design guidelines change from small high-speed vessels to giant low speed bulk carriers. A hull form design methodology was used to assess the seakeeping performance based on changes in the main dimensions or secondary form parameters, LCB, C_{Wp} and LCF. It was then possible to develop and analyse many alternative designs, applying nonlinear optimization techniques to the problem of design for seakeeping. The designer only had to provide some geometric constrains and seakeeping objectives. By systematic generation of new hull forms the authors could investigate the effect of the ship size, its main dimensions and most importantly the effect of hull shape. For the first case it was necessary to generate geo symmetrical hulls. While on the second case the variations were obtained by the changes of length and beam/drought ratio (B/T) for fixed displacement. Like in previous studies, the hull shape variation were also achieved by using the Lackenby linear distortion [29], where the main dimensions are maintained and C_B and LCB are varied. The seakeeping performance assessment was then performed based on a non-linear direct approach where the seakeeping prediction software was based on a 2-D strip theory. This way the seakeeping trends could be easily studied by comparing the ship motions for pair of designs which differed in only one parameter, leading to the selection of the hulls with most promising results. For the variations performed it was concluded that increasing both the ship length and B/T ratio reduced vertical plane motion and added the resistance. While in the particular case of smaller high speed hull forms, vertical accelerations were less sensitive to variations of form parameters such as C_B and LCB. Nevertheless, an increase in C_B seemed to reduce both heave and pitch motions while an increase in LCB only reduced heave motions, being negligible to pitch motions.

In more recent years, Özüm et al.[35] investigated the effect of hull form parameters on seakeeping assessment of fast ships at conceptual design stage. These parameters were classified into two groups: main dimensions (L, B and T) and secondary form parameter (LCB and C_P). New hull forms could be systematically generated from a parent hull, much like in previous approaches. The main dimensions were easily manipulated by scaling the offsets, with the hull length (L) changing between 10% and -10% while the beam and draft ratio (B/T), displacement and other parameters were kept constant. Alternatively, the B/T ratio was changed between 25% and -25% with L, displacement and secondary parameters kept constant. The forms factors were once again altered by the Lackenby Method [29], a common approach and widely accepted as a fast and simple for such purposes. The transfer functions were then compared to heading waves at a Froude number of 0.5. The main conclusions were:

- Reducing hull length reduces heave amplitudes and increases pitch amplitudes.
- Increasing B/T reduces vertical plane motions.
- Decreasing C_P reduces heave amplitude.
- Approaching of LCB to the aft reduces heave amplitudes.

The main dimensions seem to have greater effect on the vertical plane motions than on the form parameters. The approach taken to study the effect of hull form parameters on seakeeping, proved to be valid and worth considering. Due to its simplicity of implementation, it can easily be added during the

conceptual design stage.

Sariöz and Narli [40] investigated the effect of seakeeping criteria on seakeeping performance assessment for passenger vessels. This assessment was studied along four factors:

- The wave response characteristics of the ship which depends on the size, dimensions, form, and weight distribution characteristics.
- The nature of the sea environment.
- The ship's speed and heading which determine how the ship will encounter the environment.
- The quantitative and qualitative requirements for the well being and safety of passengers and crew on board, i.e. the seakeeping criteria.

Each point was considered as step of the analysis and some highlights are taken. In the responses characteristics it is important to underline that for a passenger vessel vertical and lateral accelerations are of main concern. These accelerations are important because they directly affect the comfort and well being of the passengers. In terms of the natural seaway in which a ship operates, it can only be described by means of a statistical model. When predicting the responses in a specified sea-way, the authors considered that calculations must be performed for all headings and for each seakeeping response which affect the performance of the vessel. To better demonstrate the importance of such considerations, as shown in Figure 2.1, the Root Mean Square (RMS) vertical acceleration levels (m/s^2) in a passenger vessel are plotted for a range of headings from head seas to following seas for one of the sea states. It is possible to see how heading seas have higher vertical accelerations, and how they increase with speed. On the other hand, following sea have smaller vertical accelerations and are reduced with increasing speeds. It serves as an indication of what to expect on similar analysis. This is however just a representative illustration and this radial lines will differ from sea state to sea state. It also shows why in many previous works only head seas were considered, since it is most likely the worst case scenario. Nevertheless, one can also argue the importance of multiple headings for a more complete study. The seakeeping criteria is generally limited for vertical and lateral accelerations, however it can also be based on motion sickness incidence (MSI) and motion induced interruptions (MIIs). Therefore, depending on exposure time and frequency of oscillation, different values of RMS vertical acceleration could be selected as seakeeping criteria. This may result in different levels of habitability for same sea conditions. It is then crucial, in a comparative seakeeping analyses, that the chosen set of criteria and its parameters are described in order to provide reliable seakeeping performance assessment.

Cepowski [10] studied the changes of design parameters on selected seakeeping criteria. This analysis was performed on a passenger-car ferries. For these types of ships the seakeeping qualities greatly influence the design and must be decided in preliminary stages of the project. A total of 3072 of hull variations were developed based on the combination of 4 different ratios of length and beam, eight hull form variations and metacentric height (GM), ranging from 0.4 m to 1.4 m every 0.2 m. For operational conditions, the following parameters were calculated: maximum significant roll amplitudes, maximum significant amplitude of vertical/lateral accelerations and maximum Motion Sickness Incidence (MSI). These results allowed the development of design guidelines, prepared form regression functions as well as artificial neural networks. Further study was conducted in Cepowski [10] to predict the motion sickness incidence index at the initial design stage. It was concluded that the designer could choose between three ranges of design parameters [L/B, B/D and C_B] to calculate the index based on vertical accelerations. The following occur/s:

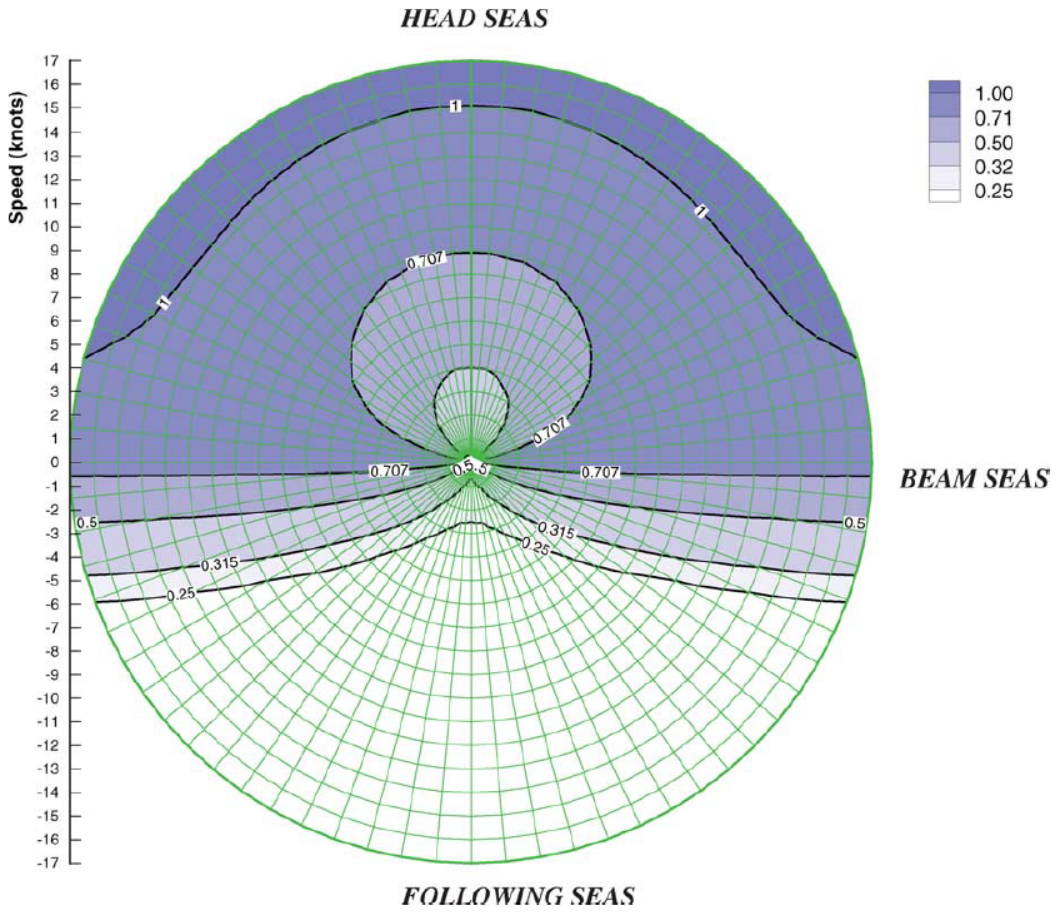

Fig. 6. Speed polar diagram of RMS vertical acceleration in sea state 5.

Figure 2.1: Speed polar diagram of RMS vertical acceleration in a specific sea state from Sariöz and Narli [40].

- High wave resistance, but MSI index has low values, minor rolling and transverse accelerations;
- Low MSI index, medium values of additional wave resistance, rolling and transverse accelerations;
- High values of MSI index, transverse accelerations and rolling, but low additional wave resistance.

Motion Sickness Incidence (MSI) is in fact a common parameter to be minimized in optimization analysis, usually for heading waves, specific sea - states and locations on the hull. Scamardella and Piscopo [41] however used the Motion Sickness Incidence (MSI) to investigate the performance of passenger's ships on multiple locations of the hull, at different sea - states and headings. They used a new index called Overall Motion Sickness Incidence (OMSI), defined as the mean Motion Sickness Index (MSI) value on the main deck. It was proposed and chosen as a parameter to be minimized in a single-objective optimization procedure, accounting for both operating scenarios and sea spectra. It should be noticed that this index OMSI was also selected as the main parameter to be minimized in this dissertation. This index is seen as particularly useful to be used in a seakeeping optimization, since a lot of information can be compressed into one parameter. By using OMSI it is possible to compare ships regarding their specific type of operation. This way the process of comparing different hulls variations is simplified and more accurate, when compared to the approaches presented before.

A hull form optimization was carried on a passenger vessel, derived by the round bilge NPL systematic series, where several new hulls were generated. These derived hulls were systematically generated,

at same Froude number and displacements, changing by the Lackenby Method [29], several form parameters, namely the block, prismatic and midship section coefficients, together with the position of the longitudinal center of buoyancy. Each coefficient was within the limit of 10% of variation.

Two different scenarios were then analysed: for one of them it was assumed that all headings had same probability of occurrence, while in the other a specific probability density function was defined. The second scenario was the most realistic and guidelines for the optimum hull generation were presented:

- Decrease the block coefficient, for fixed waterline length, breadth and displacement, increasing the immersion;
- Shift after the center of buoyancy, as far as possible, depending on both equilibrium and trim considerations;
- Increase the prismatic coefficient, decrease the midship section and water plane area ones.

This index proved to be a valid parameter to be optimized on passenger ships. These solutions deserve a further analysis, since this method was tested on only one type of hull and subtle differences may occur when changing the operating scenario and different forms of variations.

Combining many of the methods described above, Belga et al [5], optimized the seakeeping performance of a displacement catamaran to operate as fast crew supplier for an offshore platform at the Alentejo basin. Similarly to Scamardella and Piscopo [41] the average MSI at the passenger area and vertical acceleration responses at the bow were selected as the objective functions to be minimized. Heave and pitch motion were predicted based on a strip theory code only for heading waves. In the end an optimum hull was obtained and its operability was assessed in the respective operating scenario.

2.4 Summary

It is clear that predicting the ship behavior is of most importance to naval architects. Specifically, at the early stage of design, strip theory becomes a useful tool to predict ship motions. Within its range of application (small Froude, small amplitudes and slender hulls), relatively good results could be obtained using low computational power. This is particularly useful at early stages of the project.

Advancements on seakeeping analysis also opened new opportunities for researchers to improve the seakeeping qualities of a ship. In the particular case of passenger vessels, comfort has been widely studied both on its methods of prediction and on optimization procedures. In particular the advantages of such implementations right at an early design stage. Therefore, the significance of the topic is clear, in an ever more demanding industry.

Chapter 3

Background

The following chapter is dedicated to meaningful background theory required to understand the work in study. It starts with an overview on strip theory together with the method for roll damping corrections. The formulations to obtain the wave spectrum and RMS, with the respective transformations required for accounting incoming wave from multiple headings, are presented. The formulation for MSI and OMSI are presented next, together with the definition of the seasickness. Finally, the operability index which is applied to evaluate the ship performance in the study, is explained mathematically.

3.1 Strip Theory

The present work studies the overall comfort and operability along the ship, based on a seakeeping analysis. Only absolute motions and accelerations in waves are here considered. There are different methods to study the hydrodynamics of the hull in incoming waves. These include model testing, CFD solver and strip theories. The later method is selected to be used in this dissertation. It is ideal to be used at an early stage of a design project, due to its low computational power together with the reliable results. In this work, two programs, which are based on the strip theory are used to assess the ship motions in incoming waves.

Strip theories are considered two-dimensional theories. It is assumed that the motions of a three-dimensional vessel could be calculated by representing it as a number of two-dimensional elements along the ship. These are commonly referred as strips- and solve the resulting boundary value problem. The total effect on the ship is obtained by integrating the effects of all individual strips along the lengths. These theories adopt a velocity potential function throughout the fluid domain. Here it is assumed that the fluid is **homogeneous**, **inviscid** and **incompressible** and the fluid must be **irrotational**. The strip theory formulation used by both program is the slender-body theory from Salvesen et al. [39]. This theory is linear and in the frequency domain. It assumes the beam of the ship to be small in comparison to the wavelength, low forward speeds and low frequencies of oscillation.

Following the formulations in Salvesen et al. [39] it is possible to obtain the equations of motion of a ship. This thesis is not focused on the implementation of strip theory, relying on the seakeeping programs for that matter. Therefore, only the main equations and coefficients are presented. For a detailed definition of each coefficient it is advised to read Salvesen et al. [39]. Considering that **(x, y, z)** is a right-handed coordinate system fixed with respect to the mean position of the ship, assuming that oscillatory motions are linear and harmonic. The axis **z** is in the vertical upward direction and passing

through the center of gravity of the ship. The axis **x** is along the longitudinal direction of the ship. The axis **y** is perpendicular to **x** in port side direction. Also, the ship is advancing in waves and oscillating as an unrestrained rigid body. The oscillatory motions consist of three translations and three rotations. Let the translatory displacements in **(x, y, z)** be the surge (ξ_1), the sway (ξ_2) and the heave (ξ_3). Furthermore, let the rotational displacement in **(x, y, z)** be the roll (ξ_4), the pitch (ξ_5) and the yaw (ξ_6). This coordinate system and the respective linear and angular displacement is shown in Figure 3.1. Assuming that the responses are linear and harmonic, the six linear coupled differential equations of motion can be written, using subscript notation, in the abbreviated form:

$$\sum_{k=1}^{6}\left[\Big(M_{jk}+A_{jk}\Big)\ddot{\xi_k}+B_{jk}\dot{\xi_k}+C_{jk}\xi_k\right]=F_j e^{i\omega t}; \qquad j=1,...,6 \tag{3.1}$$

,where M_{jk} are the components of the generalized mass matrix for the ship A_{jk} and B_{jk} are the added-mass and damping coefficients, C_{jk} are the hydrostatic restoring restoring coefficients and F_j are the complex amplitudes of the exciting force and moment. The force and moment are given by the real part of $F_j e^{i\omega t}$. F_1, F_2 and F_3 are the amplitudes of the surge, sway and heave exciting forces, while F_4, F_5 and F_6 are the amplitudes of roll, pitch and yaw exciting moments. Frequency is represented by ω. The dots stand for time derivatives so that $\dot{\xi_k}$ and $\ddot{\xi_k}$ are velocity and acceleration terms.

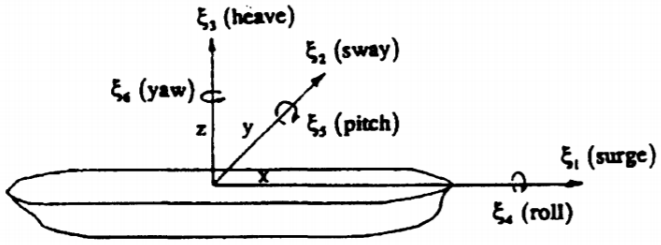

Figure 3.1: Coordinate system and six modes of ship motion, from Fonseca and Guedes Soares [17].

Assuming that the ship has lateral symmetry (symmetric about the x, z plane) and the center of gravity is located (0, 0, Z'$_g$), then the mass, added mass and damping coefficients matrices are:

$$M_{jk}=\begin{bmatrix} M & 0 & 0 & 0 & M_{Z'_g} & 0 \\ 0 & M & 0 & -M_{Z'_g} & 0 & 0 \\ 0 & 0 & M & 0 & 0 & 0 \\ 0 & -M_{Z'_g} & 0 & I_4 & 0 & -I_{46} \\ M_{Z'_g} & 0 & 0 & I_5 & 0 & \\ 0 & 0 & 0 & -I_{46} & 0 & I_6 \end{bmatrix} \tag{3.2}$$

$$A_{jk}(or B_{jk})=\begin{bmatrix} A_{11} & 0 & A_{13} & 0A_{15} & 0 & \\ 0 & A_{22} & 0 & A_{24} & 0 & A_{26} \\ A_{31} & 0 & A_{33} & 0 & A_{35} & 0 \\ 0 & A_{42} & 0 & A_{44} & 0 & A_{46} \\ A_{51} & 0 & A_{53} & 0 & A_{55} & 0 \\ 0 & A_{62} & 0 & A_{64} & 0 & A_{66} \end{bmatrix} \tag{3.3}$$

$$C_{jk} = \begin{bmatrix} 0 & 0 & 0 & 0 & 0 & 0 \\ 0 & 0 & 0 & 0 & 0 & 0 \\ 0 & 0 & C_{33} & 0 & C_{35} & 0 \\ 0 & 0 & 0 & C_{44} & 0 & 0 \\ 0 & 0 & C_{53} & 0 & C_{55} & 0 \\ 0 & 0 & 0 & 0 & 0 & 0 \end{bmatrix} \tag{3.4}$$

From Equations 3.1 to 3.4 and assuming lateral symmetry and slender hull form, the coupled equations of motion for heave and pitch are obtained:

$$(M + A_{33})\ddot{\xi_3} + B_{33}\dot{\xi_3} + C_{33}\xi_3 + A_{35}\ddot{\xi_5} + B_{35}\dot{\xi_5} + C_{35}\xi_5 = F_3 e^{i\omega t} \tag{3.5}$$

$$A_{53}\ddot{\xi_3} + B_{53}\dot{\xi_3} + C_{53}\xi_3 + (I_5 + A_{55})\ddot{\xi_5} + B_{55}\dot{\xi_5} + C_{55}\xi_5 = F_5 e^{i\omega t} \tag{3.6}$$

The same is obtained for roll motions:

$$(A_{42} - M_{Z_g'})\ddot{\xi_2} + B_{42}\dot{\xi_2} + (A_{44} + I_4)\ddot{\xi_4} + B_{44}\dot{\xi_4} + C_{44}\xi_4 + (A_{46} - I_{46})\ddot{\xi_6} + B_{46}\dot{\xi_6} = F_4 e^{i\omega t} \tag{3.7}$$

It should be noticed that all viscous effect are neglected. This assumption is justified because the viscous damping is very small for the vertical ship motions. However, according to Salvesen et al. [39] the roll-damping coefficient (B_{44}) is significantly affected by viscosity even in the absence of bilge keels, requiring its correction, see Section 3.2. The solutions for the second order linear differential equations are harmonic in the form:

$$\xi_j(t) = \Re\Big\{\xi_j^A e^{i\omega t}\Big\} = \xi_j^a cos(\omega t - \theta_j) \tag{3.8}$$

,where ξ_j^A is the complex amplitude of the harmonic motion, ξ_j^a is the real amplitude and θ_j is the phase angle that represents the delay of the response. Finally, assuming small angular motions, the absolute vertical motions ($\xi_z(x', y', t)$), at a point on the ship located at (x',y',z'), are given by:

$$\xi_z(x', y', \omega) = \Re\Big\{\big[\xi_3^A(\omega) - x'\xi_5^A(\omega) + y'\xi_4^A(\omega)\big]e^{i\omega t}\Big\} \tag{3.9}$$

3.2 Roll damping

Linear potential flow theory cannot be used for the case of sway, yaw, and roll without including a correction for viscous damping. Comparison between present theory and experiments shows that the potential roll-damping coefficient B_{44}, is significantly affected by viscous effects even in the absence of bilge keels, Salvesen et al. [39]. Therefore, calculations by a potential flow theory overestimate the roll amplitude, particularly in resonance, tampering the results. The amplitude of roll can be computed with reasonable accuracy only if viscous roll damping effects are included. The roll damping ratio may be estimated using Miller [33] method as :

$$K = K_1 + K_2 \cdot \sqrt{\phi_a} \tag{3.10}$$

With:

$$K_1 = C_v \cdot 0.00085 \cdot \frac{L_{OA}}{B_{OA}} \cdot \sqrt{\frac{L_{OA}}{\overline{GM}}} \cdot \left[\left(\frac{Fn}{C_B} \right) + \left(\frac{Fn}{C_B} \right)^2 + 2 \cdot \left(\frac{Fn}{C_B} \right)^3 \right] \tag{3.11}$$

$$K_2 = 19.25 \cdot \left[A_{bk} \cdot \sqrt{\frac{l_{bk}}{r_b}} + 0.0024 \cdot L_{OA} \cdot B_{OA} \right] \cdot \frac{r_b^3}{L_{OA} \cdot B_{OA}^3 \cdot D \cdot C_B} \tag{3.12}$$

where,

$A_{bk} = l_{bk} \cdot h_{bk}$	One sided area of bilge keel [m^2]
l_{bk}	Length of bilge keel [m]
h_{bk}	Height of bilge keel [m]
r_b	Distance center line of water plane to turn of bilge [m]
L_{OA}	Length of ship [m]
B_{OA}	Breath of ship [m]
D	Draft of ship [m]
$\overline{GM}$	Initial metacentric height [m]
Fn	Froude number
ϕ_a	Amplitude of roll [rad]
C_v	Correction factor on K_1 for speed effect (Generally considered C_v = 1)

The roll damping coefficient is calculated using the following expression 3.13, where ξ_{44} is the roll damping factor, I_{xx} and I_{44} are the inertia moment and the added inertia with respect to the x-direction axis and $W_{n,44}$ is the roll natural frequency.

$$B_{44} = 2 \cdot \xi_{44} \cdot (I_{44} + I_{xx}) \cdot W_{n,44} \tag{3.13}$$

3.3 Wave spectra theory

The formulation for the wave spectrum presented here is based on *MAXSURF* Motions user manual [6] and is a generalised spectrum formulation used by DNV, based on JONSWAP spectrum original developed by the Joint North Sea Wave Project. In the formulation, H $_{1/3}$ corresponds to the wave height and T_P is the peak period. In Figure 3.2 is presented the effect of the peak enhancement factor (γ), being clear that the resonance peak of the wave spectrum increases with γ. The spectrum itself is defined as follows:

$$S_\zeta(\omega_0) = \frac{\alpha}{\omega_0} e^{\frac{-\beta}{\omega_0}} \gamma^{e^{\frac{-1}{2\sigma^2}\left[\frac{\omega_0}{\omega_p}-1\right]^2}} \tag{3.14}$$

Where,

$$\alpha = 5\pi^4 \big(1 - 0.287 ln(\gamma)\big) \frac{H_{\frac{1}{3}}^2}{T_p} \tag{3.15}$$

$$\beta = \frac{20\pi^4}{T_p^4} \tag{3.16}$$

The peak enhancement factors are given by:

$$\begin{aligned} \gamma &= 5.0 && for && \frac{T_p}{\sqrt{H_{\frac{1}{3}}}} \leq 3.6 \\ \gamma &= e^{5.75-\frac{1.15T_p}{\sqrt{H_{\frac{1}{3}}}}} && for && 3.6 < \frac{T_p}{\sqrt{H_{\frac{1}{3}}}} \leq 5.0 \\ \gamma &= 1.0 && for && 5.0 < \frac{T_p}{\sqrt{H_{\frac{1}{3}}}} \end{aligned} \tag{3.17}$$

The step functions are given by:

$$\begin{aligned} \sigma &= 0.07 \quad for \quad \omega_0 < \omega_p \\ \sigma &= 0.09 \quad for \quad \omega_0 > \omega_p \end{aligned} \qquad Where, \quad \omega_p = \frac{2\pi}{T_p} \tag{3.18}$$

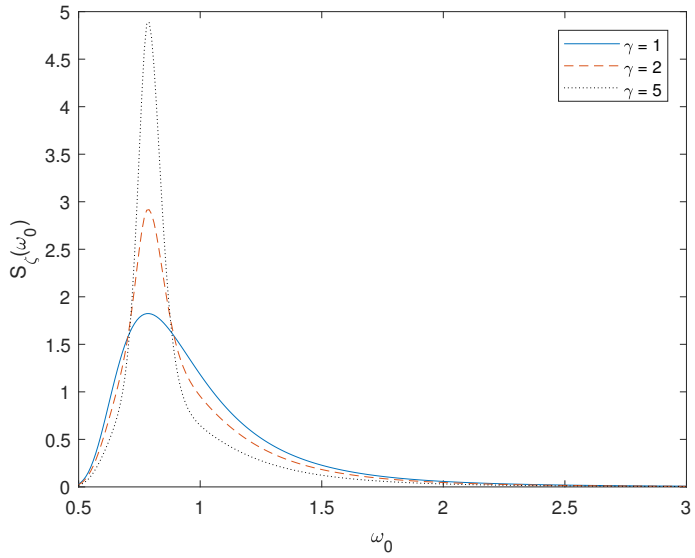

Figure 3.2: Spectrum comparison for H_s = 4.0 m, T_p = 8.0 s with γ= 1, γ= 2 and γ= 5.

3.4 Spectrum Transformations

When a ship is not sailing (zero speed) it is easy to transform a wave energy spectrum into a motion energy spectrum, accounting that transfer functions between wave energy and motion (component) energy are known. However when the speed is actually different from zero the waves will meet the ship with an apparent frequency, which is called the encounter frequency (ω_e). In fact the spectral value of the waves $S_\zeta(\omega_e)$ based on ω_e is different from the spectral value $S_\zeta(\omega)$, since there must exist an equal amount of energy in the frequency bands $\Delta\omega$ and $\Delta\omega_e$. Then the following equation is valid:

$$S_\zeta(\omega_e) \cdot d\omega_e = S_\zeta(\omega_0) \cdot d\omega_0 \tag{3.19}$$

Which gives the following relation:

$$S_\zeta(\omega_e) d\omega_e = \frac{S_\zeta(\omega_0)}{\frac{d\omega_0}{d\omega_e}} \tag{3.20}$$

Knowing that the the relation between the frequency of encounter and the wave frequency in deep

water is given by:

$$\omega_e = \omega_0 - \frac{\omega_0^2}{g} V \cdot cos\mu = \omega_0 \cdot \left(1 - \frac{V}{c} \cdot cos\mu\right) \qquad , c = g/\omega_0 \tag{3.21}$$

where,

ω_0 = wave frequency in a fixed reference (rad/s)

ω_e = frequency of encounter in a moving reference (rad/s)

V = forward ship speed (m/s)

c = wave speed (m/s)

μ= ship heading relative to wave direction (rad)

Then for deep water:

$$\frac{d\omega_0}{d\omega_e} = 1 - \frac{2\omega_0 V \cdot cos\mu}{g} \tag{3.22}$$

Back to the the equation 3.21 of the encounter frequency it is worth taking a better look and interpret its results:

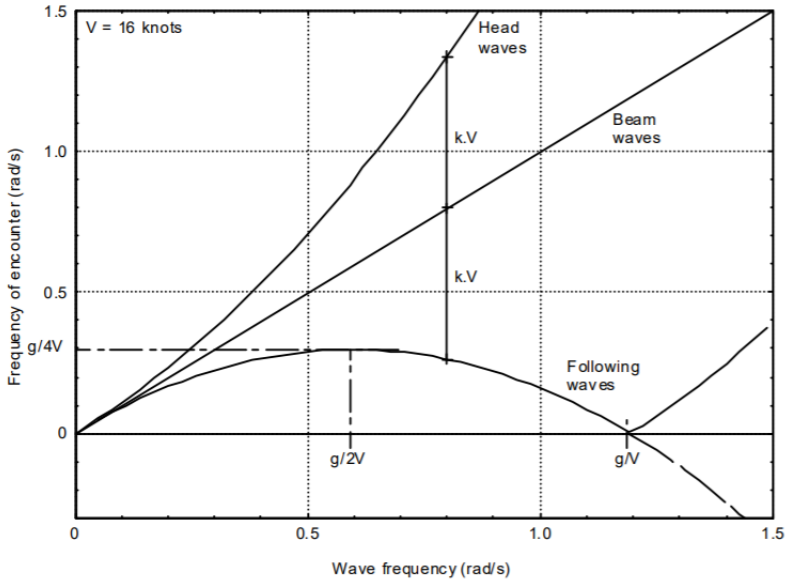

Figure 3.3: Relation between ω_e and ω, from Journée and Massie [26].

Figure 3.3 is a plot of equation 3.21 for a forward speed of 16knots, taken from Journée and Massie [26]. The following conclusions are taken from this document: The upper curve is for head waves approaching from the bow, here frequency of encounter becomes higher than the wave frequency ($\omega_e > \omega_0$). For wave approaching from the beam there is no frequency shift, ($\mu = \pm \pi/2$) so that $\omega_e = \omega_0$ as is shown in Figure 3.3. For following seas these relationships are not as clear and a deeper look should be taken:

- When $\omega_e \to 0$, the speed of the waves becomes high and ω_e is only slightly influenced by V (which is smaller than c).
- As ω_0 increases - from small values - the wave speed decreases slowly so that V becomes more and more important. Equation 3.22 gives that ω_e has a maximum when ω_0 = g/(2V), (in this case the waves are coming from behind). The corresponding ω_e value is ω_e = g/(4V), and is the highest

apparent frequency that will be observed in following waves. Since $d\omega_e/d\omega_0$ is here zero, it is expected that problems occur with $S_\zeta(\omega_e)$ at this frequency, based on the relation given in equation 3.20.

- As ω_0 increases beyond ω_0=g/(2V), the wave speeds continue to decrease so that ω_e deceases as well.
- At some even higher frequency ω_0=g/V , the wave speed (c), matches the ship speed (V) . The ship is surfing on this wave.
- Waves with frequencies higher than ω_0=g/V are moving more slowly than the ship. The ship intercepts these waves from behind so that these behave as head waves. Negative frequencies are not ”normal”, therefore, these values are shown by the dashed line and their absolute value is plotted instead.

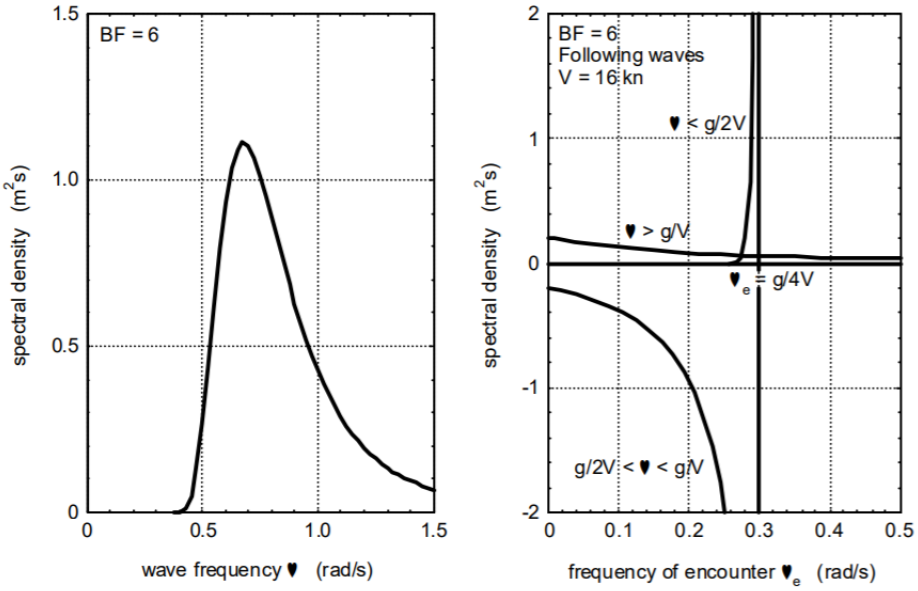

Figure 3.4: Transformed Wave Spectrum in Following Waves, plots from Journée and Massie [26].

Figure 3.4 shows how a wave spectrum is distorted when it is transformed in terms of encounter frequency in following waves. This type of distortion takes place whenever the waves have a velocity component in the same sense as the ship speed, whenever the waves approach from any direction aft of ”beam seas”. This spectrum will be hard to work with. When waves are approaching from any direction forward of ”beam seas” encounter frequencies only become higher than the absolute frequencies, no special problems are encountered.

3.5 RMS Vertical accelerations

The present work is focused on assessing the performance of two different passenger ships on multiple locations. It is then of the most importance to correctly assess them in a realistic sea-way. Remote locations are expressed in a reference frame (x', y' ,z'), fixed with the mid-ship. The seakeeping results from the seakeeping program are also presented in the inertial reference frame at the center of gravity (same as LCB), Chapter 4. From the previous section the absolute vertical displacement (ξ_z) at a

remote location on the vessel (x', y', z'), is given by Equation 3.9. This equation is also used in Belga et al. [5], where only heave and pitch motions were considered, because only heading seas were studied. In the present work, multiple heading seas are considered, therefore roll motions are also included.

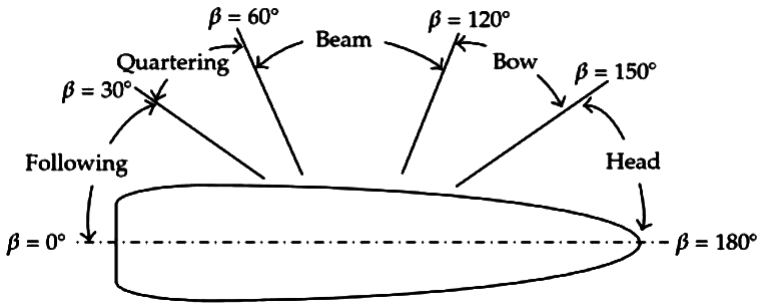

Figure 3.5: Headings

$$\xi_z(x', y', \omega) = \Re\Big\{ \big[\xi_3^A(\omega) - x'\xi_5^A(\omega) + y'\xi_4^A(\omega)\big] e^{i\omega t} \Big\} \tag{3.9}$$

,where ξ_j^A with j = 3,4,5 is the complex amplitude of the harmonic heave, roll and pitch motion, respectively.

The wave spectrum $S_\zeta(\omega_e)$ is given by equation 3.23, accounting the relative speed between the ship (V) and the encountering waves (β), which are defined according the scheme in Figure 3.5.

$$S_\zeta(\omega_e) = \frac{S_\zeta(\omega_0)}{1 - \frac{2\omega_0 V cos\beta}{g}} \tag{3.23}$$

Let $\omega=\omega_e$, the ship vertical responses on a given sea spectrum S_z are then given by

$$S_z(x', y', \omega_e) = |\xi_z(x', y', \omega_e)|^2 S_\zeta(\omega_e) \tag{3.24}$$

With the encounter frequency (ω_e) and the the vertical responses (S_z) it becomes possible to obtain the spectral moments m_{0z}, m_{2z} and m_{4z}. These spectral moments are essential to calculate the MSI and thus the OMSI.

$$m_{0z} = \int_{\omega_e} S_z(x, \omega_e) d\omega_e \tag{3.25}$$

$$m_{2z} = \int_{\omega_e} \omega_e^2 S_z(x, \omega_e) d\omega_e \tag{3.26}$$

$$m_{4z} = \int_{\omega_e} \omega_e^4 S_z(x, \omega_e) d\omega_e \tag{3.27}$$

This methodology is fine for calculations only in heading waves, yet, in this dissertation we are interested in studying following seas too. As seen before both wave spectrum and encounter frequency are distorted, creating problems when calculating this spectral moments, see Section 3.4. For that reason the alternative relation described by Journée and Massie [26], to avoid such problems is used instead:

$$m_{0z} = \int_0^\infty S_z(\omega_e) \cdot d\omega_e = \int_0^\infty S_z(\omega_0) \cdot d\omega_0 \tag{3.28}$$

$$m_{2z} = \int_0^\infty \omega_e^2 \cdot S_z(\omega_e) \cdot d\omega_e = \int_0^\infty \omega_e^2 \cdot S_z(\omega_0) \cdot d\omega_0 \tag{3.29}$$

$$m_{4z} = \int_0^\infty \omega_e^4 \cdot S_z(\omega_e) \cdot d\omega_e = \int_0^\infty \omega_e^4 \cdot S_z(\omega_0) \cdot d\omega_0 \tag{3.30}$$

By using this methodology it is not required to obtain $S_z(\omega_e)$, since $S_z(\omega_0)$ is used instead,that is obtained from Equation 3.31.

$$S_z(x', y', \omega_0) = |\xi_z(x', y', \omega_0)|^2 S_\zeta(\omega_0) \tag{3.31}$$

Once the spectral moments are obtained it becomes easy to obtain frequency independent responses, such as: The Root Mean Squared (RMS) displacement (RMS_z), velocity (RMS_{vz}) and accelerations RMS_{az}. These values have been widely used since it can simplify the analysis of statistical measurements into one factor, instead of looking into the whole range of frequencies.

$$RMS_z = \sqrt{m_{0z}} \tag{3.32}$$

$$RMS_{vz} = \sqrt{m_{2z}} \tag{3.33}$$

$$RMS_{az} = \sqrt{m_{4z}} \tag{3.34}$$

3.6 An introduction to seasickness

Before studying the different hull variations based on numerical models that predict seasickness incidence, it is important to have a better understanding of what seasickness actually is. Motion sickness is a generic denomination used to describe the discomfort on a moving environment: on ships, air crafts, vehicles, a swing, an amusement park ride, in zero gravity environments (space) and even in elevators. The culmination of the different symptoms associated lead to vomit. In fact, the term motion sickness is used in two different scenarios. The first implies that the sickness is a kind of disease, when in fact it is a perfectly normal response to motions from a healthy individual without any functional disorders. Secondly, it can be induced in absence of motion as during a virtual reality simulation, e.g. in wide screen IMAX cinemas that create strong sensations of motions and replicates motions sickness symptoms as presented by Stevens and Parsons [42]. The first case will be the point of interest in this dissertation.

3.6.1 Physiology

The human body as three different systems related with the detection of motion as described by Arribas and Piñeiro [1]:

- The vestibular system placed in the inner ear. Its mission is to detect the relative motion of head and body relative to earth and generate a reflective motor activity. The linear acceleration in the three main directions is detected by the otoliths and sends this information to the brain where is responded by either motion or head tilt. This system also includes three semicircular canals that detect angular accelerations based in the displacement of an internal fluid inside the canals. This too is processed by the brain and assists to control equilibrium.

- The proprioceptive system corresponds to pressure sensors in the skin, muscles and joints. They react to forces and displacements producing a sense of body movement or applied force. These are import for the body interpretation of motion.
- The visual system, i.e. our eyes, detect the motion of the environment and send information to the brain. Here the information is processed and is given a correspondent response to the motion of the environment.

In fact, seasickness occurs when there are conflicting signals between these three systems. To be more specific, the vestibular system sends information to the brain about self-motion that does not match with the information provided by the visual or the proprioceptive systems. A good example in passengers ships is when a passenger is inside a cabin, while the ship is advancing in waves. Here the accelerations are detected by the vestibular system, but the visual system can not notice any motion. However, the conflict can happen among sensations of the same system, i.e. a conflict between linear and angular accelerations detected in the vestibular system. For instance, spinning (angular accelerations) while advancing (linear acceleration) can produce a conflict and cause motion sickness.

3.6.2 Motion sickness in maritime environment

In maritime environment, motion sickness is actually refereed as seasickness. In a ship the seasickness is mainly caused by its motions, although there are specific ship motions that cause people to become seasick, the exact nature of the relation of the ship's motion to the sickness it causes is not well defined. Both shipboard surveys and laboratory studies have been conducted to determine the effects of motion type (roll, pitch, and heave), motion frequency and acceleration, and exposure duration. However, in most related studies the vertical component is considered to have the major influence in seasickness with a maximum of sensitivity occurring at 0.167Hz, Griffin [20].

Even if not aware of these motions passengers start to feel discomfort that is many times wrongfully attributed to food, smells or temperature. First symptoms occur in the stomach followed by a sensation of nausea. In response the brain sends more blood to the stomach and surface blood vessels of the face trend to constrict reducing the blood flow in the head producing face pallor. In addition, passengers start sweating even in cool environments. Symptoms that lead to an increase of salivation, body warmth and light drowsiness, culminating in vomit, Griffin [20].

Consequently, seasickness leads to certain performance implications for the crew. Stevens and Parsons in [42] differentiate between general and specific effects of a given motion. General effects refer to any task or performance carried out in a moving environment. They might be of a motivational nature (i.e., motion sickness), an energetical nature (i.e., motion induced fatigue caused by added muscular effort to maintain balance), or of a bio mechanical nature (i.e., interference with task performance due to loss of balance). Specific effects are defined as those that interfere with specific human abilities such as cognition or perception. In the case of a passenger ship, these consequences affect the passenger who ultimately can not enjoy the travel or benefit from the many activities offered, representing in fact less revenue.

3.7 Motion Sickness Index (MSI)

As seen before, motion sickness deeply affects humans at sea and predicting how it occurs at in a certain ship and in a specific sea way is a great concern for naval architects. Many proposals have been

developed over the years, but Motion Sickness Index (MSI) is still one of the most famous and used today, as discussed in Chapter 2. The original model was developed by O'Hanlon and McCauley [34] and it assessed the number of passengers that vomit after two hours. This model was further developed by McCauley [31] to include a variable time domain. The formulation here presented to obtain MSI is based on this second iteration of the model and is the same one used by *MAXSURF* Motions [7]. It was described by Colwell [12] and depends on the average RMS vertical acceleration $|RMS_{\text{az}}|$ and the average peak frequency of the vertical motions of the ship $|f_{\text{e}}|$ and the voyage time (or period to which MSI is being tested) in minutes (t).

$$MSI\% = 100 \times \Phi(Z_a)\Phi(Z_t) \tag{3.35}$$

Where $\Phi(Z)$ is the standard normal distribution function:

$$\Phi(Z) = \frac{1}{\sqrt{2\pi}} e^{-\frac{z^2}{2}} \tag{3.36}$$

And,

$$Z_a = 2.128 log_{10}(a) - 9.277 log_{10}(f_e) - 5.809 \left[log_{10}(f_e)\right]^2 - 1.851 \tag{3.37}$$

$$Z_t = 1.134 Z_a + 1.989 log_{10}(t) - 2.904 \tag{3.38}$$

$$a = \frac{|RMS_{\text{az}}|}{g} = \frac{0.798\sqrt{m_{4z}}}{g} \qquad |f_e| = \frac{\sqrt{\frac{m_{4z}}{m_{2z}}}}{2\pi} \tag{3.39}$$

3.8 Overall Motion Sickness Index (OMSI)

On classical seakeeping analysis the procedures to compare the parent hull with ship variation discard the operating scenarios and sea spectra. The classic rule of thumb is selecting the best hull as the one who minimizes heave and pitch RAOs. Only head regular waves are usually considered, since they are considered to be the worst case scenario. However, it is more reliable, to consider multiple sea-states that the ship may encounter during its lifetime compared to one single sea-sates. Also, considering head seas as the worst case scenario is not always true, since MSI peaks may also occur at transverse headings depending on the wave peak period, which will be later discussed on Section 5.4. Here it is also shown that locations along the deck are not affected equally, since peaks of MSI are different, depending on the type of headings. For such reasons it was considered that using the Overall Motion Sickness Index (OMSI) developed by Scamardella and Piscopo [41] was the ideal parameter to be minimized, on ship variations that seek to improve comfort on passenger ships. The improved hulls are therefore the solutions with the smallest values of OMSI. Here MSI is considered on multiple locations along the deck, heading angles and sea states are averaged into a single factor, the OMSI. In more detail OMSI is defined as the mean MSI over the deck for any assigned sea-state and heading angle, as:

$$OMSI_{(H_{1/3},T_p)_j,\beta_k} = \frac{\int_{A_{deck}} MSI_{(H_{1/3},T_p)_j,\beta_k,(x',y',z'_{deck})} dA}{A_{deck}} \tag{3.40}$$

,where (x', y', z'_{deck}) denotes the coordinates of the ith of N_c remote control location points on the main deck area (A_{deck}) and βmeans the heading. OMSI is then defined for any assigned sea-state and heading

angles as:

$$OMSI_{(H_{1/3},T_p)_j,\beta_k} = \frac{1}{N_c}\sum_{i=1}^{Nc} MSI_{(H_{1/3},T_p)_j,\beta_k,(x',y',z'_{deck})_i} \tag{3.41}$$

Finally, accounting for all heading angles and peak periods:

$$OMSI = \frac{1}{N_c}\sum_{j=1}^{Ns} p_j \sum_{k=1}^{N_\beta} p_\beta \sum_{i=1}^{N_c} MSI_{(H_{1/3},T_p)_j,\beta_k,(x',y',z'_{deck})_i} \tag{3.42}$$

,where N_c, N_s and N_β denote the number of remote control location points on the main deck, sea states and heading angles, respectively. Both the sea-states and heading angles have a certain probability of occurrence p_j and p_β, respectively.

3.9 Operability index

Another way of comparing a ship hull in terms of its seakeeping performance is with the operability index. Fonseca and Guedes Soares [18] stated: "the calculation of the operability index, which represents the percentage of time during which the ship is operational, depends on the wave climate of the ocean area where the ship operates, the dynamic response of the ship to the waves, and the ship mission. The relation between the ship operability and the mission characteristics is established through the seakeeping criteria". The seakeeping criteria given by Tezdogan et al. [45] is used in this study. In the criteria, the operability index is defined as:

$$Op(\%) = \frac{\sum_{H_{1/3},T_p} n_{ss,\beta}(H_{1/3} < H_{1/3}^{lim})}{N} \cdot 100 \tag{3.43}$$

The operability index is a ratio, between the number of sea-sates (for all available peak periods) with significant wave heights, that do not exceed the maximum significant wave height ($n_{ss,\beta}$), over the total number of sates (N) in a certain wave scatter diagram.

It is a common approach to calculate the distribution of the maximum significant wave height $H_{1/3max}(T_p,\beta)$ for all mean wave periods of interest, using methods as the one presented by Fonseca and Guedes Soares [18]. Thus, avoiding the laborious work of calculating a certain ship response and compare it to the seakeeping criteria. However, in order to calculate OMSI, both absolute vertical accelerations and MSIs are obtained for all the points along the deck, at each sea-state. This means that the actual results can be directly compared with the seakeeping criteria, and therefore obtain the operability index. Unlike previous implementations of this method where only one or two locations are studied, in the present multiple locations along the deck are available. This means that the seakeeping criteria can be compared always with the maximum point along the deck, for each sea-state, regardless of its location. Leading to more reliable results.

Chapter 4

Comparison between programs of seakeeping analysis

It is increasingly important for a ship to carry out its mission within acceptable standards of comfort, safety and efficiency. To do so ship responses such as roll motions, absolute motions or accelerations are set to specific limits. It can be done at an early stage of a project, by studying absolute motions and accelerations based on seakeeping methods. There are many options to assess motions such as model tests, full-scale trials, or numerical calculations. Full-scale trials obtain the most realistic results, except for testing extreme weather conditions, but they are hard to perform at early stages of design. Model tests are prohibitively expensive, coupled with the inability of many model basins to produce sea conditions of interest for some types of craft and therefore less accessible to the design process. For such reasons, seakeeping programs based on strip theory are a frequent tool to predict ship motions, even in an era with more powerful methods such as Computational Fluid Dynamics (CFD) solvers. These tools are of particular interest during the early stages of project, because of its low computational power and simplicity in generating fast results.

Strip theory was selected as the tool for seakeeping analysis. It is to be embedded on hull optimization procedures, on passenger's comfort, of two different types of passenger ships. Programs using the strip theory, must be time efficient while maintaining good level of accuracy. In the present chapter was made a comparison between two available code alternatives, **CENTEC-SK** and ***MAXSURF* Motions**, at different headings and for a fixed Froude number. The goal of such comparison was to select the most adequate software to be used in dissertation, which as shown was **CENTEC-SK**. Belga [4] made a similar comparison on the same programs but only for head waves and multiple Froude numbers instead. Both codes perform the computations in the frequency domain, following the common method of Salvesen et al. [39].

4.1 Overview of seakeeping program, *CENTEC-SK*

CENTEC-SK was developed at CENTEC (Center for Marine Technology and Ocean Engineering) at Instituto Superior Técnico (IST), Lisbon. It is a frequency domain strip-theory code or the linear version of Fonseca and Guedes Soares [17]. The available documentation was used, however many of its features were not documented. It is known that it follows the frequency domain formulation of Salvesen et al. [39] without transom terms in the equations. According to Belga [4] the numerical solution for the 2-D radiation potential in forced harmonic motions, which allows to determine the sectional added masses,

damping coefficients and diffraction force, is obtained via multi-parameter conformal mapping Ramos and Guedes Soares [38]. The Linear potential flow theory requires the correction for viscous damping for the case of roll motions. This in-house code relies on text-based data entry system and generating an input file is quite a laborious process. On the other hand, the processing speed is very fast regardless of the input file. Table 4.1 compares the two programs on some of the geometry settings, being clear that *MAXSURF* Motions can analyse more complex geometries. Table 4.2 is a comparison on coordinate systems used by both programs. Motion results coordinate systems are of particular importance, since point coordinates studied further on, depend on this referential system. The information on both tables regarding this seakeeping code, *CENTEC-SK*, is based on Belga [4].

4.2 Overview of seakeeping program *MAXSURF* Motions

MAXSURF Motions is one module within *MAXSURF* Connected Edition V21 which is a commercially available software developed by Bentley Systems [7]. This software is very well documented. The configuration set for comparison uses the linear strip theory of Salvesen et al. [39] and without transom corrections. The numerical solution for 2-D radiation potential is also obtained via multi-parameter conformal mapping. The roll response is calculated using linear roll damping theory. This program is very user friendly and the modules are easy to integrate between each other, making it simple to perform changes on the input file. However, the running time can be very long and it is difficult to perform multiple tests.

Table 4.1: Characteristics of seakeeping programs,Belga [4].

Parameter	**Fonseca**	**MAXSURF Motions**
Maximum number of cross sections	40	200
Minimum number of equally spaced cross section	21	30
Maximum number of offset points per cross section	20	15
Minimum number of offset points per half cross section	8	3
Cross sections defined with equal number of offset mapping terms	YES	YES
Offset points approximately equally distant along cross section	YES	-
Maximum number of wavelengths used for motion results	30	500
Level of flexibility when setting wavelength range	HIGH	LOW
Computational speed with highest settings	HIGH	LOW

Table 4.2: Programs coordinate system, Belga [4].

	Program	**Coordinate Origin**	**+ x-axis**	**+y-axis**	**+z-axis**
Geometry Data	Fonseca	fwdPP, centerline, DWL	aft	port	upwards
	MAXSURF Motions	-	forward	starboard	upwards
Inputs	Fonseca	amidship, centerplane, DWL	forward	port	upwards
	MAXSURF Motions	amidship, centerplane, baseline	forward	starboard	upwards
Motion Results	Fonseca	LCG, centerplane, baseline	forward	port	upwards
	MAXSURF Motions	LCG, centerplane, baseline	forward	starboard	upwards

4.3 Programs Validation

Even though *MAXSURF* Motions is very well documented, and all the formulation is available, no further comparisons between the programs and their implementations of the linear strip theory by Salvesen et al. [39] are made. Such study would be out of the scope of this work. The main objective of this chapter is to validate the seakeeping program as an adequate tool for the present study in this dissertation. The rest of this seakeeping program comparison will focus on the results of each program compared to actual experimental results. This way is possible to make an informed decision on which program is best suited for the type of ship and required conditions. It is also a method of validating the seakeeping results obtained for the two different passenger ship at study.

The comparison process is simplified for the present study. It is done by analyzing the accuracy of the RAOs from the programs with experimental results available in the literature. Since neither one of the two ships at study here have available experimental results, the S-175 containership was selected as the alternative ship, with similar characteristics, to be used instead. The main characteristics of this vessel are presented in Table 4.3 and its body plane is shown in Figure 4.1 from ITTC [24].

The validation is performed by comparing the measured data and the calculations for the responses in regular waves for the S-175 containership with a forward speed corresponding to a Froud number of Fn = 0.275. This comparison focuses on the transfer functions for heave, roll and pitch at six different heading angles (β=180º, β=150º, β=120º,β=90º, β=60º and β=30º), where β=180º is head seas, β=90º is beam seas and β=0º is following seas, following International Towing Tank Conference ITTC standard definitions. The results are plotted against the non-dimensional wave frequency $\omega\sqrt{L/g}$ with a 31 evenly spaced frequencies in regular waves. The responses have been measured at a wave height of 1/50 of Lpp. The non-dimensional parameters, such as heave per wave amplitude, pitch and roll per wave slope are presented in the results. The validation for the above modes of motion for the S-175 container ship in regular waves, based on the transfer function of the motion, is carried out by comparing the computational results from the numerical code with experimental date available in the literature. The experimental datum used in the validation process is from three organizations Ishikawajima-Harima Heavy Industries (IHI), Sumitomo Heavy Industry (SHI) and Ship Research Institute (SRI), presented in the summery report of the seakeeping committee of the 15th and 16th International Towing Tank Conferences, ITTC [24]. Three different institutions were selected because there were no consistent experimental results for all headings of interest thus becoming the best solution to validate both programs. It should be noticed that the experimental data was not enough on the measured roll transfer function, specially, at the resonance frequency. Here the large effect of damping is clear, for that reason such results can not be confirmed with the same accuracy as the other two.

In Figures 4.2 - 4.4, the heave, roll and pitch motions are compared. As seen in Figure 4.2, showing the heave RAOs as function of the non-dimensional wave frequency, *CENTEC-SK* and *MAXSURF* Motions are in agreement regarding frequency. Both programs seem consistent with the experimental results, however on head seas they both overestimate the resonance peak, with *CENTEC-SK* taking a slight edge between the two. As it is shown in Figures 4.2a and 4.2b.

Regarding the comparison between roll RAOs from Figure 4.3, there are some noticeable divergences between the two programs. Knowing that *MAXSURF* Motions has no correction on the roll damping, the over prediction at resonance peak is quite noticeable. Also, *Foncesa* has a good frequency alignment with the experimental results. *MAXSURF* Motions's resonance peaks generally occur

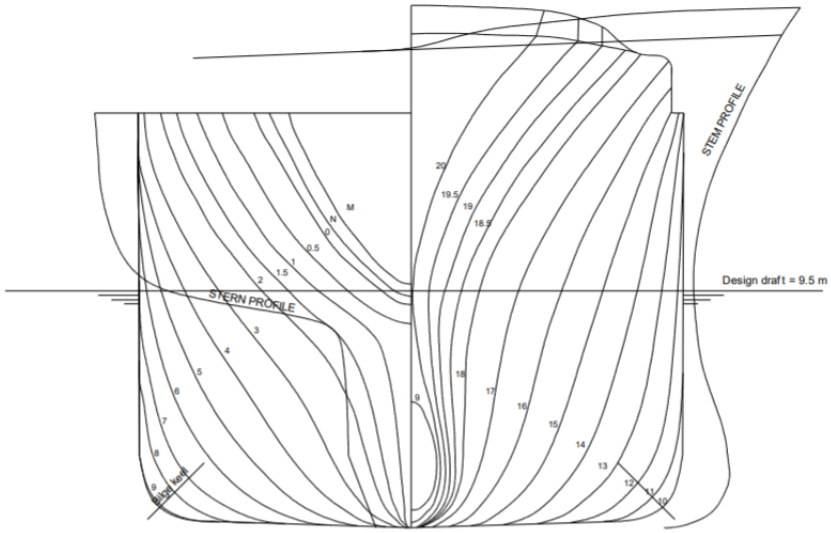

Figure 4.1: Body Plan for the S-175 Containership, ITTC of 1983 [24]

Table 4.3: Main Dimensions of the S-175 ContainerShip, ITTC of 1983 [24]

Main dimensions	**S-175 Containership**
Length between perpendiculars [m]	175
Beam [m]	25.4
Depth [m]	15.4
Draft [m]	9.5
Displacement [Kg]	24742000
Longitudinal Center of Buoyancy *	1.417
Block Coefficient	0.5716
Mid-Ship Section Coefficient	0.97
Vertical Center of Gravity [m]	9.52
Metacentric Height [m]	1
Pitch radius of gyration *	0.24
Roll radius of gyration**	0.328
*Expressed as a percentage of length between perpendicular.	
**Expressed as a percentage of breath.	

at smaller frequencies, quite clear for β= 60º, as shown in Figure 4.3e. At β= 30º shown in Figure 4.3f, both programs are in line with different experimental results. While *MAXSURF* Motions is consistent with the results from SRI Model Test, *CENTEC-SK* is consistent with the results from SHI Model Test. This incoherence may be solved by looking at the other program results in the study by ITTC [24]. By doing so it concluded that *CENTEC-SK* is closer to the rest of those programs and confirmed that even the results from SRI Model Test are divergent from the rest, for this particular heading.

Finally, the comparison between pitch RAOs as function of the non-dimensional wave frequency, is presented in Figure 4.4. On head seas the experimental and programs results are in clear agreement, with a slight over prediction of peak resonance compared to SRI Model Test, as shown in Figures 4.4a and 4.4b. However, for beam seas *MAXSURF* Motions clearly over predicts the pitch RAOs while *CENTEC-SK* under predicts the same results compared to SRI Model test, as seen in Figure 4.4d.

Such differences between the two programs are reduced when approaching following seas, as shown in Figure 4.4f. From these results it is taken that *CENTEC-SK* is more consistent with experimental results and due to its fast computational performance it becomes the ideal program to be used on this dissertation.

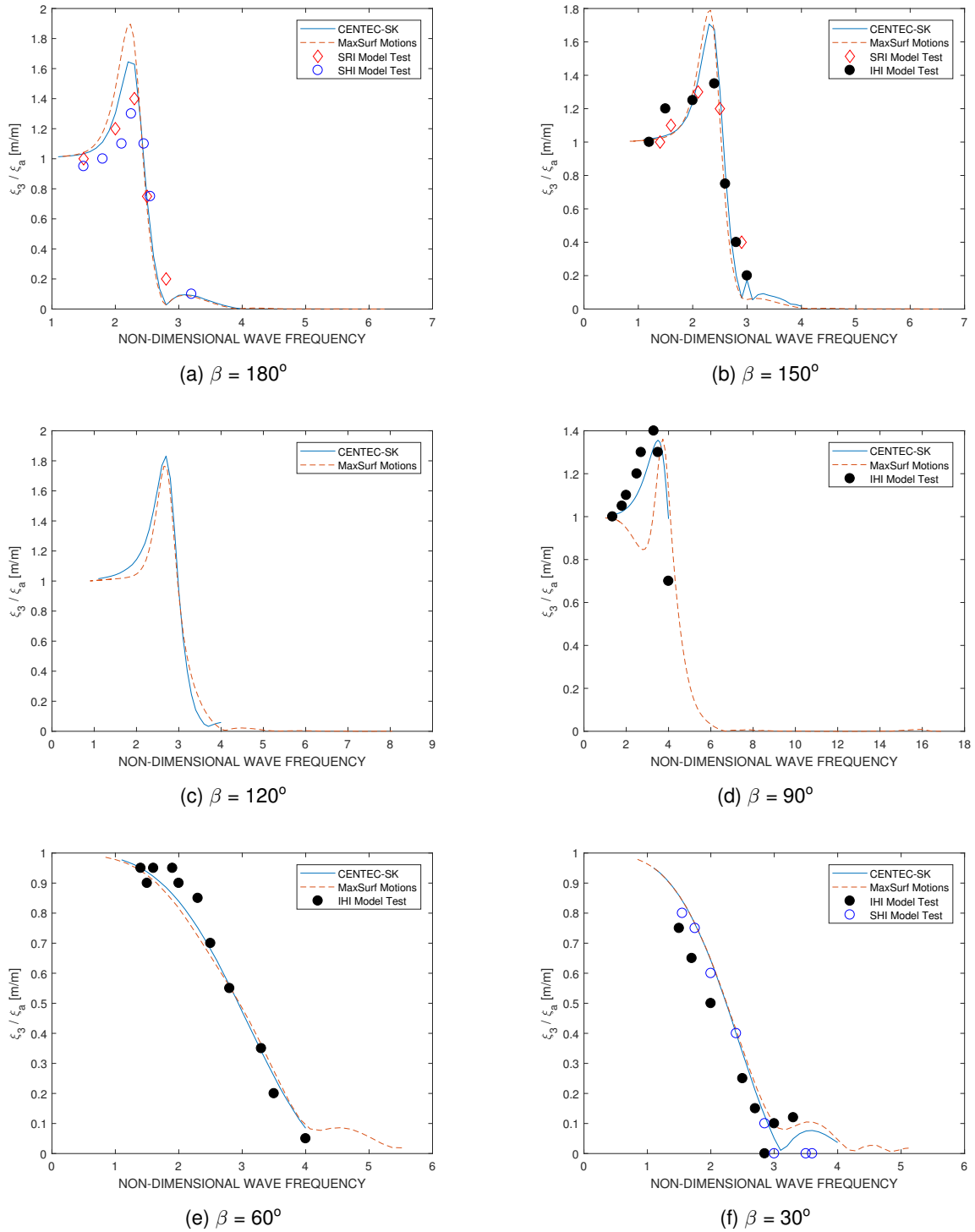

(a) β = 180°

(b) β = 150°

(c) β = 120°

(d) β = 90°

(e) β = 60°

(f) β = 30°

Figure 4.2: Heave RAOs as function of the non-dimensional wave frequency.

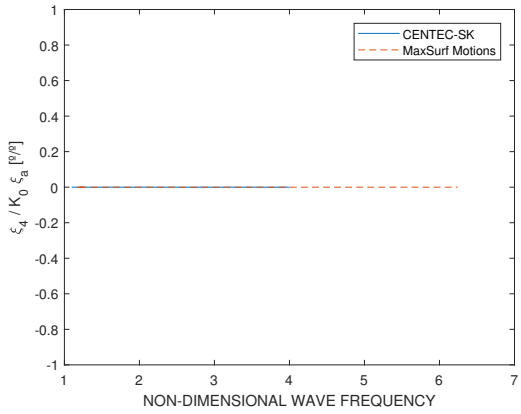

(a) β = 180º

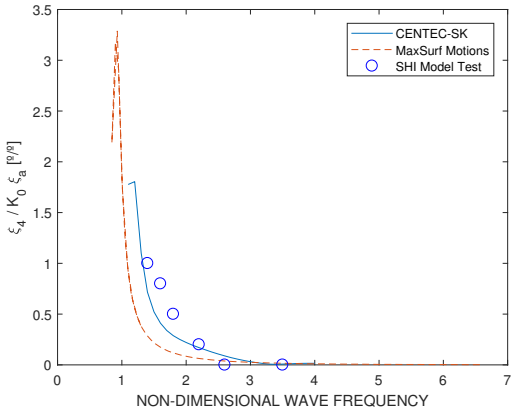

(b) β = 150º

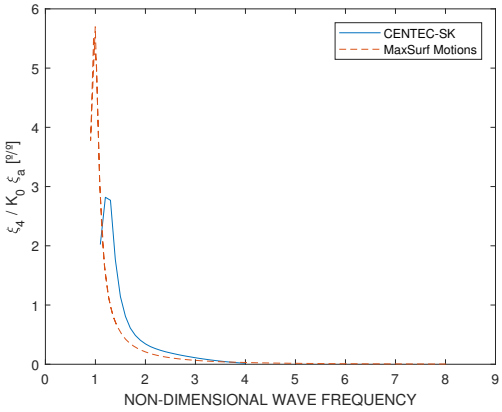

(c) β = 120º

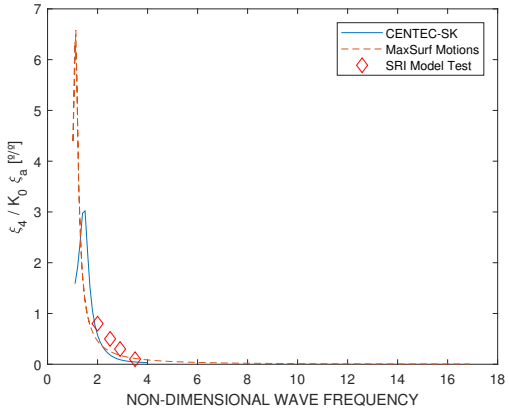

(d) β = 90º

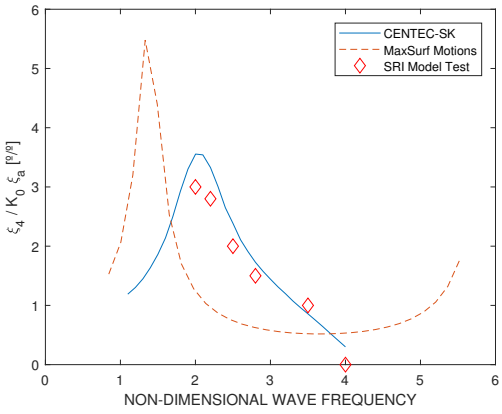

(e) β = 60º

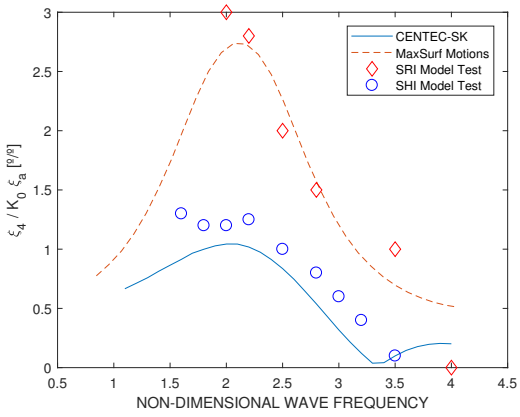

(f) β = 30º

Figure 4.3: Roll RAOs as function of the non-dimensional wave frequency.

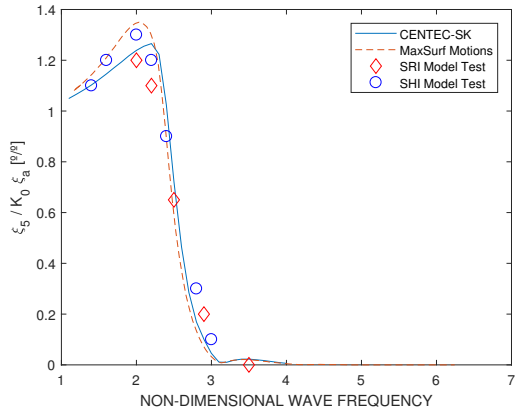

(a) β = 180º

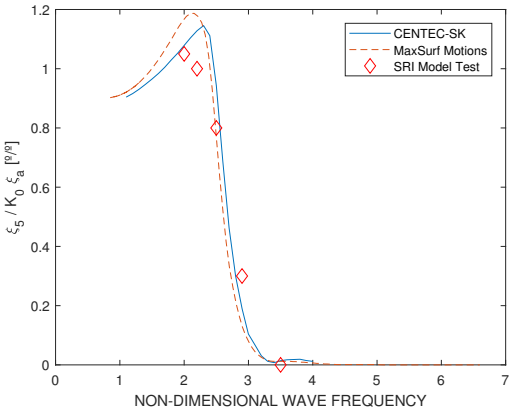

(b) β = 150º

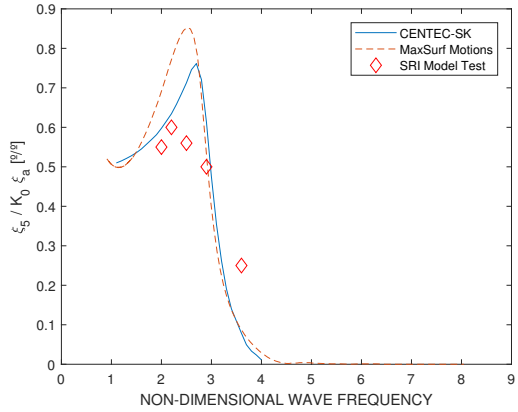

(c) β = 120º

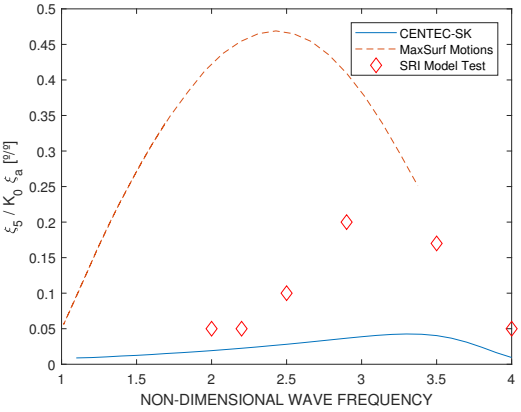

(d) β = 90º

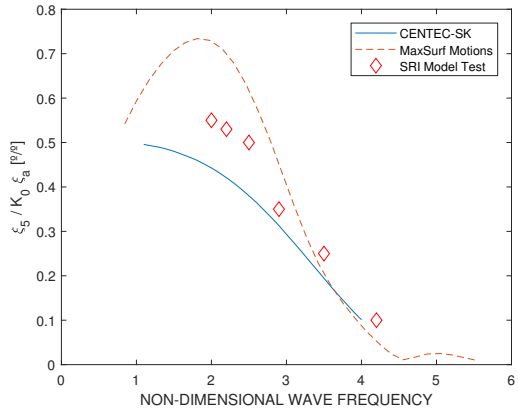

(e) β = 60º

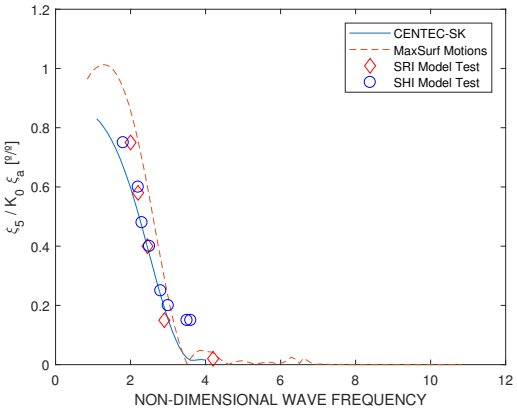

(f) β = 30º

Figure 4.4: Pitch RAOs as function of the non-dimensional wave frequency.

4.4 Summary

Since the start of this dissertation it was clear that using strip theory for the seakeeping analysis was the best solution. To do so, two different programs were available, namely *CENTEC-SK* and *MAXSURF* Motions.

From the characteristics comparison between the two programs it was concluded that *MAXSURF* Motions was the most user friendly of the two. Also, it had the best documentation, compared to *CENTEC-SK*. *MAXSURF* Motions input files were easier to work with. All the transformations were very intuitive and easy to cross between the various modules of *MAXSURF*. The input files from *CENTEC-SK*, required a specific type of input file in the form of ".DAT" format. This input file is frequently different between versions, thus requiring the creation of an auxiliary computer code, wrote in *MATLAB*, to ensure consistency and reduce time. Even though *MAXSURF* Motions proved to have many points in its favour it had a major drawback, which was its computational time. Compared to *CENTEC-SK*, the computational time from *MAXSURF* Motions is so much higher. Therefore, it would be impracticable for calculating OMSI, since it required multiple sea states and headings. Also, the output files from *MAXSURF* Motions are harder to integrate with *MATLAB*, the ideal tool for the calculation of OMSI.

For the S-175 containership, the comparisons showed that both programs predicted consistent results regarding heave and pitch motions. Particularly in heave motions, no noticeable differences were found between the two programs at any of the 6 headings studied. On pitch motions *MAXSURF* Motions over predicted the results, for headings between the beam and following seas.

Regarding roll motions the results were not confirmed by the experimental results, since the frequency region for the resonance peak, the one of most interest, was not within the region of the experimental results. However, it was clear that *MAXSURF* Motions over predicts the resonance peak of roll motions compared to *CENTEC-SK*. Finally, it is easier to include roll damping corrections on *CENTEC-SK*, which showed a clear effect on the results.

It was concluded that *CENTEC-SK* code was the most suitable tool for this dissertation. Therefore, *CENTEC-SK* was used to obtain all seakeeping results. This code has some drawbacks like lack of official documentation and laborious input files. However, its fast computation and flexibility to integrate with *MATLAB*, make it the best tool for multiple and reliable seakeeping calculations.

Chapter 5

Characterization of the seakeeping improvement procedures

In the first part of this dissertation, the prior work on the optimization of hulls using seakeeping analysis was introduced. The tools and methods were selected and introduced as a basis for this dissertation. In the present chapter such methods are put into practice with the goal of finding hull variations that are improved for comfort of passengers in specific sea ways.

It is well known that ship design is a cycle with many different stages of process. At each iteration of the project the ship becomes more complex and optimized. Therefore, improvement procedures are performed along multiple stages of the process and focused on different categories accordingly: such as construction costs, carrying capacity, safety, comfort, hull resistance, service speed, among others. To say that different problems can be addressed at different times and it is very important to correctly identify the best timing for each one.

On the present work, the focus is on strategies of improving passenger ship hulls at an early stage of design, while there is still flexibility to major changes without compromising other components of a project, that are dependent on fixed parameters of a ship hull. For that reason no major constrains are selected but the influence of the performed variations is considered instead. To be specific, for this dissertation an improved hull is refereed to hull variations that improves comfort of its passengers. Other seakeeping characteristics of the ship may be affected by comfort oriented solutions. Such effects should also be accounted and evaluated by naval architects, when considering some of the solutions here used. However, in this dissertation, no study is presented on these seakeeping characteristics outside the scope of passengers comfort.

This chapter serves to introduce the two different passenger ships in study and their respective operating scenarios, the respective hull variations performed to each ship. It is also performed an analysis to the parameters used for assessing the seakeeping performances of each hull variation.

5.1 Parent ships characteristics

Passenger ships are a particular group that is concerned for comfort above many other characteristics. For that reason it becomes of particular interest to study optimization procedures that focus on improving the comfort of its passengers. In the present case, the comfort improvements are based on

the reduction of the Overall Motion Sickness Index (OMSI), where the method is tested for two different scenarios. In the first scenario is studied a larger area where all positions assessed have the same importance and all benefit from comfort improvements. On the second scenario only one particular section is improved. To do so two different ships were selected according to its improvement requirements, both ship characteristics are presented on Subsections 5.1.1 and 5.1.2 respectively.

5.1.1 Passenger ship for river and coastal waters [SHIP1]

The first vessel particularly benefits from an overall study of its comfort without discriminating any particular area since the passengers are distributed evenly across the length of the ship, as seen in Figure 5.1. This river going vessel, is supposed to operate on two to three days trips and is therefore equipped with cabins placed all along the deck. Originally this vessel was to operate on rivers, but there is interest using a similar ship on coastal areas where it would be facing slightly harsher conditions (Section 5.2). Because of the new sea conditions and cabins distributions, this ship becomes and ideal candidate to study OMSI along the deck and improve it in terms of comfort. The main characteristics of this passenger ship for river and coastal waters, that may from now on also be referred as SHIP1, constitute the parent ship from which all new hull variations are derived.

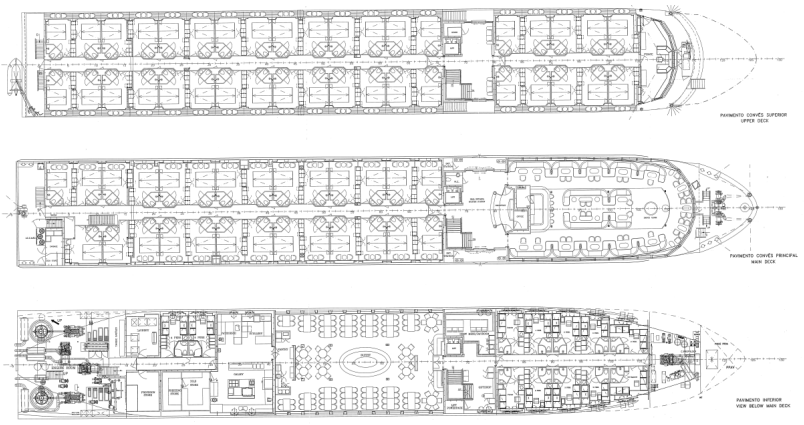

Figure 5.1: Part of the general arrangement from SHIP1.

This parent ship has simple lines as shown in Firgure 5.2, which is helpful to make the variations in *MAXSURF* Modeler [6]. The main dimensions and form parameters are presented on Table 5.1. These characteristics are based on the referential centered at midship, like the one used in *CENTEC-SK* code (Section 4.1). The seakeeping analysis on this ship will be performed at a speed of 16 Knots (Fn = 0.304). This speed corresponds to a maximum based on similar ships in coastal operations and is fixed through the tests. It is also worth noticing that the value of the vertical center of gravity (KG) is the same in all hull variations. The longitudinal center of buoyancy (LCB) and the longitudinal center of gravity (LCG) are always in the same position. This assumption is based on Kukner and Sarioz [28] where is stated: ”For all the variant hulls, the position of the longitudinal center of gravity is assumed to be in the same vertical plane as the longitudinal center of buoyancy. It is well known that exact knowledge of the ship weight distribution is not available during the earliest stages of design and variations of the position of LCG will not significantly affect the seakeeping performance characteristics”. In total 98 points are studied with its locations fixed with the referential at the midship. The point distribution is presented in Figure 5.3.

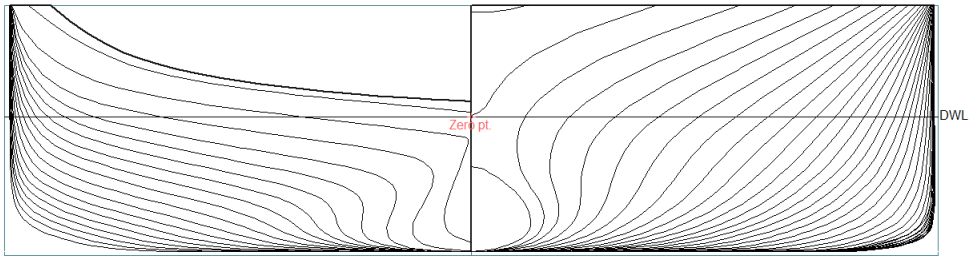

Figure 5.2: Parent hull forms from *MAXSURF* Modeler [SHIP1].

Table 5.1: Parent hull main dimensions and form parameters [SHIP1].

Displacement	$\triangle$	960.5	[t]
Draft to baseline	T	1.6	[m]
Waterline length	L_{WL}	75	[m]
Waterline beam	B_{WL}	11	[m]
Prismatic coefficient	C_P	0.717	[-]
Block Coefficient	C_B	0.71	[-]
Midship section coefficient	C_M	0.99	[-]
Waterplane area coefficient	C_{WP}	0.841	[-]
LCB=LCG from MS (-ve aft)	LCB =LCG	-1.5	[m]
Vertical center of buoyancy	KB	0.859	[m]
Vertical center of gravity	KG	3.58	[m]
Speed (Maximum)	V	16	[kn]

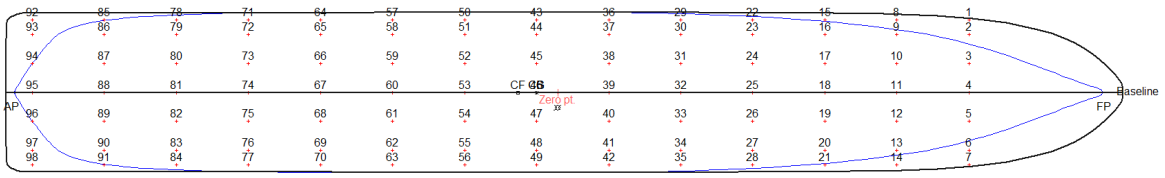

Figure 5.3: Distribution of points along the deck [SHIP1]

5.1.2 Ocean liner passenger ship [SHIP2]

The second ship is an ocean liner passenger ship, that may also be referred as SHIP2. This second ship has larger dimensions and is to operate in more agitated seas (Section 5.2). Like SHIP1 this second ship is also a passenger ship with cabins and many different public areas. However, the focus will be on the self-service area located on aft of the ship, shown in Figure 5.4. A region that is known to cause discomfort on its passengers. Such problem has been tackled from the point of vibration, using finite element analysis by Esteves and Gordo [16], but it would be interesting to approach the same problem using a seakeeping analysis. It is a great complement to the study of OMSI on passenger ships, because a smaller area in a specific region of the ship is being studied. Also, the operating scenario faced by SHIP2 is more severe compared to SHIP1. This parent ship also has simple lines as shown in Figure 5.5, which is helpful make the variations in *MAXSURF* Modeler. The main dimensions and form parameters are presented on Table 5.2. These characteristics are based on the referential centered at midship, like the one used in *CENTEC-SK* code (Section 4.1). Like before the vertical center of gravity (KG) is fixed for all hull variations. Together with the assumption that the longitudinal center of buoyancy (LCB) and the longitudinal center of gravity (LCG) are in the same location.

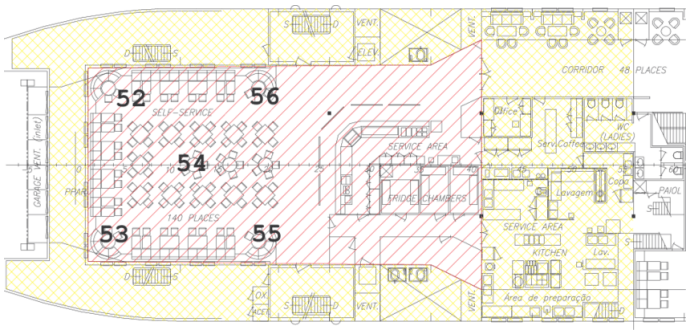

Figure 5.4: Self service area SHIP2, deck 5, aft area until frame 60, from Esteves and Gordo [16] [SHIP2].

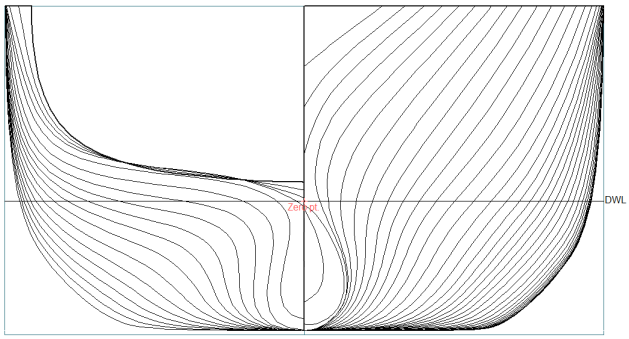

Figure 5.5: Parent hull forms from *MAXSURF* Modeler [SHIP2].

The seakeeping analysis on SHIP2 will be performed at a service speed of 21 Knots (Fn = 0.349). This speed corresponds to the service speed of the ship. In total 65 points are studied, with its locations fixed with the referential at the midship. The point distribution is presented in Figure 5.6.

Table 5.2: Parent hull main dimensions and form parameters [SHIP2].

Displacement	$\triangle$	5085	[t]
Draft to baseline	T	4.5	[m]
Waterline length	L_{WL}	98	[m]
Waterline beam	B_{WL}	20	[m]
Prismatic coefficient	C_P	0.642	[-]
Block Coefficient	C_B	0.563	[-]
Midship section coefficient	C_M	0.877	[-]
Waterplane area coefficient	C_{WP}	0.719	[-]
LCB=LCG from MS (-ve aft)	LCB =LCG	-2.9	[m]
Vertical center of buoyancy	KB	2.5	[m]
Vertical center of gravity	KG	6.5	[m]
Speed (Service)	V	21	[kn]

5.2 Operation sites

The seakeeping analysis in carried out in two different ships as stated before. Both ships operate in two different conditions of sea. While the first ship operates in coastal waters along Algarve, the second ship is to operate in rougher conditions in the Atlantic Ocean connecting Algarve to Madeira. Knowing the conditions of sea is an important aspect when calculating the OMSI. More specifically information

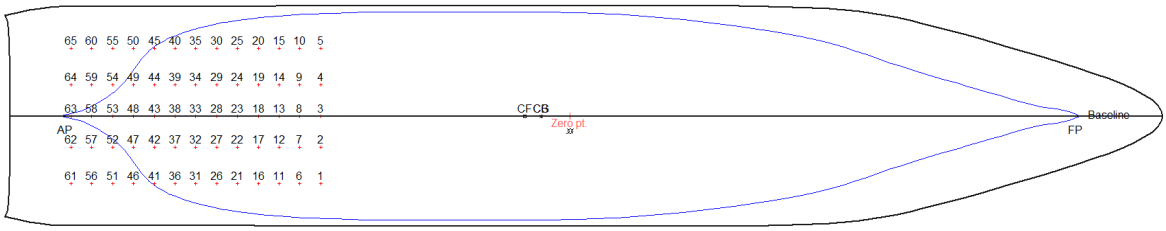

Figure 5.6: Distribution of points along the deck [SHIP2]

like wave height and wave periods are used to obtain the wave spectrum. The most common type of wave headings will help to focus on specific motions to be considered.

In the present study, the comfort analysis is carried along a particular region, in various sea conditions, throughout a long period. Therefore, it requires a long-term sea state description of sea. The significant wave height and mean wave period will vary in a long-term prediction of the sea. To do so, it is required to know the joint frequency of the significant height and mean wave period. This type of information can be used in many ways, for example to obtain long-term statistics of the wave amplitude and wave height. Like when looking for the probability of a specific wave height along the wave periods. This information is used to calculate the OMSI, when considering the probability of the various sea-states (Section 3.8). Also, important when studying the operability of the ship during the year, for specific limiting criteria of operation, the operability index (Section 3.8).

In this section are presented the sea conditions of each operation site. These are essential to accurately predict the OMSI and the Operability index.

5.2.1 Coast of Algarve [Operating Scenario 1]

SHIP1 operates on the basin of Algarve, for touristic trips along the coast, see Figure 5.7, here refereed as **Operating Scenario 1**. The characterization of the sea is done using a scatter diagram presented on Table 5.3. It was constructed based on data collected by CENTEC (Center for Marine Technology and Ocean Engineering) at Instituto Superior Técnico (IST). This data was gathered in one point near the coast of Algarve [Φ37^{o}N, L -8.5^{o}W], as shown in Figure 5.7, for a period between 1958 and 2001. There are 10 different intervals of wave height ($H_{1/3}$) to 22 different peak periods (T_P). The wave spectrum for each sea state $S_\zeta(\omega_0)$ is calculated based on Section 3.3.

Statistical information of sea direction is also available and considering a trip from West to East, the ship faces the worst scenario of encountering waves. It is mainly constituted by head and bow seas as show in Figure 5.9 and 5.8. For this type of operation: beam, quartering and following seas will have little influence on the OMSI. It means that the best results should be on hull variations that mainly improve comfort on head seas, which correspond to around 62% on encountered seas.

5.2.2 Atlantic Ocean region between Algarve and Madeira [Operating Scenario 2]

SHIP2 operates on the Atlantic Ocean connecting Algarve to Madeira, transporting passengers between the two regions. This operating scenario is here refereed as **Operating Scenario 2**. The characterization of the sea is done using a scatter diagram presented in Table 5.4. It was constructed

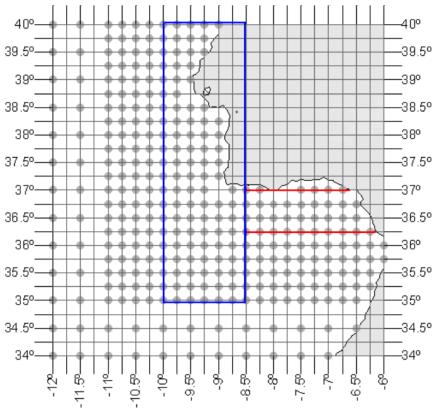

Figure 5.7: Map of collected point in the region of Algarve.

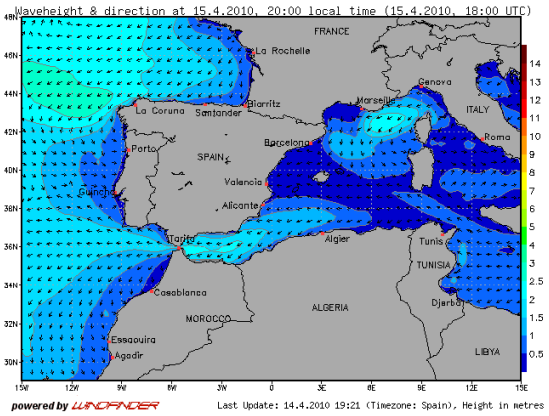

Figure 5.8: Wave height and direction of the waves in the region of Algarve

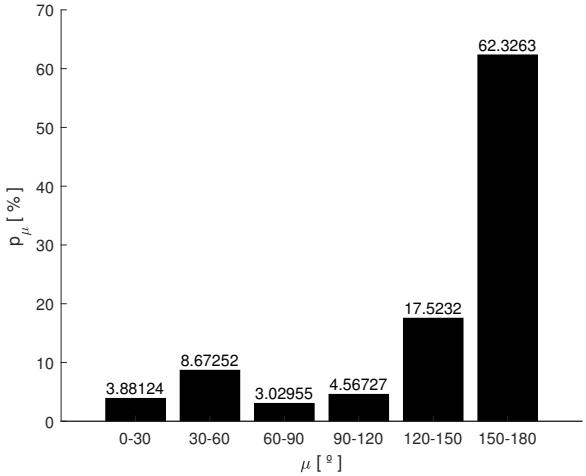

Figure 5.9: Probable fractions of time at various ship-wave headings [SHIP1]

Table 5.3: Joint frequency of significant wave height and spectral peak period. Representative data for the coast of Algarve.

Significant wave height [m]	Spectral peak period (s)																			
	3	4	5	6	7	8	9	10	11	12	13	14	15	16	17	18	19	20	21	22	Sum
1	508	9992	18888	6858	2900	2871	4174	4963	5661	5847	4854	3171	1651	0	676	356	0	65	0	13	73448
2	0	101	5072	8450	6026	1332	1609	1913	2443	2838	3692	3582	2688	0	1419	899	0	111	0	34	42209
3	0	0	2	251	1971	1251	828	735	649	552	727	661	562	0	377	374	0	32	0	6	8978
4	0	0	0	2	38	223	500	427	378	199	212	197	217	0	83	134	0	2	0	0	2612
5	0	0	0	0	0	5	42	142	215	182	83	50	56	0	59	55	0	1	0	0	890
6	0	0	0	0	0	0	0	11	60	99	35	26	21	0	27	15	0	1	0	0	295
7	0	0	0	0	0	0	0	0	6	25	24	14	14	0	8	15	0	0	0	0	106
8	0	0	0	0	0	0	0	0	1	2	2	2	1	0	2	12	0	0	0	0	22
9	0	0	0	0	0	0	0	0	0	1	1	1	0	0	0	1	0	0	0	0	4
10	0	0	0	0	0	0	0	0	0	0	1	2	0	0	0	0	0	0	0	0	3
Sum	508	10093	23962	15561	10935	5682	7153	8191	9413	9745	9631	7706	5210	0	2651	1861	0	212	0	53	128567

based on data collected by the European Center for Medium-Range Weather Forecasts (ECMWF). This data is representative of one point in the middle of the route [Φ35º N, L 15º W], for a period between 1979 and 2013. There are 10 different intervals of wave height ($H_{1/3}$) to 20 different peak periods (T_P). The wave spectrum for each sea state $S_\zeta(\omega_0)$ is to be calculated based on Section 3.3. Statistical information of sea direction is also available and a trip from Northeast to Southwest is considered. For this trip the ship is expected to encounter mainly head and bow seas and sometimes beam seas as

show in Figure 5.10.

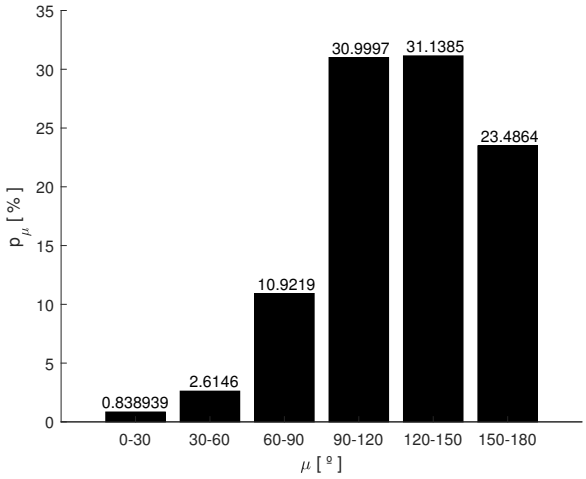

Figure 5.10: Probable fractions of time at various ship-wave headings [SHIP2]

Table 5.4: Joint frequency of significant wave height and spectral peak period. Representative data for the Atlantic Ocean (Region between Algarve and Madeira)

Significant wave height [m]	**Spectral peak period (s)**																
	5	**6**	**7**	**8**	**9**	**10**	**11**	**12**	**13**	**14**	**15**	**16**	**17**	**18**	**19**	**20**	**Sum**
1	6	38	244	238	241	128	58	42	17	26	4	0	4	0	0	0	1046
2	7	360	2235	2160	3094	3318	3638	4125	2870	1007	239	8	26	3	0	0	23090
3	0	11	570	1183	1583	1237	1290	2380	4150	4008	1505	59	258	38	0	2	18274
4	0	0	0	77	278	426	477	526	809	1502	1529	89	447	69	0	2	6231
5	0	0	0	2	8	64	130	216	218	298	404	36	358	71	0	2	1807
6	0	0	0	0	1	3	15	54	73	69	115	12	108	39	1	5	495
7	0	0	0	0	0	0	0	4	14	20	37	5	52	15	0	0	147
8	0	0	0	0	0	0	0	0	1	5	21	1	6	3	0	0	37
9	0	0	0	0	0	0	0	0	0	1	3	0	1	3	0	0	8
10	0	0	0	0	0	0	0	0	0	0	1	0	0	0	0	0	1
Sum	13	409	3049	3660	5205	5176	5608	7347	8152	6936	3858	210	1260	241	1	11	51136

5.2.3 Comparison between operating scenarios

As seen before SHIP1 is to operate on Operating Scenario 1 and SHIP2 is to operate on Operating Scenario 2. Different sea conditions are to be expected by each ship.

Based on the characteristics of SHIP1, it is clear that it was design for relatively calm conditions of sea. Such conditions are expected on Operating Scenario 1. Here the significant wave height is mainly between 0-1 m and sometimes between 1-2 m. The range of spectral peak periods is between 4-14 s, as shown on Table 5.3. This ship is also to expect a very predictable type of encountering waves, manly heading waves, which makes it easier to perform purposely oriented hull alterations. On the other hand, SHIP2 is an ocean going passenger carrier. Based on its design characteristics it is clear that it is prepared to face harsher conditions. That is exactly what is expected from Operating Scenario 2, where significant wave heights are between 2-4 m or even 4-5m, as shown on Table 5.4. These significant wave heights are higher than in Operating Scenario 1.

Another major different between SHIP1 and SHIP2 is that the second ship has a less predictable type of incoming waves. Even though it is expected to face mainly head and bow seas, beam seas are also representative on this operating scenario. Such differences will allow a deeper understanding on the use of OMSI, as a way of comparing comfort levels between different ships and hulls. It will be also possible to see if the type of sea-state or wave direction have any influence on the final results.

5.3 Derivation of new hull forms

Several hull variations were obtained from both parent hull. Such variations were divided into two categories. The first focused on the systematical variation of form parameters such as the longitudinal center of buoyancy (LCB),the block coefficient (C_B) and the midship section coefficient (C_M), using the Lackenby Method [29]. The second type of systematical variations only depended on main dimensions, such as the length at waterline (L_{WL}), beam at waterline (B_{WL}) and draft (T). This methodology for developing new hull forms is based on work of similar researchers, Grigoropoulos and Loukakis [21], Kukner and Sariöz [28], Özüm et al.[35], Cepowski [10], Scamardella and Piscopo [41] and Belga et al.[5], who proved that seakeeping performances are affected by these parameters.

Six different types of hull variations were tested in this dissertation. All six on SHIP1 and four on SHIP2. Each hull variation was performed using *MAXSURF* Modeler from *Bentley Systems* [6], where all the transformations were easily accomplished for a large number of hulls. In order to make the discussion as clear as possible, each type of hull transformations was called **Set *n***. With *n* being a number between 1-6 that corresponds to each method of transformation. In the following tables the data refereeing to each hull variation from both parent ships are presented, where the data in bold refer to the parent hull/ship.

5.3.1 Hull transformations for SHIP1

The first type of hull variations are presented on Tables 5.5-5.7. These three tables consist of new hull combinations of C_B and LCB. With the Block coefficient (C_B) ranging between 0.66-0.76 for three different values of LCB, 50%, 52% and 54%, measured form the forward perpendicular. Physically it means that an LCB = 50% is half of L_{WL}. The variations in C_B are smaller than 10% comparatively to the parent hull to avoid unreasonable distortions.

The main difference between these three tables is the process to obtain the new C_B and LCB. That is, in one method the C_B was obtained by changing the ships displacement, in the other C_B was obtained by changing the ship's draft. In the third and last one, C_B was obtained by changing both ship's draft and waterline beam. The goal is to study any possible influence in the final results, based on how the same coefficients are transformed. Even thought the coefficients are the same in these three tables, the way they were obtained are not. For that reason each transformation type of C_B and LCB is considered different and therefore called Set 1, Set 2 and Set 3. The other types of hull transformations namely Set 4, Set 5 and Set 6 are independent of each other, since each coefficient is different and transformed by only one method instead. A more detailed analysis on how each **Set *n*** is obtained for SHIP1, is now discussed:

Set 1 of hull variations, corresponds to the first approach of changing the C_B, where the displace-

ments and shape coefficients like C_P and C_{WP} are free to change. While C_M, L_{WL}, B_{WL} and T are fixed to the parent values. Both the length overall (L_{OA}) and the beam overall (B_{OA}), may suffer some changes due to the Lackenby Method [29]. In Table 5.5 significant information of each new hull derivation from the parent ship (SHIP1), is presented. It should be noticed that C_P increases with C_B, as does C_{WP} and the displacement. Also, C_P and the displacement do not change with LCB, unlike C_{WP} that decreases for bigger LCBs.

Table 5.5: Hull form parameters for Set 1 of variations. Fixed C_M = 0.99, L_{WL} = 75 m, B_{WL} = 11 m and T = 1.6 m. Parent ship: SHIP1.

	C_B = 0.66	**C_B= 0.68**	**C_B = 0.70**	**C_B = 0.71**	**C_B= 072**	**C_B = 0.74**	**C_B = 0.76**
LCB = 50%							
C_P	0.67	0.69	0.707		0.727	0.748	0.780
C_{WP}	0.817	0.828	0.843	-	0.857	0.871	0.885
Δ	901 t	920 t	948 t		974 t	1001 t	1028 t
LCB = 52%							
C_P	0.67	0.69	0.707	**0.717**	0.727	0.748	0.78
C_{WP}	0.809	0.818	0.833	**0.841**	0.848	0.862	0.876
Δ	901 t	920 t	948 t	**960.5 t**	974 t	1001 t	1028 t
LCB = 54%							
C_P	0.67	0.69	0.707		0.727	0.748	0.78
C_{WP}	0.801	0.809	0.824	-	0.838	0.853	0.867
Δ	901 t	920 t	948 t		974 t	1001 t	1028 t

Set 2 of hull variations, corresponds to the second approach of changing the C_B, where T, C_P and C_{WP} were free to vary instead. The displacement is now fixed to the parent hull, as is C_M, L_{WL}, B_{WL}. Again the length overall (L_{OA}) and beam overall (B_{OA}), may suffer some changes due to the Lackenby Method [29]. In Table 5.6 significant information of each new hull derivation from the parent ship (SHIP1) is presented. Like before C_P and C_{WP} increase with C_B. While T reduces with bigger C_B's and is not affected by changes in LCB.

Table 5.6: Hull form parameters for Set 2 of variations. Fixed C_M = 0.99, L_{WL} = 75 m, B_{WL} = 11 m and Δ= 960.5 t. Parent ship: SHIP1

	C_B = 0.66	**C_B= 0.68**	**C_B = 0.70**	**C_B = 0.71**	**C_B= 072**	**C_B = 0.74**	**C_B = 0.76**
LCB = 50%							
C_P	0.667	0.687	0.707		0.727	0.748	0.768
C_{WP}	0.809	0.825	0.84	-	0.855	0.869	0.883
T	1.721 m	1.671 m	1.623 m		1.578 m	1.535 m	1.495 m
LCB = 52%							
C_P	0.667	0.687	0.707	**0.717**	0.727	0.748	0.768
C_{WP}	0.803	0.818	0.833	**0.841**	0.848	0.862	0.876
T	1.721 m	1.671 m	1.623 m	**1.6 m**	1.578 m	1.535 m	1.495 m
LCB = 54%							
C_P	0.667	0.687	0.707		0.727	0.748	0.768
C_{WP}	0.794	0.810	0.825	-	0.839	0.853	0.867
T	1.721 m	1.671 m	1.623 m		1.578 m	1.535 m	1.495 m

Set 3 of hull variations, corresponds to the third and final approach of changing the C_B, where T, B_{WL}, C_P and C_{WP} are free to vary instead. Displacement is fixed to the parent hull, as is C_M, L_{WL}. Again the length overall (L_{OA}) and beam overall (B_{OA}), may suffer some changes due to the Lackenby Method [29]. In Table 5.7 significant information of each new hull derivation from the parent ship (SHIP1), is presented. Like before C_P and C_{WP} increase with C_B. T and B_{WL} reduce with bigger C_B's and are not

affected by changes in LCB. It should be noticed that the ratio B_{WL}/T is maintained constant for each new C_B, and is equal to B_{WL}/T = 6.9, the same has in the parent hull.

Table 5.7: Hull form parameters for Set 3 of variations. Fixed C_M = 0.99, L_{WL} = 75 m, B_{WL}/T = 6.9 and Δ= 960.5 t. Parent ship: SHIP1.

	C_B = 0.66	C_B= 0.68	C_B = 0.70	C_B = 0.71	C_B= 072	C_B = 0.74	C_B = 0.76
LCB = 50%							
C_P	0.666	0.687	0.707		0.728	0.748	0.768
C_{WP}	0.813	0.828	0.843		0.857	0.871	0.885
T	1.659 m	1.635 m	1.611 m	-	1.589 m	1.567 m	1.546 m
B_{WL}	11.41 m	11.24 m	11.078 m		10.923 m	10.775 m	10.632 m
LCB = 52%							
C_P	0.666	0.687	0.707	**0.717**	0.728	0.748	0.768
C_{WP}	0.803	0.818	0.833	**0.841**	0.848	0.862	0.876
T	1.659 m	1.635 m	1.611 m	**1.6 m**	1.589 m	1.567 m	1.546 m
B_{WL}	11.41 m	11.24 m	11.078 m	**11 m**	10.923 m	10.775 m	10.632 m
LCB = 54%							
C_P	0.666	0.687	0.707		0.728	0.748	0.768
C_{WP}	0.794	0.809	0.824		0.838	0.853	0.867
T	1.659 m	1.635 m	1.611 m	-	1.589 m	1.567 m	1.546 m
B_{WL}	11.41 m	11.24 m	11.078 m		10.923 m	10.775 m	10.632 m

Set 4 of hull variations, corresponds to transformations on C_M for a fixed LCB. Table 5.8 contains significant information of each new hull derivation from the parent ship (SHIP1). For SHIP1 C_M ranges between 0.99 - 0.95. The data in bold corresponds to the parent hull and as we can see it corresponds to the highest value of C_M, making only sense to study transformations with smaller values of C_M. Here C_B is kept constant just like B_{WL}, T and the displacement. On the other hand C_P and C_{WP} are free to change with C_M, with both C_P and C_{WP} increasing the smaller C_M is. All variations are obtained for the same LCB = 52%, since the focus is on C_M in this particular case.

Table 5.8: Hull form parameters for Set 4 of variations. Fixed C_B = 0.71, B_{WL} = 11 m, T = 1.6 m and Δ= 960.5 t.Parent ship: SHIP1.

	C_M = 0.99	C_M = 0.98	C_M = 0.97	C_M = 0.96	C_M = 0.95
LCB = 52%					
C_P	**0.717**	0.725	0.733	0.742	0.75
C_{WP}	**0.841**	0.845	0.847	0.852	0.855

Set 5 of hull variations, corresponds to transformations on the waterline length (L_{WL}), the same as Lpp. This is one of the two geometrical variations in study. Table 5.9 contains significant information of each new hull derivation from the parent ship (SHIP1). In this case the waterline length (L_{WL}) is set as the variable to be changed. Four different hulls were derived, by increasing and reducing L_{WL} by 10%. The parent hull corresponds to L_{WL} = 100%, with its data presented in bold. In this type of variation all form parameters, B_{WL}/T and displacement are kept constant. On the other hand, L_{WL}, B_{WL} and T change accordingly.

Set 6 is the last type of hull variation, corresponding to transformations based on the B_{WL}/T ratio. It is the second type of geometrical variations in study. In Table 5.10 significant information of each new hull derivation from the parent ship (SHIP1), is presented. Four different hulls were derived by increasing and reducing B_{WL}/T by 25%. In this type of variation form parameters, L_{WL} and displacement are kept constant, while B_{WL} and T change accordingly.

Table 5.9: Hull form parameters for Set 5 of variations. Fixed C_B = 0.71, C_P = 0.717, C_M = 0.99, B_{WL}/T = 6.87 and Δ= 960.5 t. Parent ship: SHIP1.

	L_{WL} = 90%	**L_{WL} = 95%**	**L_{WL} = 100%**	**L_{WL} = 105%**	**L_{WL} = 110%**
LCB = 52%					
L_{WL}	67.5 m	71.25 m	**75 m**	78.75 m	82.5 m
B_{WL}	11.60 m	11.30 m	**11 m**	10.74 m	10.50 m
T	1.69 m	1.64 m	**1.6 m**	1.561 m	1.53 m

Table 5.10: Hull form parameters for Set 6 of variations. Fixed C_B = 0.71, C_P = 0.717, C_M = 0.99, L_{WL} = 75 m and Δ= 960.5 t. Parent ship: SHIP1

	B_{WL}/T = 5.2	**B_{WL}/T = 5.8**	**B_{WL}/T = 6.87**	**B_{WL}/T = 7.9**	**B_{WL}/T = 8.6**
LCB = 52%					
B_{WL}	9.5 m	10.15 m	**11 m**	11.8 m	12.3 m
T	1.852 m	1.734 m	**1.6 m**	1.491 m	1.431 m

5.3.2 Hull transformations for SHIP2

The transformations on SHIP2 were performed based on the exact same methods used for SHIP1. The difference is that only one Set of hull variation was used to change the C_B and LCB, namely Set 2. The purpose of the other two (Set 1 and Set 3) was achieved by studying SHIP1. Like for SHIP1, Set 4, Set 5 and Set 6 were used the exact same way on SHIP2. The respective results for hull transformations based on Set 2, Set 4, Set 5 and Set 6 can then be found from Table 5.11-5.14. Again, the data in bold is correspondent to the parent hull.

The coefficients changes were consistent with SHIP1. However, the coefficient C_M could now be increased and decreased by 10%, instead of only being reduced like it was done for SHIP1. When this coefficient was increased, C_M = 0.92 and C_M = 0.96, some distortions seemed to be introduced by *MaxSurf* Modeler, particularly in the bulb region. Such distortions may lead to inconsistencies and therefore inconclusive results.

Table 5.11: Hull form parameters for Set 2 of variations. Fixed C_M = 0.877, B_{WL} = 20 m and Δ= 5085 t. Parent ship:SHIP2.

	C_B = 0.50	**C_B= 0.53**	**C_B = 0.56**	**C_B = 0.58**	**C_B = 0.60**
LCB = 50%					
C_P	0.57	0.604		0.661	0.684
C_{WP}	0.652	0.688	-	0.745	0.768
T	5.07 m	4.78 m		4.37 m	4.23 m
LCB = 53%					
C_P	0.57	0.604	**0.642**	0.661	0.684
C_{WP}	0.644	0.680	**0.719**	0.738	0.76
T	5.07 m	4.78 m	**4.5 m**	4.37 m	4.23 m
LCB = 56%					
C_P	0.57	0.604		0.661	0.684
C_{WP}	0.636	0.672	-	0.730	0.752
T	5.07 m	4.78 m		4.37 m	4.23 m

Table 5.12: Hull form parameters for Set 4 of variations. Fixed C_B = 0.563, B_{WL} = 20 m, T = 4.5 m and Δ= 5085 t. Parent ship: SHIP2.

	C_M = 0.79	**C_M = 0.83**	**C_M = 0.87**	**C_M = 0.92**	**C_M = 0.96**
LCB = 53%					
C_P	0.714	0.679	**0.642**	0.612	0.587
C_{WP}	0.758	0.738	**0.719**	0.71	0.702

Table 5.13: Hull form parameters for Set 5 of variations. Fixed C_B = 0.563, C_P = 0.642, C_M = 0.877, B_{WL}/T = 4.4 and Δ= 5085 t. Parent ship: SHIP2.

	L_{WL} = 90%	**L_{WL} = 95%**	**L_{WL} = 100%**	**L_{WL} = 105%**	**L_{WL} = 110%**
LCB = 53%					
L_{WL}	93 m	96 m	**98 m**	100 m	19.50 m
B_{WL}	20.52 m	20.20 m	**20 m**	19.69 m	4.39 m
T	4.62 m	4.54 m	**4.5 m**	3.362 m	3.310 m

Table 5.14: Hull form parameters for Set 6 of variations. Fixed C_B = 0.563, C_P = 0.642, C_M = 0.877, L_{WL} = 98 m and Δ= 5085 t. Parent ship: SHIP2.

	B_{WL}/T = 3.33	**B_{WL}/T = 3.77**	**B_{WL}/T = 4.44**	**B_{WL}/T = 5.10**	**B_{WL}/T = 5.55**
LCB = 53%					
B_{WL}	17.4 m	18.5 m	**20 m**	21.5 m	22.35 m
T	5.17 m	4.87 m	**4.5 m**	4.20 m	4.03 m

5.4 Motion sickness index distribution

On board of a ship not all places are equally comfortable. Generally, near the center of gravity the motions of the ship tend to be less significant, compared to the bow or the stern. The same is true for the side beams of starboard or port side. In the present section an assessment of such variations is done for a set of peak periods and heading angles.

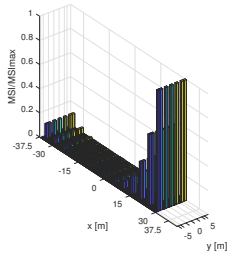

(a) Heading angle β = 180^o with MSI_{max} = 0.0913 %

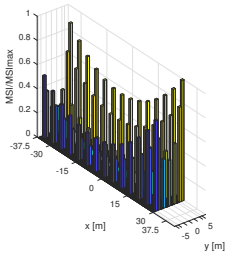

(b) Heading angle β = 120^o with MSI_{max} = 8.91 %

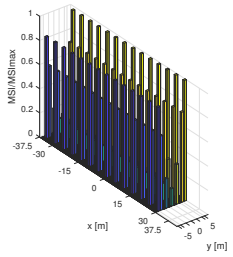

(c) Heading angle β = 90^o with MSI_{max} = 17.57 %

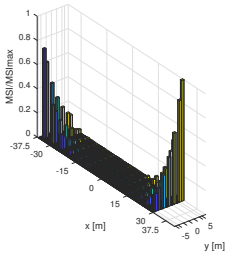

(d) Heading angle β = 60^o with MSI_{max} = 2.1205E-04 %

Figure 5.11: MSI distributions along the deck for a T_p = 5 s [SHIP1].

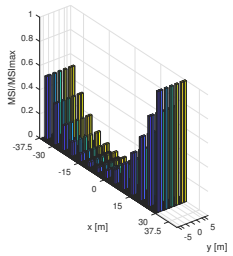

(a) Heading angle β = 180^o with MSI$_{max}$ = 6.79 %

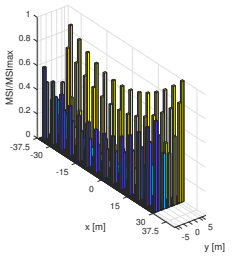

(b) Heading angle β = 120^o with MSI$_{max}$ = 9.95 %

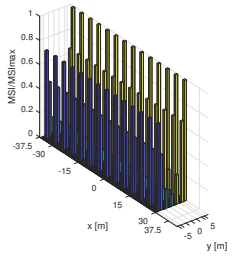

(c) Heading angle β = 90^o with MSI$_{max}$ = 4.75 %

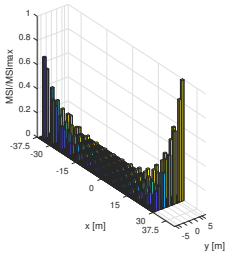

(d) Heading angle β = 60^o with MSI$_{max}$ = 3.555E-04 %

Figure 5.12: MSI distributions along the deck for a T$_p$ = 10 s [SHIP1].

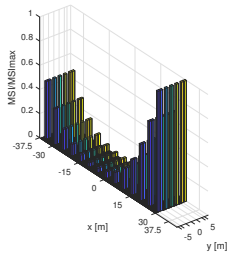

(a) Heading angle β = 180^o with MSI$_{max}$ = 1.93 %

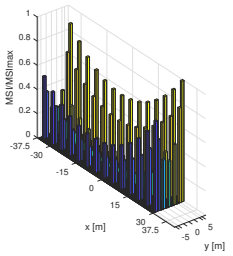

(b) Heading angle β = 120^o with MSI$_{max}$ = 2.06 %

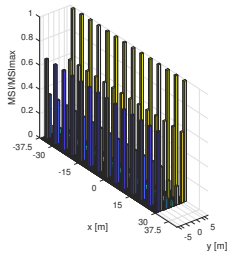

(c) Heading angle β = 90^o with MSI$_{max}$ = 0.5940 %

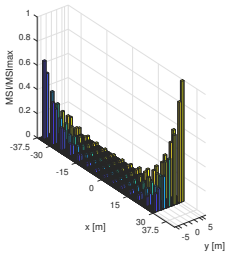

(d) Heading angle β = 60^o with MSI$_{max}$ = 5.077E-06 %

Figure 5.13: MSI distributions along the deck for a T$_p$ = 15 s [SHIP1].

Figures 5.11 - 5.13 show how MSI is distributed on the deck of SHIP1. The MSI/MSI$_{max}$ is represented in the form of a bar on these figures. The biggest bars correspond to MSI/MSI$_{max}$ = 1, which are the location of maximum MSI on a particular ship, sea-state and heading. This way it easier to understand the most meaningful locations to be studied and compare the MSI distributions between different sea-states and headings. In order to find how each location is influenced by the ship motions at different sea-states: Three different peak periods T$_p$ are selected, 5s, 10s and 15s with a constant significant wave height H$_s$ = 1 m. For each specific sea state four different plots of MSI/MSI$_{max}$ are presented, corresponding to heading angles of 180^o, 120^o, 90^o and 60^o, illustrating head seas, bow seas, beam seas and quartering seas respectively.

For the first sea-state, T_p = 5s and H_s = 1 m, the distributions of MSI/MSI_{max} clearly change along each coordinate of the deck together with each heading as seen in Figure 5.11. For a heading angle of 180º the bow is most affected compared to the stern and equally affected along the breath, as seen on Figure 5.11a. Here the maximum MSI_{max} = 0.0913%. On the other hand for heading angles of 120º the difference between MSI/MSI_{max} at stern and bow is not as significant. The values at the bow are still higher than in the stern, however MSI_{max} = 8.91% is now more significant than before and there is a change of magnitude along the breath, as seen in Figure 5.11b.

Such differences between MSI/MSI_{max} along the breath is even more significant for beam seas, as shown in Figure 5.11c. With the highest MSI_{max} = 17.57% of the four headings for this sea-state. Unlike before MSI/MSI_{max} is constant along the length of the ship. But it changes along the breath, with smaller values along the center line. Finally, in a heading angle of 60º the MSI/MSI_{max} distribution is similar to what is found before for heading angles of 120º, as shown in Figure 5.11d, with significant differences between bow and stern compared to the midship location. It is also worth noticing that an MSI_{max} = 2.1205E-04% is significantly low compared to other head and beam seas. Such small value has no significant physical meaning, since it can in fact be considered zero. These significant digits are only presented, so the reader can understand how small the magnitude of MSI is on these types of headings. On quartering and following seas, the MSI is therefore negligible for the calculation of OMSI as confirmed on the other sea-states

For the second sea state, T_p = 5s and H_s = 1 m presented by Figure 5.12, similar conclusions in terms of MSI/MSI_{max} compared to the first sea-state are found. Yet not everything is similar. To start in head seas, see Figure 5.12a, the MSI_{max} = 6.79 % is a clear increase compared too before. It is also clear, a greater effect of motion sickness in the stern of the ship, while still finding maximums of MSI/MSI_{max} at the bow and minimum at the midship. On the other hand, for a heading of 120º, see Figure 5.12b, the same type of MSI/MSI_{max} distribution occurs, with a MSI_{max} = 9.95 % similar to the previous sea-state. On beam seas the MSI/MSI_{max} distribution maintains constant along the length and changes along the breath, as shown in Figure 5.12c. Though with an MSI_{max} = 4.75 %, motions sickness seemed to improve for the new peak period T_p = 10 s. For quartering seas no significant changes are found both in terms of MSI/MSI_{max} or maximum MSI which is MSI_{max} = 3.555E-04 %, similar to the previous sea state where no passengers suffer sea-sickness.

In the last sea state here compared, T_p = 15s and H_s = 1 m shown in Figure 5.13 is possible to see the progress of motions sickness incidence (MSI) along the various peak periods T_p. On head seas, see Figure 5.13a, the same type of MSI/MSI_{max} distribution is observed. However, the MSI_{max} = 1.93 % is reduced compared to the second sea-state, indicating that the motion sickness incidence (MSI) is differently affected by peak periods. Similar conclusions are taken from bow seas, shown in Figure 5.13b, where MSI/MSI_{max} distribution maintains constant and a reduction of the maximum MSI value to MSI_{max} = 2.06 %, consistent with heading of 180º. Like on beam seas, see Figure 5.13c, the maximum MSI continued to decrease to MSI_{max} = 0.5940 %, considerably smaller than in the first sea-state. Again in headings of 60º, see Figure 5.13d, no major changes were observed, only to notice that MSI_{max} = 5.077E-06 %, still considerably smaller than on all other headings, meaning that no passenger would be affected.

As show, peak periods clearly influence motions sickness incidence (MSI). Lower peak periods (T_p) seem to greatly effect beam seas compared to higher ones. The opposite is also true for head seas,

where smaller peak periods (T_p) have smaller values of motion sickness incidence compared to higher ones. These conclusions are confirmed by Figure 5.14a, where the overall motion sickness index (OMSI) is plotted versus the peak periods (T_p). Here a range of heading angles, 180º, 150º, 120º, 90º, 60º and 30º, is being considered with equal probability of occurrence, for various significant wave heights H_s. Clearly the influence of peak periods is observed, with higher values occurring between T_p = 5s and T_p = 10s. In order to assess how heading waves influence OMSI, a similar plot is found in Figure 5.14b, with the difference that each heading has its own weight i.e probability of occurrence. SHIP1 operates on the Operating Scenario 1, where head seas are more likely to occur than beam seas. Comparing the two tables is seen that the OMSI is increased around T_p = 10s, while near T_p = 5s OMSI is greatly reduced. Therefore, it confirms the influence of headings in the results of OMSI. This serves to show how one heading, one sea state or one location are not enough to assess the comfort of a passenger ship. That is because different locations respond differently and what is an improvement in some conditions, may be unfavorable to others. This case is in agreement with the conclusions obtained by Scamardella and Piscopo in [41]. Therefore, the OMSI index for different sea sates and heading and respective probability of occurrence is a suitable parameter to be minimized in the particular case of a passenger ship.

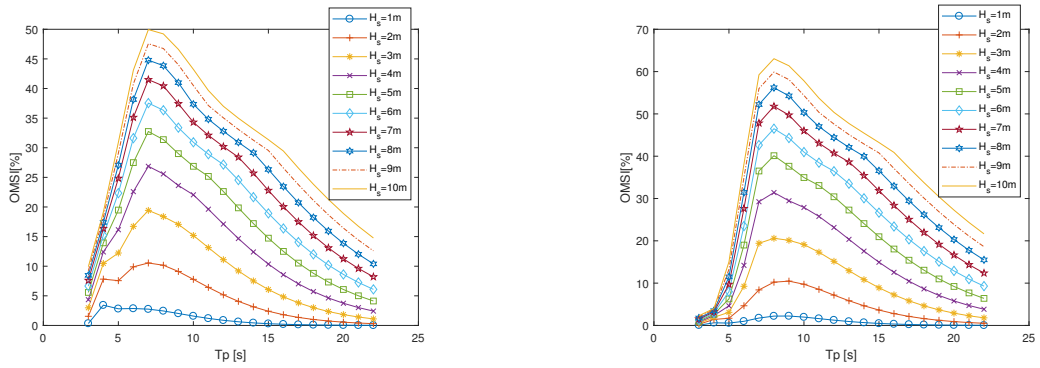

(a) Same headings probability

(b) Different headings probability

Figure 5.14: OMSI distribution at different sea states [SHIP2].

Similar conclusions regarding the points distribution along deck, together with the influence of the peak period and ship headings, can be taken for SHIP2. However, it is worth noticing that the calculations of OMSI, only consider a small distribution of points located on the aft part of the ship, as shown on Figure 5.15. Here it is clear that MSI/MSI_{max} ratio is still larger on the aft part of the ship for head and bow seas. This ratio is still uniform along the length of the studied region in beam seas. The main difference to be expected is on the magnitude of the OMSI. The location in study is on one extremity, meaning that the small values at the midship won't balance the higher ones at the stern, when calculating OMSI. Therefore, considering point locations on only one of the ship's extremities, will increase the average value of MSI on the calculation of OMSI. The changes in operating scenario are also clear for SHIP2, where the values of OMSI are increased, see Figure 5.16. As shown before, when all headings have the same probability of occurrence the value of OMSI is different from when each heading has its own weight. This is clear when looking at Figure 5.16b, that used the probability of each heading from Operating Scenario 2 to calculate OMSI. Following seas have small values of MSI and have little contribute to OMSI, specially when comparing following seas to head and bow seas, that have large values of MSI and high probability of occurrence. But one key difference between the two operating scenarios is that Operating Scenario 2 has a more uniform distribution of its heading's probability. That is clear when comparing Figure 5.14 and 5.16 in the region of T_p = 5s. For SHIP2 the values of OMSI did not reduce abruptly like they did on SHIP1, meaning the final Overall Motions Sickness Index (OMSI), from Equation 3.42, will be larger on SHIP2 than on SHIP1.

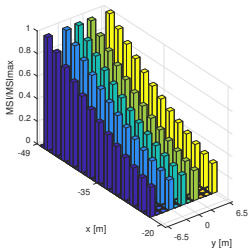

(a) Heading angle β = 180^o with MSI_{max} = 6.85 %

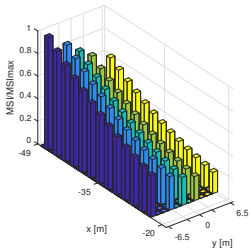

(b) Heading angle β = 120^o with MSI_{max} = 4.77 %

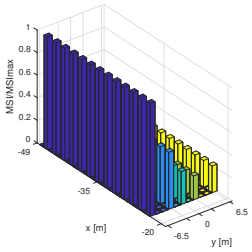

(c) Heading angle β = 90^o with MSI_{max} = 0.56 %

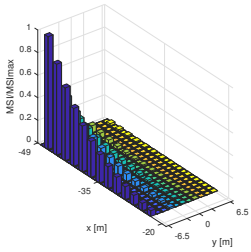

(d) Heading angle β = 60^o with MSI_{max} = 5.3E-06 %

Figure 5.15: MSI distributions along the deck for a T_p = 10 s [SHIP2].

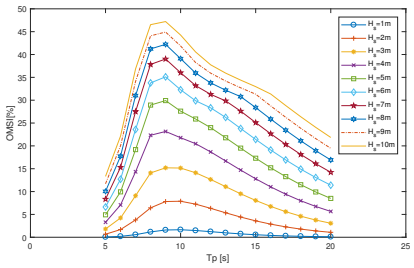

(a) Same headings probability

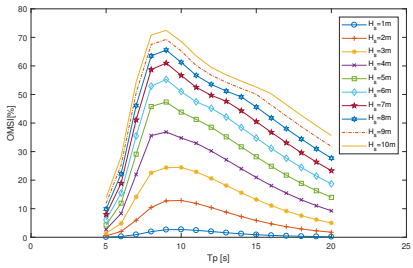

(b) Different headings probability

Figure 5.16: OMSI distribution at different sea states [SHIP2].

5.5 Summary

Throughout this chapter the characteristics of the two ships were presented. On both ships passenger's comfort is to be improved based on OMSI. On SHIP1 passenger's comfort is to be improved along the deck, while on SHIP2 only a strategic region of the aft part is considered. Two different operating scenarios were presented, each suited for the type of operation of each ship. Also, six types of hull transformations were presented. Based on previous researchers, these transformations are expected to influence the seakeeping characteristics of the ship and so the passenger's comfort. The discussion on how such transformations may affect the ship positively or negatively are presented on the following chapter. Finally, it was confirmed the influence of peak periods and heading angles on the MSI distribution along the deck. OMSI is therefore a suitable parameter to be minimized when studying comfort on passenger ships, since in one index the influence of multiple headings and sea-states is accounted based on their weight for the operation of the ship. This way the results are expected to be more accurate, than selecting only one sea-state or one heading.

Chapter 6

Overall Motions Sickness Index Analysis

Both passenger ships and operating scenarios have been introduced in the previous chapters, as well as the background required to perform a seakeeping analysis based on conform levels of passenger in a ship. This chapter is dedicated to present the results and conclusions obtained in this dissertation. It starts by comparing the comfort levels on each hull variation based on the OMSI. Such analysis is complemented by a comparison between hull variations regarding heave, roll and pitch RAOs. Absolute vertical accelerations on strategic points along the deck are are also compared to the parent hull. The ship resistance is studied for each hull variation, to understand how it is affected by each type of hull transformation. Finally, the operability index is assessed for the best solutions on each type of hull variation (**Set *n***).

6.1 Results from OMSI analysis

The Overall Motion Sickness Index (OMSI) is analysed for all types of hull variation, at their respective sea environment and for six different headings. The maximum service speed is considered, which for the passenger ship for river and coastal water in Algarve (SHIP1) is 16kn and for the ocean liner passenger ship to Madeira (SHIP2) is 21kn. Each OMSI is presented in the form of a table the same way the hull variations were presented back in Section 5.3.

6.1.1 OMSI results for hull variation based on SHIP1

Hull variations derived from changing the C_B and shifting the LCB position indicate that OMSI is reduced by both increasing C_B and moving LCB forward, as seen in Tables 6.1, 6.2 and 6.3. For SHIP1 the effect off shifting LCB is not as clear as of changing C_B. This can be explained by the type of points distribution along the deck, as shown Figure 5.3. Since they are equally distributed along the ship deck, any improvements on one extremity of the ship will degrade the others. Nevertheless, the method still gives an optimized solution, based on the configurations that have smaller MSI values overall. In this dissertation, an optimized solution is considered when the OMSI is reduced. Such results can in fact be different as they are dependent on the type of points distribution, as we will see further ahead. It is also important to notice that the improvements on OMSI are consistent in all three tables. That is, regardless of the method used to change C_B and LCB. Either using Set 1, Set 2 or Set 3, the OMSI was smaller on the highest C_B and lowest LCB. It is clear that in all three cases the increase of C_B at a constant C_M will

always benefit the OMSI.

The variations performed using a C_B = 0.76 together with a shift of LCB to the midship give the most comfortable hull. When C_B is transformed using the Set 1 for hull variations (variable displacement) the reduction of OMSI was in the order of 12.9% compared to the parent hull. Using Set 2 for hull variation (variable T do change the C_B) the reduction on OMSI was in the order of 17.7%, compared to the parent hull. On the Set 3 of hull variations (variable T and B_{WL}) the reduction on the OMSI was in the order of 12.4%. These results variations presented in Table 6.2 seem to consistently give slightly better results of OMSI. Such differences are explained by the fact that the B_{WL}/T is different for each new C_B and as seen further ahead, an increase in this ratio is beneficial for the OMSI. Nevertheless, the goal of using three different sets to change C_B and LCB was achieved. On one side the results were consistent on all three sets, showing that the results are not affected by how each coefficient was obtained. Still, it was possible to select a solution that least affected the original design of the hull. For SHIP1 it is better to only change the draft of the ship, instead of changing the displacement (Set 1) or even the beam and draft simultaneously (Set 3).

Table 6.1: Values of OMSI on each hull variation based on Set 1 [SHIP1].

	CB = 0.66	**CB = 0.68**	**CB = 0.70**	**CB = 0.71**	**CB = 0.72**	**CB=0.74**	**CB=0.76**
LCB = 50%	4.637	4.487	4.280	-	4.089	3.942	3.787
LCB = 52%	4.761	4.630	4.438	**4.349**	4.228	4.048	3.854
LCB = 54%	4.869	4.758	4.511	-	4.032	4.078	3.863

Table 6.2: Values of OMSI on each hull variation based on Set 2 [SHIP1].

	CB = 0.66	**CB = 0.68**	**CB = 0.70**	**CB = 0.71**	**CB = 0.72**	**CB=0.74**	**CB=0.76**
LCB = 50%	4.727	4.538	4.383	-	4.102	3.862	3.581
LCB = 52%	4.855	4.612	4.489	**4.349**	4.386	4.018	3.652
LCB = 54%	4.985	4.662	4.535	-	4.281	3.987	3.725

Table 6.3: Values of OMSI on each hull variation based on Set 3 [SHIP1].

	CB = 0.66	**CB = 0.68**	**CB = 0.70**	**CB = 0.71**	**CB = 0.72**	**CB=0.74**	**CB=0.76**
LCB = 50%	4.728	4.055	4.261	-	4.101	3.975	3.808
LCB = 52%	4.870	4.294	4.483	**4.349**	4.254	4.051	3.863
LCB = 54%	4.818	4.367	4.572	-	4.365	4.158	3.900

The form variations obtained by reducing C_M (Set 4) are beneficial to the OMSI. As shown in Table 6.4, such reductions consistently give smaller values of the OMSI. The smallest of all is for a C_M = 0.95, where OMSI is reduced by 7.2% compared to the parent hull. These reductions may not seem as significant but it is worth noticing that a C_M = 0.95 is less than 5% difference compared to C_M = 0.99. This is an interesting result, because the seakeeping is improved without no major changes in the hull.

The first geometrical variation in study is Set 5 the variation of L_{WL}. Based on Table 6.5, the increase in L_{WL} clearly reduces the OMSI. In particular an increase by 10% reduced the OMSI by 28.5% compared to the parent hull. That is the lowest OMSI from all the transformations performed to SHIP1.

Table 6.4: Values of OMSI on each hull variation based on Set 4 [SHIP1].

	CM = 0.99	**CM = 0.98**	**CM = 0.97**	**CM = 0.96**	**CM = 0.95**
LCB = 52%	**4.349**	4.213	4.147	4.157	4.038

Table 6.5: Values of OMSI on each hull variation based on Set 5 [SHIP1].

	L_{WL}= 90 %	**L_{WL} = 95%**	**L_{WL} = 100%**	**L_{WL} = 105%**	**L_{WL} = 110%**
LCB = 52%	5.378	4.836	**4.349**	3.808	3.109

Finally, the results for the second type of geometrical variation or Set 6 were obtained. Increasing the B_{WL}/T ratio reduced the OMSI, as shown in Table 6.6. This change in ratio already seemed to give the advantage to the transformations of C_B by only changing T, as shown on Table 6.2. The increase in ratio by 25% reduced the OMSI by 8.2%, which is not as significant as changes in L_{WL}.

Table 6.6: Values of OMSI on each hull variation based on Set 6 [SHIP1].

	B_{WL}/T = 75%	**B_{WL}/T = 85%**	**B_{WL}/T = 100%**	**B_{WL}/T = 115%**	**B_{WL}/T = 125%**
LCB = 52%	4.553	4.440	**4.349**	4.042	3.992

6.1.2 OMSI results for hull variation based on SHIP2

The OMSI of different hull variations was also studied on SHIP2. This is a different ship but still with the same type of hull transformations, namely: Set 2, Set 4, Set 5 and Set 6. By using another ship with the same type of transformations the performance of OMSI from different ships, sea-state conditions and locations can be studied. It is noticed that the results of OMSI for SHIP2 are much higher than for SHIP1. Now the parent hull [SHIP2] has an OMSI = 16.106. This value is considerably higher than an OMSI = 4.349 from SHIP1. This can be explained by the harsher sea conditions and by the smaller area on the aft part, where points are distributed.

For SHIP2 only Set 2 was used to perform hull variations of C_B and LCB. According to Table 6.7, increasing C_B also contributed to reduce the OMSI. In fact, the OMSI is reduced by 17.6% when comparing the parent hull with the hull variation with the lowest OMSI, as expected from the previous results. On the other hand, the best hull variation is now the one where LCB = 56%, which is the one further away from the midship. That is a predictable result, that shows how reducing the distance between the area where comfort is to be improved and the center of buoyancy is clearly a valid way of reducing the OMSI, on a certain location. However, it should be noticed that the opposite is also true and some areas of the ship will be degraded by such actions.

Table 6.7: Values of OMSI on each hull variation based on Set 2 [SHIP2].

	CB = 0.50	**CB = 0.53**	**CB = 0.56**	**CB=0.58**	**CB=0.60**
LCB = 50%	18.137	17.987	-	16.915	15.552
LCB = 53%	16.588	16.332	**16.106**	15.025	15.098
LCB = 56%	15.938	15.739	-	14.678	13.267

Reductions of C_M once again proved to be effective on reducing OMSI, as shown in Table 6.8. With a reduction of 14.5% from the parent hull. Yet the increase of C_M also improved the OMSI, which is not

to be expected. A possible reason for these unexpected results may be due to the distortions on the hull, particularly on the bulb as refereed on subsection 5.3.2. This distortion improved OMSI in the order of 9.4%. However, the validity of such transformation can not be confirmed, since the distortions on the bulb may also influence the results.

Table 6.8: Values of OMSI on each hull variation based on Set 4 [SHIP2].

	CM = 0.79	**CM = 0.83**	**CM = 0.87**	**CM = 0.92**	**CM = 0.96**
LCB = 53%	13.775	15.654	**16.106**	14.756	14.591

More in line with previous results are the geometrical hull variations. As seen in Table 6.9 the increase in L_{WL} reduced once again the OMSI. This reduction was in the order of 9.2% compared to the parent hull. The increase in ratio B_{WL}/T also proved beneficial to reduce the OMSI, as shown on Table 6.10. Such reduction was 10.4% less compared to the parent hull. The two types of geometrical variations obtained similar values of OMSI on SHIP2, while for SHIP1 the increase in L_{WL} was clearly a better alternative than increasing B_{WL}/T. This shows that each variation does not influence every ship/hull exactly the same way. The best alternatives depend on the type of ship, their operating scenario and the significant type of headings. An optimization is then affected by both the types of hull, the method used, together with sea environments and locations to be improved.

Table 6.9: Values of OMSI on each hull variation based on Set 5 [SHIP2].

	L_{WL}= 90 %	**L_{WL} = 95%**	**L_{WL} = 100%**	**L_{WL} = 105%**	**L_{WL} = 110%**
LCB = 53%	16.553	16.569	**16.106**	14.892	14.625

Table 6.10: Values of OMSI on each hull variation based on Set 6 [SHIP2].

	B_{WL}/T = 75%	**B_{WL}/T = 85%**	**B_{WL}/T = 100%**	**B_{WL}/T = 115%**	**B_{WL}/T = 125%**
LCB = 53%	18.122	16.802	**16.106**	14.369	14.435

6.2 Comparison between heave, roll and pitch motions

In the following section, the analysis of heave, pitch and roll motions of some significant hull variations at four different headings (180º, 120º, 90º and 60º) is presented. This will help to understand how each hull variation contributes for the reduction of OMSI. This section also serves to show that much more information needs to be processed when comparing the plots of ship motions, instead of using an index like OMSI.

6.2.1 Comparison of ship motions between parent and derived hull [SHIP1]

The first comparison is between the parent hull from SHIP1 and three hull variations, all with the same C_B = 0.76 and different LCBs of 50%, 52% and 54%. Figures 6.1 - 6.3 are representative plots of heave, roll and pitch RAO divided by the wave frequency for the type of transformations using C_B and LCB. The data in these figures is referent to hull transformations based on Set 2. Similar plots can be found on Appendix A for the other two alternatives, Set 1 and Set 3. These were not included directly in

the main text, because they present the exact same type of information and would interfere with space constrains.

Figure 6.1 compares heave RAO divided by wave amplitude as function of the wave frequency at four different headings. Here it is clear that increasing C_B reduced heave RAO in all types of heading, which is in accordance with Kukner and Sariöz [28]. The influence of LCB on heave RAO is small or even negligible.The Roll RAO is also improved with an increase in C_B, as shown in Figure 6.2. In head waves or β=180º the roll RAO is zero as expected and no differences are to be accounted. On the other hand for a β= 120º and β= 90º the peaks are reduced on the hulls with C_B=0.76, as shown on Figures 6.2b and 6.2c respectively. For β= 60º the roll RAO shown in Figure 6.2d has no major changes from increasing the C_B. The effect of LCB on roll RAO is not clear but looking at these results it seems to have no influence on roll RAO.

Finally, the pitch RAO for the same four headings and hull variations is shown in Figure 6.3. The reductions in pitch RAO are very subtle compared to heave and roll. Any reduction will be due to LCB variations and not from any increase in C_B, like in the other two. Those reductions are clearer for beam seas, as shown in Figure 6.3c, but it should be noticed that the magnitude of pitch RAO is very small or even neglectable on these type of headings. Variations in pitch are clearer for SHIP2 and any conclusion should be confirmed further ahead. From this analysis it is possible to understand why OMSI reduced on these hull variations. The reduction in heave and pitch motion also reduce MSI and therefore OMSI. It also shows that using this method to compare the seakeeping characteristics of a ship hull is a much harder process compared to using the index OMSI, since the differences in peak RAOs are sometimes very subtle.

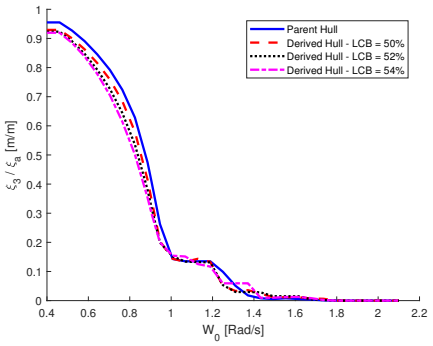

(a) β = 180º

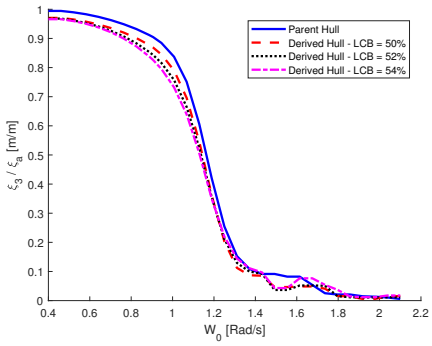

(b) β = 120º

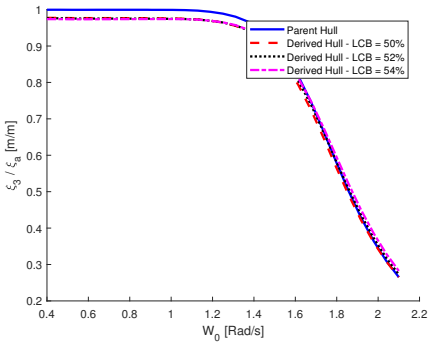

(c) β = 90º

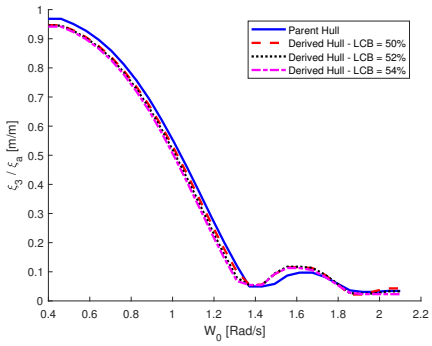

(d) β = 60º

Figure 6.1: Heave RAOs. Parent Ship: SHIP1 with C_B = 0.71. Derived Hulls: Set 2 with C_B = 0.76.

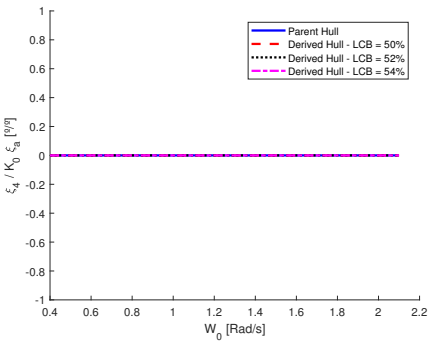

(a) β = 180º

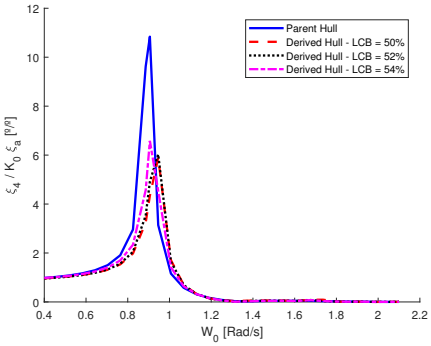

(b) β = 120º

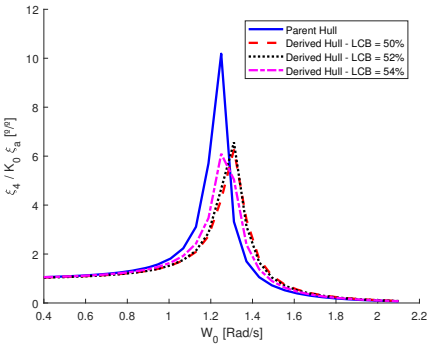

(c) β = 90º

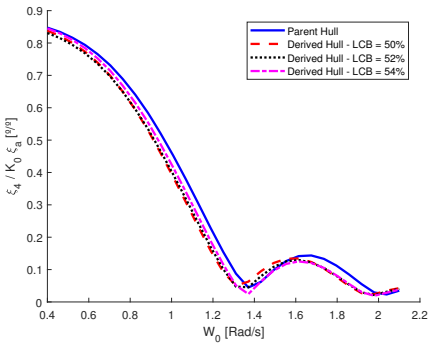

(d) β = 60º

Figure 6.2: Roll RAOs. Parent Ship: SHIP1 with C_B = 0.71. Derived Hulls: Set 2 with C_B = 0.76.

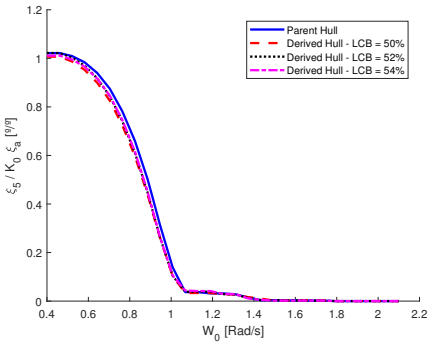

(a) β = 180º

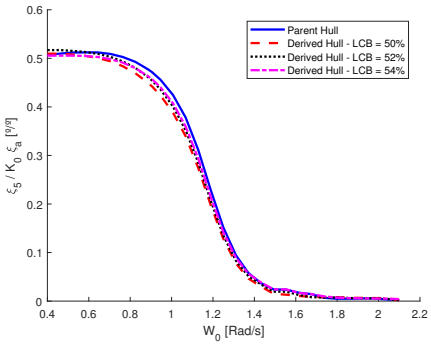

(b) β = 120º

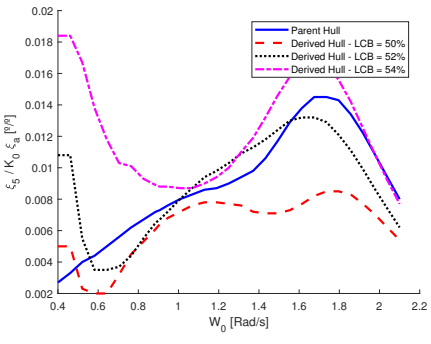

(c) β = 90º

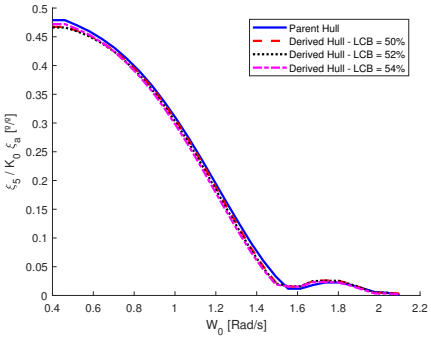

(d) β = 60º

Figure 6.3: Pitch RAOs. Parent Ship: SHIP1 with C_B = 0.71. Derived Hulls: Set 2 with C_B = 0.76.

The ship motions for hull variations based on Set 4, are presented in Figures 6.4-6.6. The parent hull (SHIP1) with a C_M = 0.99 was compared to two other hull variations. One with C_M = 0.97 and the other with C_M = 0.95. Figure 6.4 gives the comparison between heave RAO divided by wave amplitude as function of the wave frequency. The reductions in C_M do not seem to influence the heave motions. Roll motions on the other hand are influenced by the variation of C_M. The peak of roll RAO reduces with C_M for headings of β= 120^o and β= 90^o, as seen in Figures 6.5b and 6.5c respectively. For β= 60^o these differences do not occur, as confirmed by Figure 6.5d. Pitch motions are not affected by C_M for either of the four headings. Therefore, the differences in ship motions for this type of variation are very difficult to assess, since both hulls are still very similar. It is still relevant to notice how these combinations with similar RAO also presented smaller differences in OMSI. Again, it proves the inequity of comparing ship hulls by its RAOs.

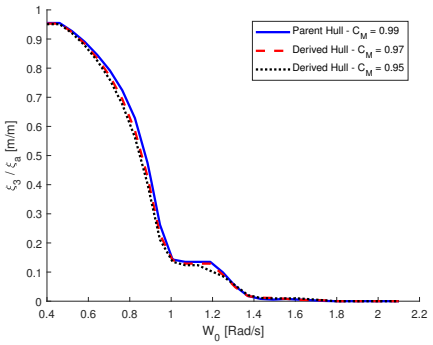

(a) β = 180^o

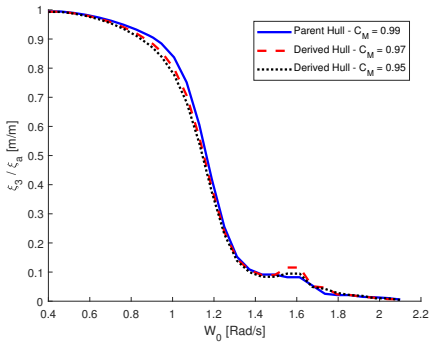

(b) β = 120^o

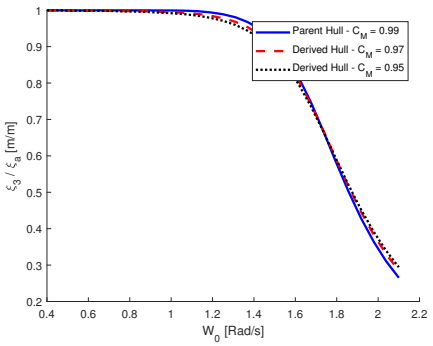

(c) β = 90^o

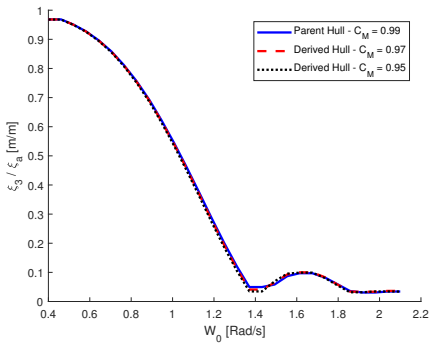

(d) β = 60^o

Figure 6.4: Heave RAOs. Parent Ship: SHIP1. Derived Hulls: Set 4.

In order to show the influence of the variations of L_{WL} on the ship motions, the results of the parent hull were compared with the values from two transformations based on Set 5. Namely,the results on the hull with L_{WL} = 90% and L_{WL} = 110% are compared to the one from the parent hull (SHIP1).

Figure 6.7 compares the heave RAO divided by wave amplitude as function of the wave frequency. Here it is clear that increasing L_{WL} contributes for reducing heave motions,while reducing L_{WL} increases heave motions. On the other hand, roll motions are as affected by variations in L_{WL}. As seen Figure 6.8, the increasing in L_{WL} did not change the roll peak. This peak is reduced with smaller values of L_{WL} instead. Regarding pitch motions the hull variations performed as expected. Based on Figure 6.9, pitch RAO was reduced when L_{WL} was increased and it was consistent for all heading waves. Like for heave motions the reductions in L_{WL}, also increase pitch RAO.

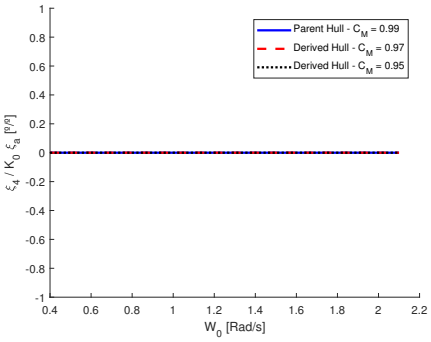

(a) β = 180º

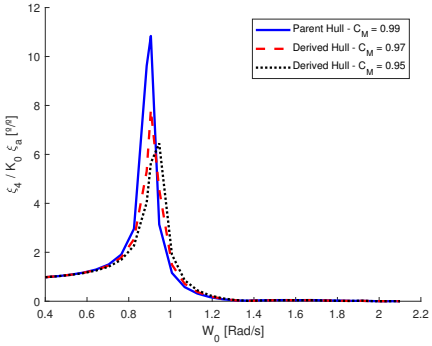

(b) β = 120º

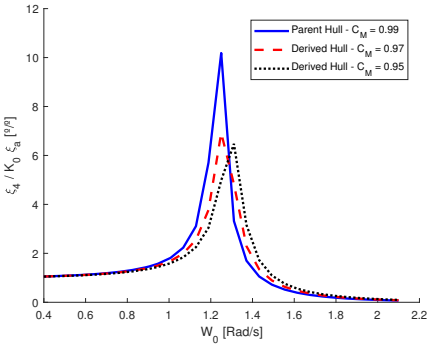

(c) β = 90º

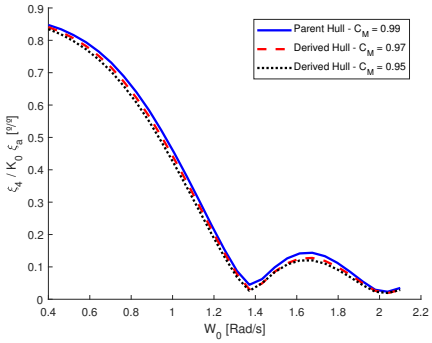

(d) β = 60º

Figure 6.5: Roll RAOs. Parent Ship: SHIP1. Derived Hulls: Set 4.

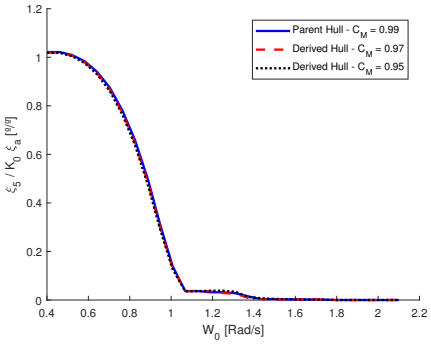

(a) β = 180º

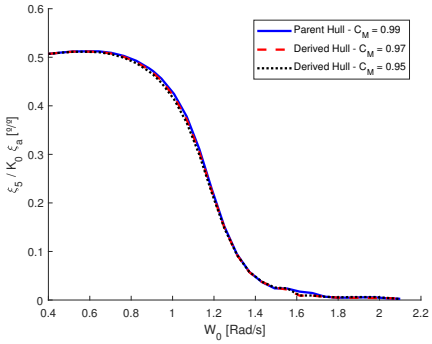

(b) β = 120º

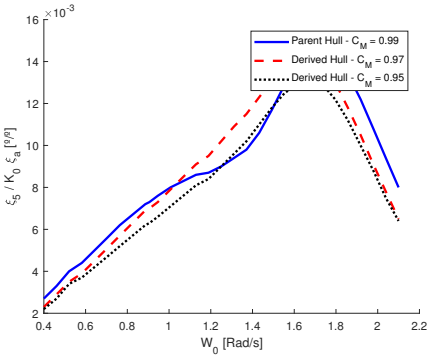

(c) β = 90º

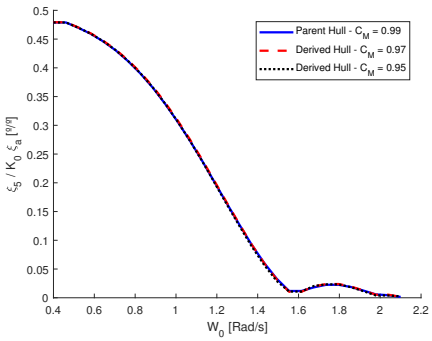

(d) β = 60º

Figure 6.6: Pitch RAOs. Parent Ship: SHIP1. Derived Hulls: Set 4.

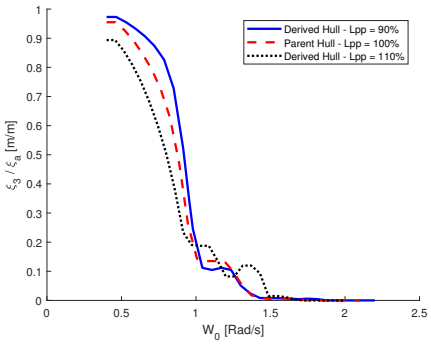

(a) β = 180°

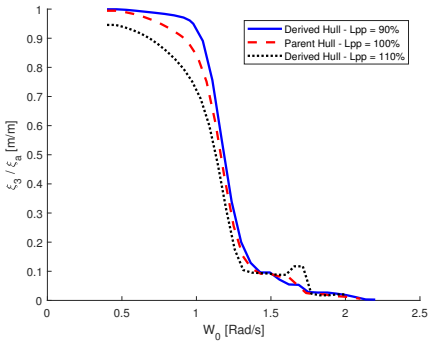

(b) β = 120°

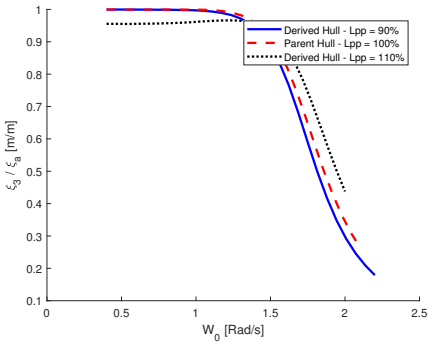

(c) β = 90°

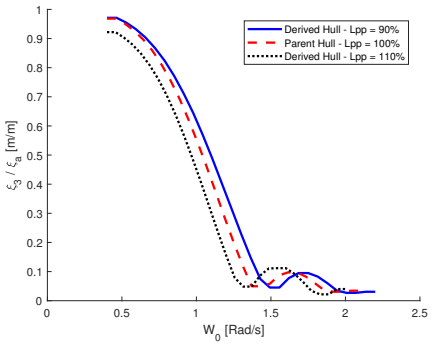

(d) β = 60°

Figure 6.7: Heave RAOs. Parent Ship: SHIP1. Derived Hulls: Set 5.

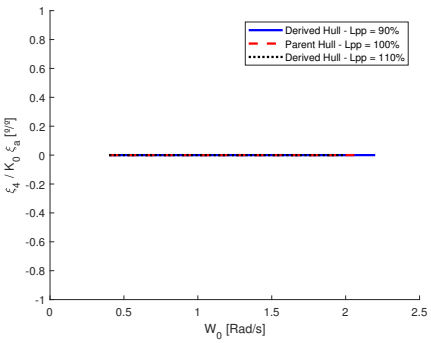

(a) β = 180°

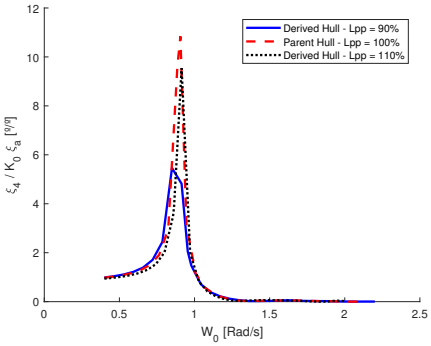

(b) β = 120°

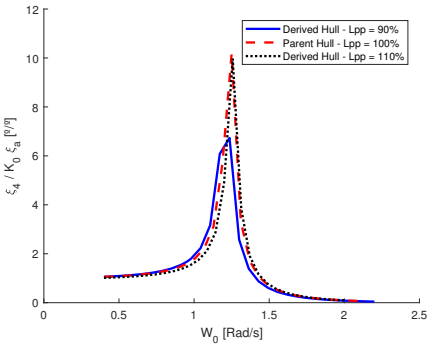

(c) β = 90°

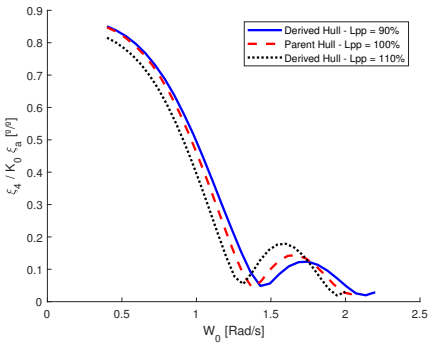

(d) β = 60°

Figure 6.8: Roll RAOs. Parent Ship: SHIP1. Derived Hulls: Set 5.

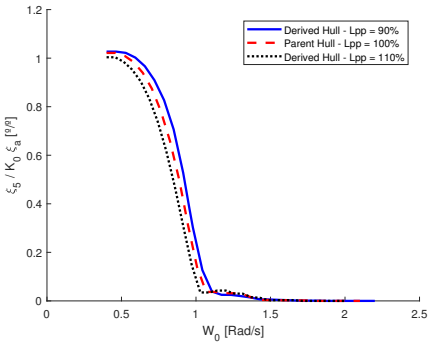

(a) β = 180º

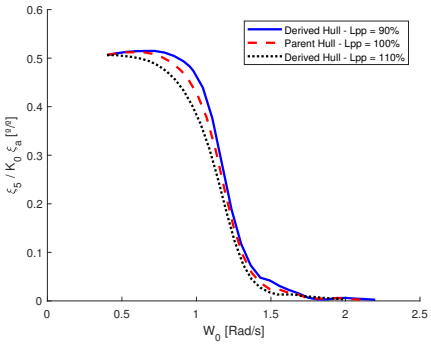

(b) β = 120º

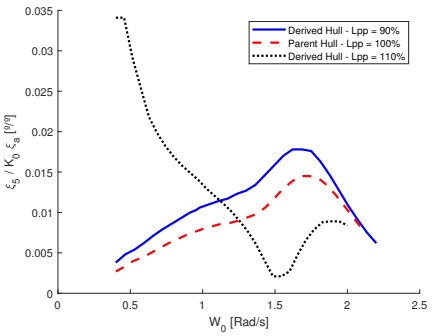

(c) β = 90º

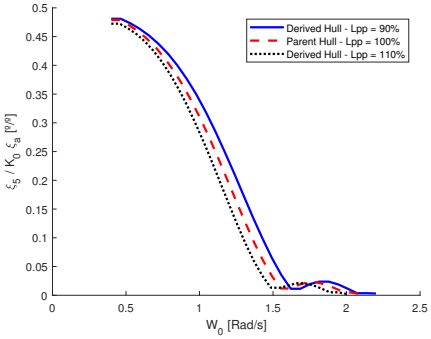

(d) β = 60º

Figure 6.9: Pitch RAOs. Parent Ship: SHIP1. Derived Hulls: Set 5.

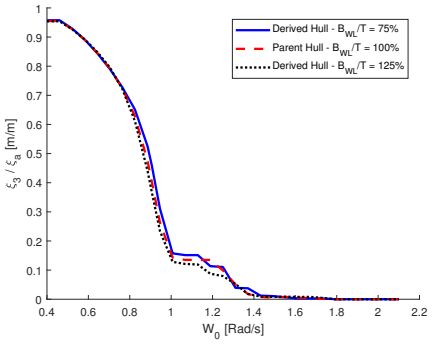

(a) β = 180º

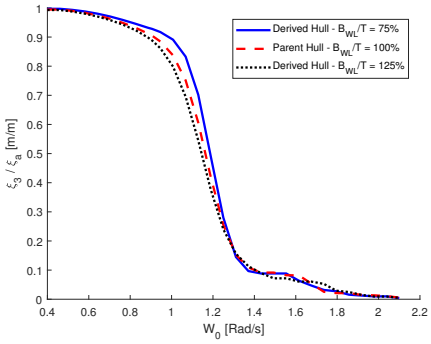

(b) β = 120º

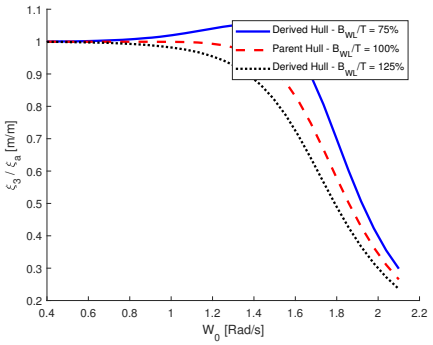

(c) β = 90º

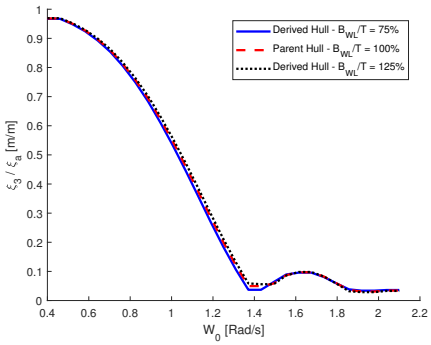

(d) β = 60º

Figure 6.10: Heave RAOs. Parent Ship: SHIP1. Derived Hulls: Set 6.

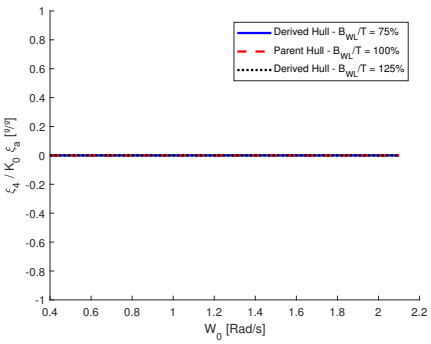

(a) β = 180º

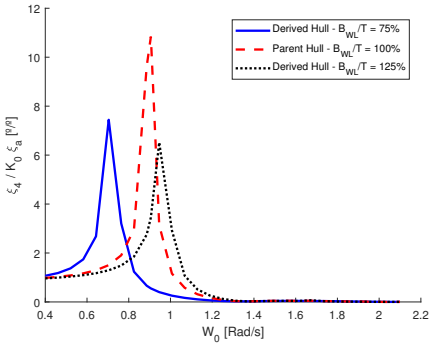

(b) β = 120º

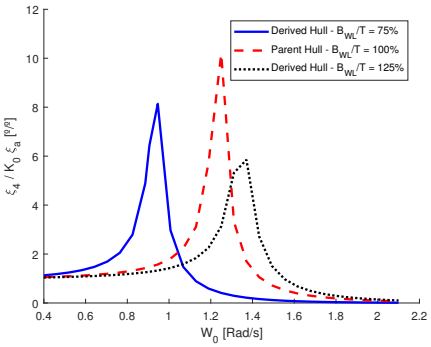

(c) β = 90º

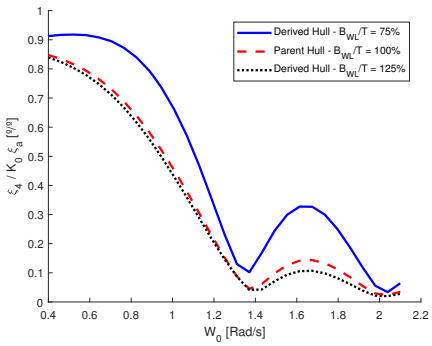

(d) β = 60º

Figure 6.11: Roll RAOs. Parent Ship: SHIP1. Derived Hulls: Set 6.

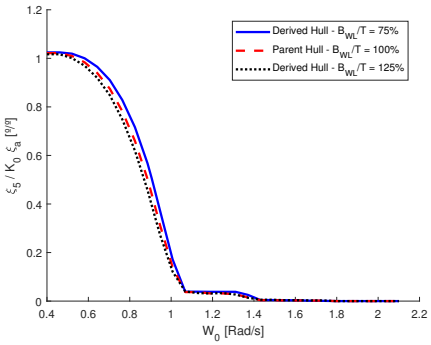

(a) β = 180º

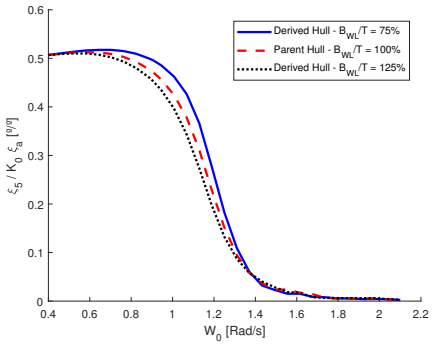

(b) β = 120º

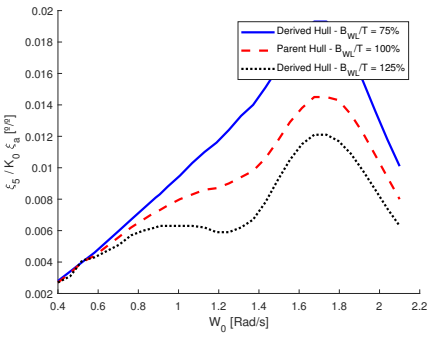

(c) β = 90º

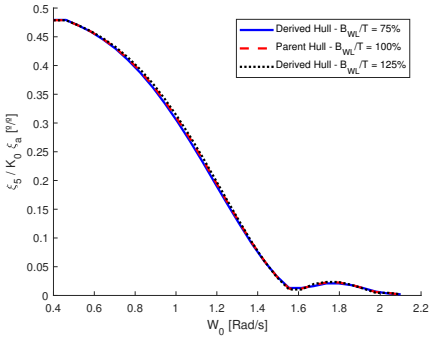

(d) β = 60º

Figure 6.12: Pitch RAOs. Parent Ship: SHIP1. Derived Hulls: Set 6.

On the second type of geometrical variations, Set 6 of hull variations where the ratio B_{WL}/T is both increases and reduced, the following conclusions relative to ship motions are obtained. As seen before the increase in ratio contributes for reducing OMSI. The increase by 25% in ratio obtained the best results and with a reduction by 25% the OMSI increased the most. For that reason, the motions of these two variations are compared. Starting by comparing heave motions, the ratio variation clearly influences the heave RAO on most wave headings, as shown in Figure 6.7, being most noticeable for beam seas. This heave RAO is reduced when the ratio is increased and the heave RAO is increased when the ratio is reduced, as shown in Figure 6.10c. That is exactly what has expected based on the results from OMSI. Roll motions presented in Figure 6.11 shifted to smaller wave frequencies for both β= 120º and β= 90º when B_{WL}/T ratio is reduced. For β= 60º roll RAO is increased at the same B_{WL}/T ratio reduction. The increase in B_{WL}/T ratio stayed relatively consistent with the parent hull (SHIP1). On the other hand, the effect of B_{WL}/T ratio is less clear on pitch motions. Only small reductions of pitch RAO, for β= 180º and β= 120º, are observed on transformations where B_{WL}/T ratio is being increased, as shown in Figure 6.12a and Figure 6.12b respectively. For following seas, shown in Figure 6.12d, the B_{WL}/T ratio has little or no influence on pitch motions. Nevertheless, the improvements in heading seas contribute the most for reducing OMSI, compared to following seas that statistically do not occur as much.

6.2.2 Comparison of ship motions between parent and derived hull [SHIP2]

A similar analysis regarding ship motions is made for SHIP2. The same transformations were performed on both ships and similar results are to be expected on their ship motions. For that reason and due to lack of space on the main text, the RAOs of heave, roll and pitch are added to Appendix A.2. Even though some conclusions are similar, the result obtained for SHIP2 have more significant differences between peaks of heave and pitch motions. Those will help to confirm some results presented for SHIP1.

The transformations using on C_B and LCB, based on Set 2 of hull variation, are discussed first. It was confirmed that heave and pitch motions are reduced by increasing C_B, being particularly significant in heading seas. Shifting LCB to the aft reduced heave motions for head and bow seas. Also, shifting LCB closer to the midship reduced pitch motions in head, bow and beam seas, but was unfavorable in following seas. Both transformations were less conclusive regarding roll motions. It was only noticeable that an LCB = 56% increased the peak roll for β= 120º and β= 90º.

Unlike for SHIP1, the transformations on C_M or Set 4, proved to have an influence on ship motions. In this particular hull the results of OMSI were unexpectedly reduced when C_M was increased. However, such results are strange, since the heave RAO is increased when C_M is increased. When C_M is reduced the peak is also reduced, as it was expected. The reduction of C_M also reduced the pitch RAOs, making these type of transformations much more effective on SHIP2 compared to SHIP1.

Changes on L_{WL}, Set 5 of hull variations, are now less noticeable on heave RAO. Nevertheless, increasing L_{WL} still reduced slightly the heave RAO. On roll motions the same changes show no influence, which was unexpected since for SHIP1, the influences of L_{WL} was quite clear. In terms of pitch motions the changes in L_{WL} behaved the same as before, where increasing L_{WL} reduced pitch RAOS regardless the type of heading.

Changes in B_{WL}/T ratio, Set 6 of hull variation, proved to be more efficient on SHIP2 and it is clear when looking at its motions. The influence of B_{WL}/T ratio was easily distinguished and a higher ratio

definitely gave a smaller peak in heave. Also, the roll motions were clearer and an increase by 25% in B_{WL}/T greatly reduced the roll peaks for β= 120º and β= 90º. Increasing B_{WL}/T also shifts the peak to smaller wave frequencies, while reducing it shifts the peaks to higher wave frequencies. As in previous cases pitch motions were smaller for bigger B_{WL}/T ratios and bigger for smaller B_{WL}/T ratios.

6.3 Absolute vertical accelerations

Absolute vertical accelerations responses as function of encounter frequency are compared in this section. Since so many sea-states, headings and deck locations were used it would be impractical to compare every single one of them. For that reason a sea-state with $H_{1/3}$ = 1 m and T_P = 9 s was selected for comparison and the same headings used to compare RAOs were used to compare absolute vertical accelerations. Different points were selected to be studied on both ships and their locations are found on Table 6.11 and Table 6.12.

Table 6.11: Remote location points on SHIP1.

Description	**Units**	**1**	**2**	**3**	**4**	**5**	**6**
Longitudinal Position (+ fwd MS)	m	29	0	-35	29	0	-35
Offset from center line	m	0	0	0	-5	-5	-5

Table 6.12: Remote location points on SHIP2.

Description	**Units**	**1**	**2**	**3**
Longitudinal Position (+ fwd MS)	m	-36	-36	-36
Offset from center line	m	-6	0	6

6.3.1 Comparison of absolute vertical accelerations between hull variations and SHIP1.

Like in the previous section only one of methods to change C_B and LCB was selected to be compared (Set 2), since vertical acceleration performed the same way regardless how C_B was derived. Figure 6.13 and 6.14 compare absolute vertical accelerations as function of encounter frequency on SHIP1 at the points 1, 2, 3 and 4, 5, 6 respectively. The optimum hull used for comparison has a C_B = 0.76 and LCB = 50%. Absolute vertical accelerations are reduced in a configuration where OMSI is smaller. On head waves these vertical accelerations are consistently smaller regardless the longitudinal and horizontal location, as confirmed by Figures 6.13a and 6.14a. The same is true for points on the center line for the other three type of headings. However, for this particular sea-state, on offset points from the center line, the absolute vertical accelerations are actually increased as exemplified on Figure 6.14b and 6.14c. It means that this type of hull variation will not improve comfort on all locations equally, regardless the type of heading or sea state. It shows why considering multiple locations, sea states and headings to ultimately improve comfort is perhaps more beneficial than choosing just one set of conditions.

Changing C_B and LCB influenced the peak of absolute vertical accelerations, the same happens when changing C_M. On SHIP1 the OMSI on a parent hull with a C_M = 0.99 was reduced with a reduction to C_M = 0.95, which in itself corresponds to a small variation. Therefore, any comparisons of absolute vertical accelerations between the two hull are expected to have subtle differences too. Regarding the

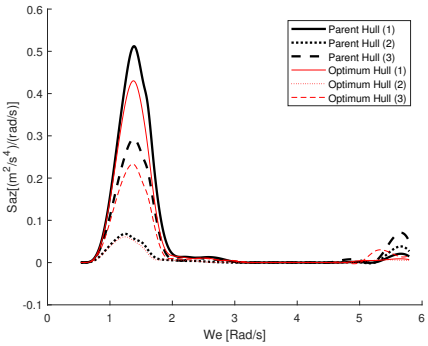

(a) β = 180°

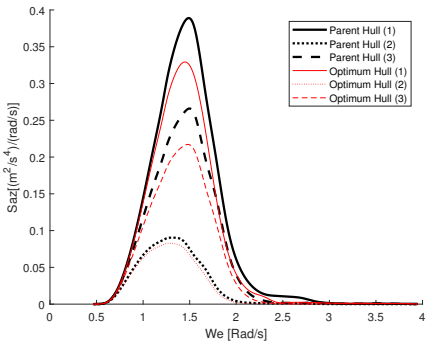

(b) β = 120°

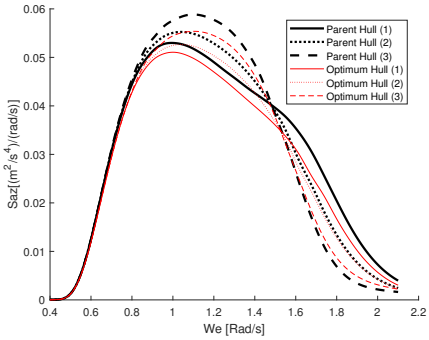

(c) β = 90°

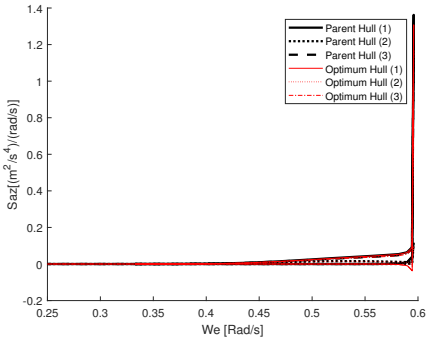

(d) β = 60°

Figure 6.13: Absolute vertical acceleration. Parent hull: SHIP1 (C_B = 0.71, LCB = 52%) Optimum hull: Set2 (C_B = 0.76, LCB = 50%) , at points 1, 2 and 3.

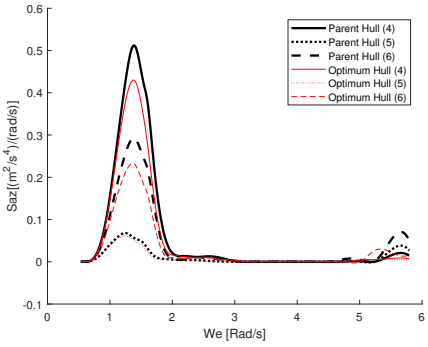

(a) β = 180°

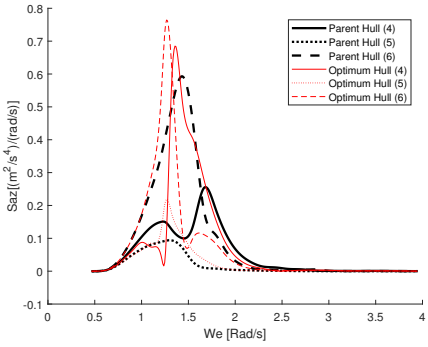

(b) β = 120°

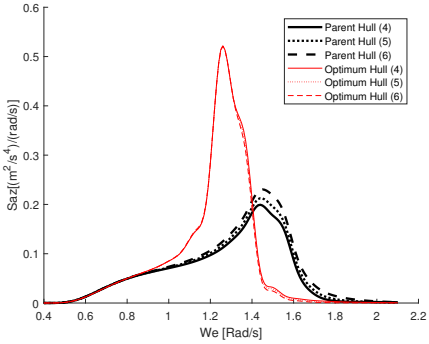

(c) β = 90°

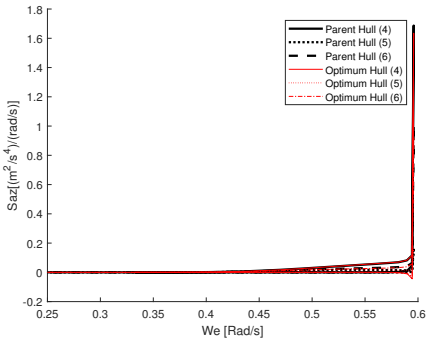

(d) β = 60°

Figure 6.14: Absolute vertical acceleration. Parent hull: SHIP1 (C_B = 0.71, LCB = 52%) Optimum hull: Set2 (C_B = 0.76, LCB = 50%) , at points 4, 5 and 6.

points on the center line, shown in Figure 6.15 for β= 180º and β= 120º, it is seen that the points located in the forward position reduce the peak of absolute vertical accelerations unlike points on the aft that actually increase it. If these accelerations had the same magnitude on both locations, the variation on C_M could be seen as unnecessary. However, since the locations with higher accelerations are actually being reduced, it is a positive result. Also, the points located offset from the center line, shown in Figure 6.16, have their absolute vertical accelerations improved, in particular for beam seas as shown in Figure 6.16c. This confirms the results obtained from OMSI.

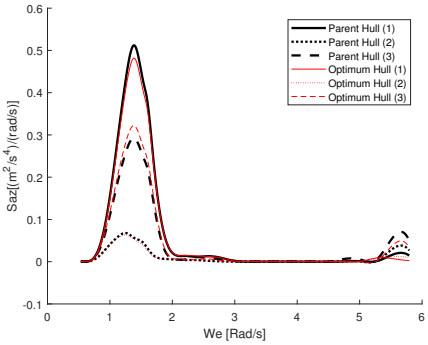

(a) β = 180º

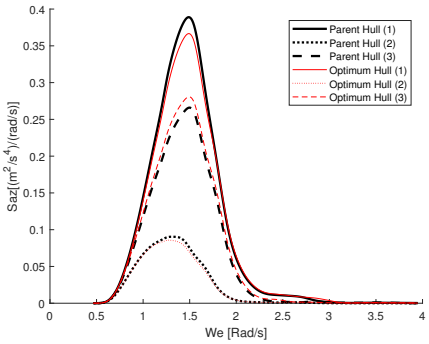

(b) β = 120º

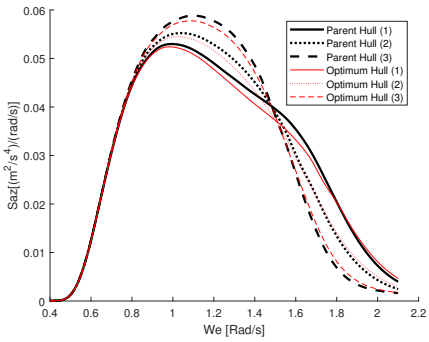

(c) β = 90º

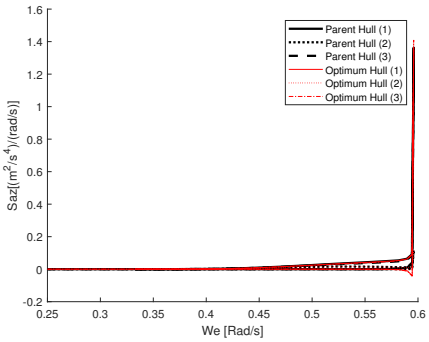

(d) β = 60º

Figure 6.15: Absolute vertical acceleration. Parent hull: SHIP1 (C_M = 0.99, LCB = 52%) Optimum hull: Set 4 (C_M = 0.95, LCB = 52%) , at points 1, 2 and 3.

It was shown that increasing the length of a ship contributes to reduce the OMSI and the motions of a ship. That is also clear when looking at the comparison of absolute vertical accelerations between the parent hull and its hull variation with a 10% increase in L_{WL}. Looking at Figure 6.17 all points on the center line of the ship see their absolute vertical accelerations reduced, quite significantly along the length of the ship. This is also true for offset points for heading equal to β= 180º. For other headings these offset points have their vertical accelerations increase, as shown in Figure 6.18.

For this sea-state, the variations of B_{WL}/T ratio presented the same type of absolute vertical accelerations as the variations of length. However such differences between parent and optimum hull were not significant. Figure 6.19 shows that increasing the ratio B_{WL}/T reduced absolute vertical accelerations on all point along the center line regardless the heading. On the other hand, the offset points from the center line, shown in Figure 6.20, have their absolute vertical accelerations increase for β= 120º and β= 90º.

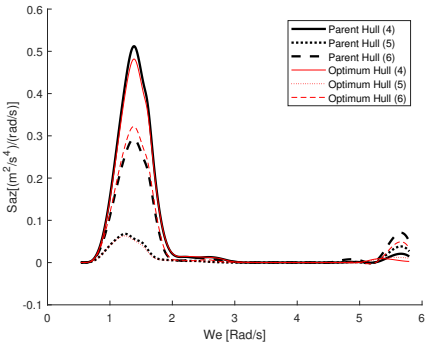

(a) β = 180°

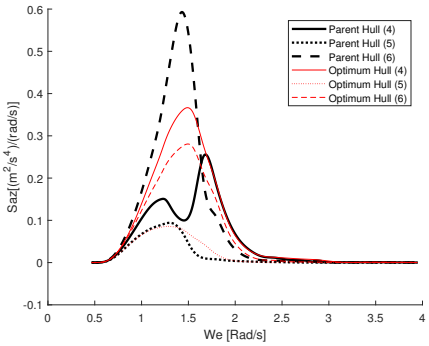

(b) β = 120°

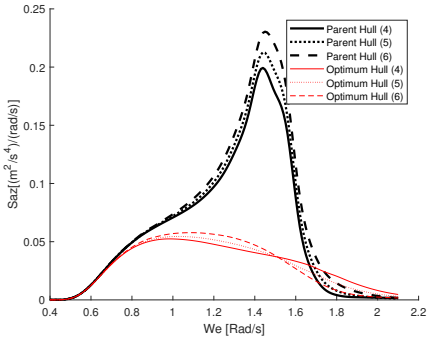

(c) β = 90°

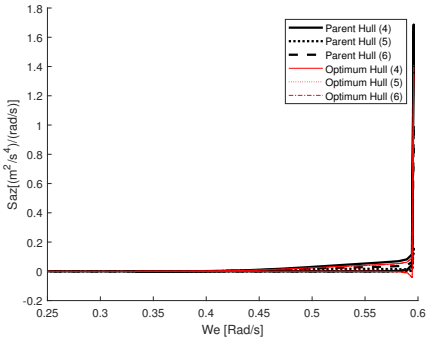

(d) β = 60°

Figure 6.16: Absolute vertical acceleration. Parent hull: SHIP1 (C_M = 0.99, LCB = 52%) Optimum hull: Set 4 (C_M = 0.95, LCB = 52%) , at points 4, 5 and 6.

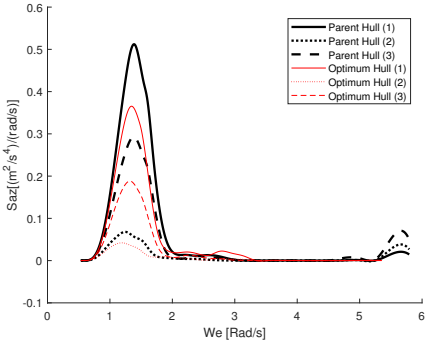

(a) β = 180°

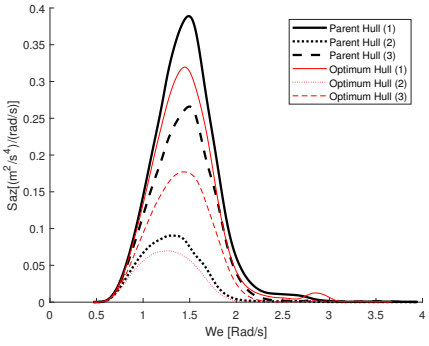

(b) β = 120°

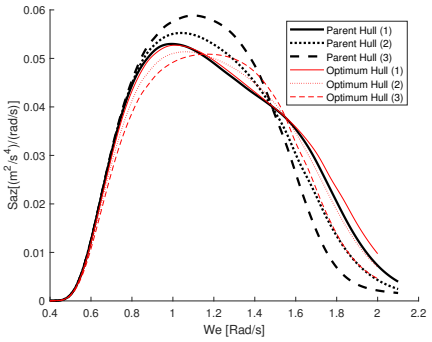

(c) β = 90°

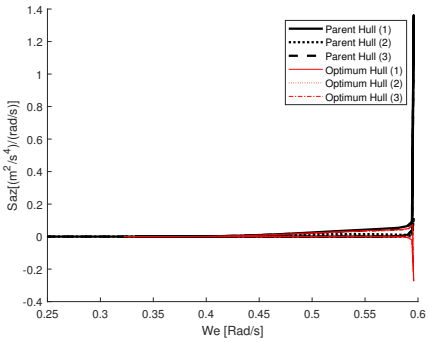

(d) β = 60°

Figure 6.17: Absolute vertical acceleration. Parent hull: SHIP1 (L_{WL} = 100%, LCB = 52%) Optimum hull: Set 5 (L_{WL} = 110%, LCB = 52%) , at points 1, 2 and 3.

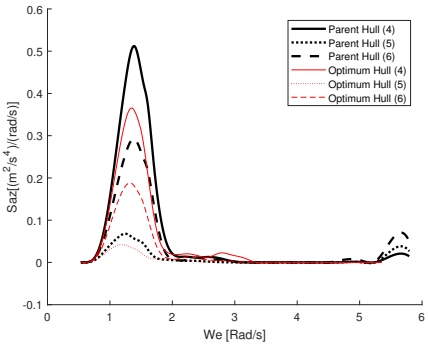

(a) β = 180°

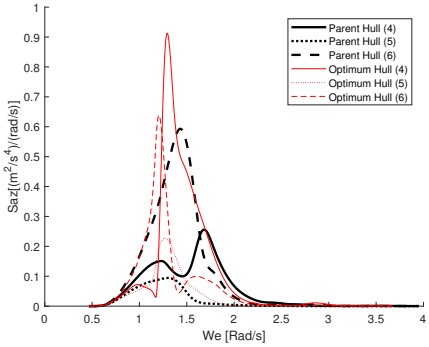

(b) β = 120°

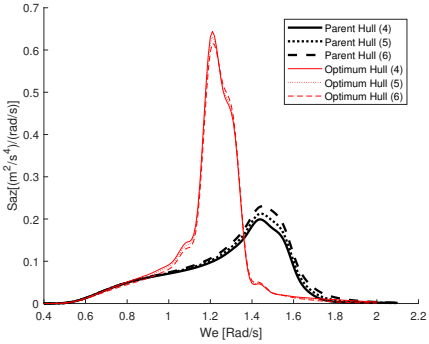

(c) β = 90°

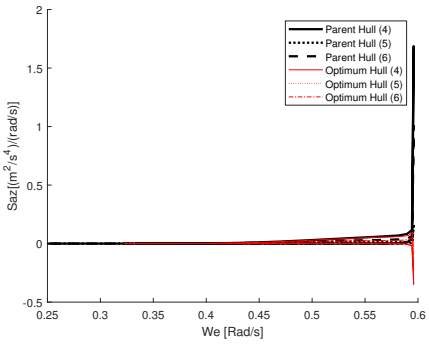

(d) β = 60°

Figure 6.18: Absolute vertical acceleration. Parent hull: SHIP1 (L_{WL} = 100%, LCB = 52%) Optimum hull: Set 5 (L_{WL} = 110%, LCB = 52%) , at points 4, 5 and 6.

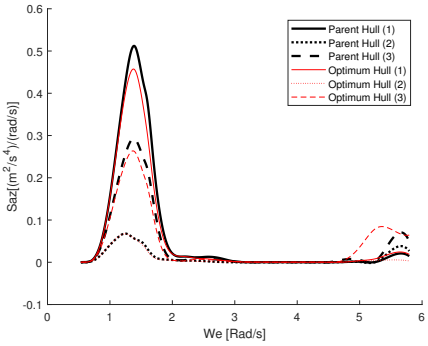

(a) β = 180°

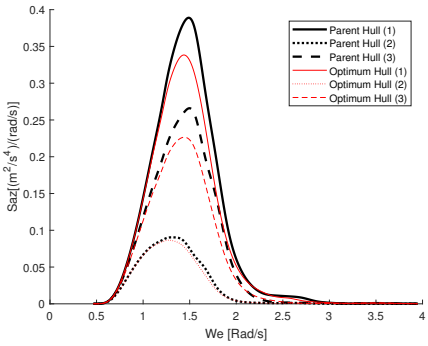

(b) β = 120°

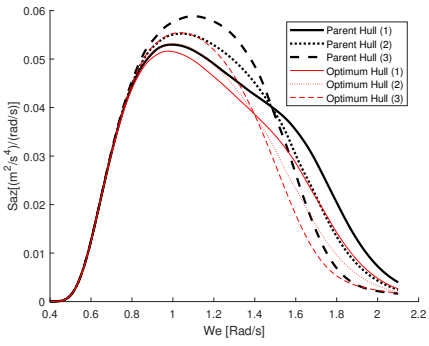

(c) β = 90°

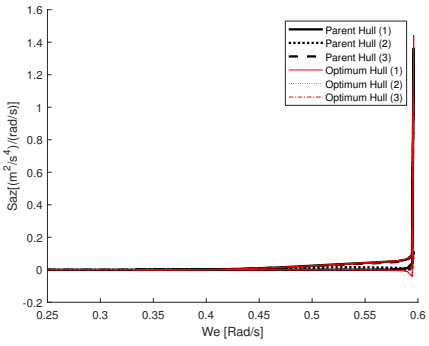

(d) β = 60°

Figure 6.19: Absolute vertical acceleration. Parent hull: SHIP1 (B_{WL}/T = 100%, LCB = 52%) Optimum hull: Set 6 (B_{WL}/T = 125%, LCB = 52%) , at points 1, 2 and 3.

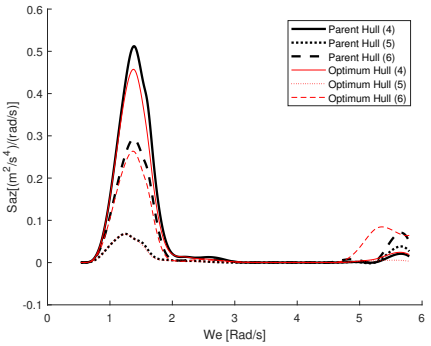

(a) β = 180º

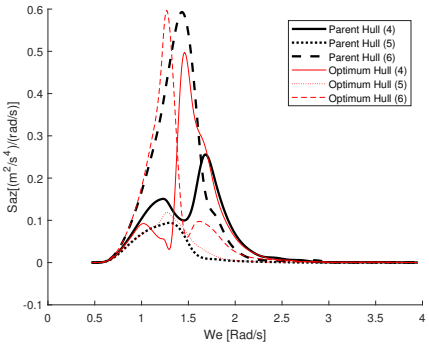

(b) β = 120º

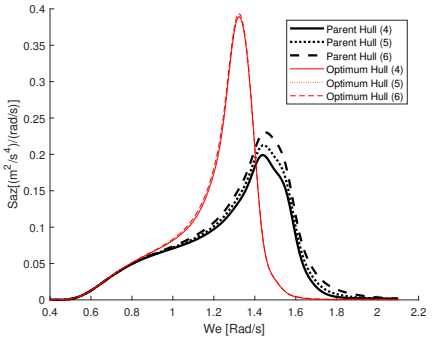

(c) β = 90º

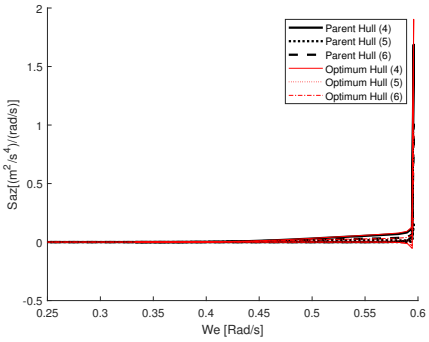

(d) β = 60º

Figure 6.20: Absolute vertical acceleration. Parent hull: SHIP1 (B_{WL}/T = 100%, LCB = 52%) Optimum hull: Set 6 (B_{WL}/T = 125%, LCB = 52%) , at points 4, 5 and 6.

6.3.2 Comparison of absolute vertical accelerations between hull variations and SHIP2.

On SHIP2 comfort is to be improved in a region on the aft part of the ship. For that reason, three points were selected to compare the absolute vertical accelerations. Such points can be found above, on Table 6.12. This will serve as complement to the analyse above, since the points are now distributed along the breath of the ship instead of the length.

Starting by looking at Figure 6.21, the first thing to notice is that the changes in C_B and LCB (Set 1 of hull variations) which gave the smallest OMSI and also reduced the absolute vertical accelerations for heading waves. However, it also increased the vertical accelerations on beam seas. Again, these transformations will not improve vertical accelerations and therefore comfort for all conditions. Mainly, because the method is focused on improving a most likely set of combinations that are to be expected.

Another point to take notice it that when comparing the absolute vertical accelerations at points along the breath, their magnitude is not the same. As previously seen on Section 5.4, with the exception of β= 180º of course. It is confirmed by Figure 6.21a, where only two lines seam to appear because at β= 180º all points behave the same way. For β= 120º and β= 90º the negative offset point tend to have higher absolute vertical accelerations compared to the positive ones, as show on Figures 6.21b and 6.21c respectively. This same exact pattern of absolute vertical accelerations is verified for the other type of hull variations, Set 4, Set 5 and Set 6, shown in Figures 6.22, 6.23 and 6.24 respectively. No other differences are verified, therefore no extra information can be taken from these other plots.

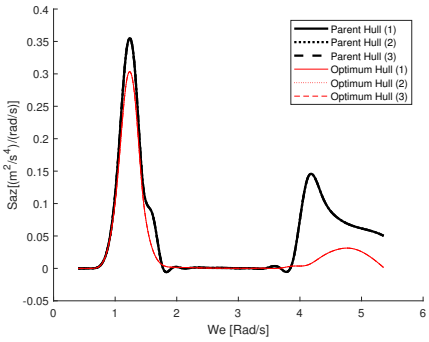

(a) β = 180°

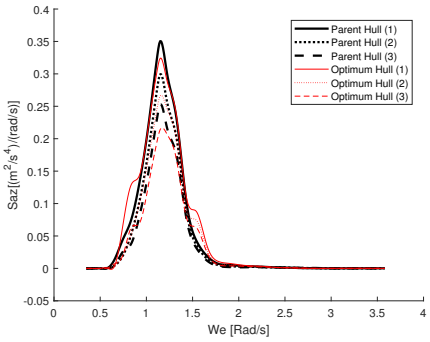

(b) β = 120°

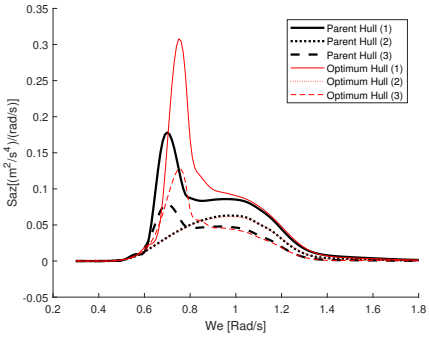

(c) β = 90°

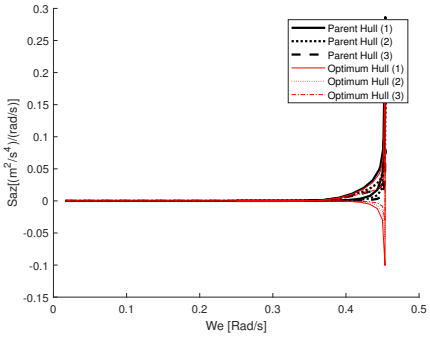

(d) β = 60°

Figure 6.21: Absolute vertical acceleration. Parent hull: SHIP2 (C_B = 0.56, LCB = 53%) Optimum hull: Set2 (C_B = 0.60, LCB = 56%), at points 1, 2 and 3.

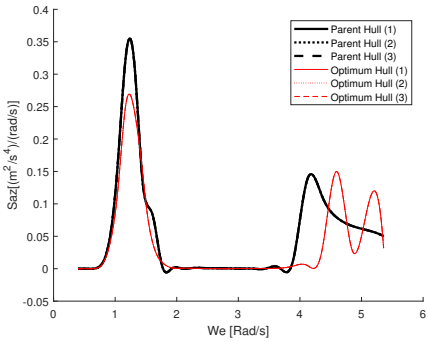

(a) β = 180°

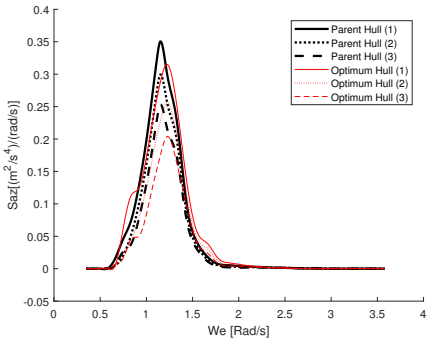

(b) β = 120°

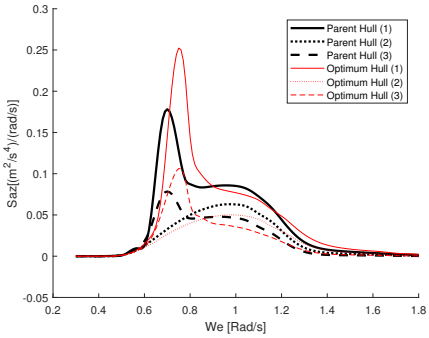

(c) β = 90°

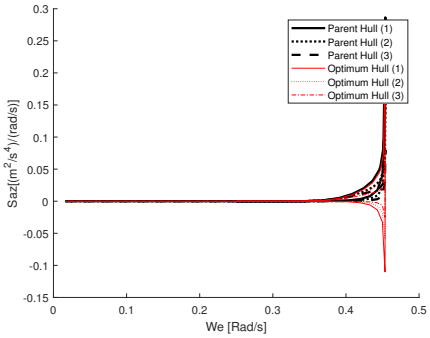

(d) β = 60°

Figure 6.22: Absolute vertical acceleration. Parent hull: SHIP2 (C_M = 0.87, LCB = 53%) Optimum hull: Set 4 (C_B = 0.87, LCB = 56%) , at points 1, 2 and 3.

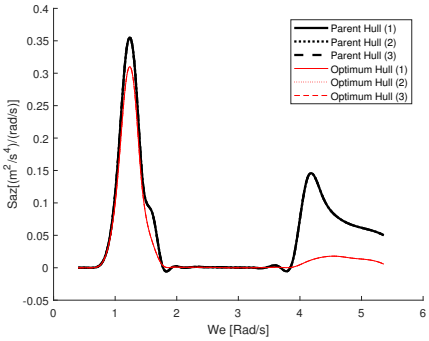

(a) β = 180°

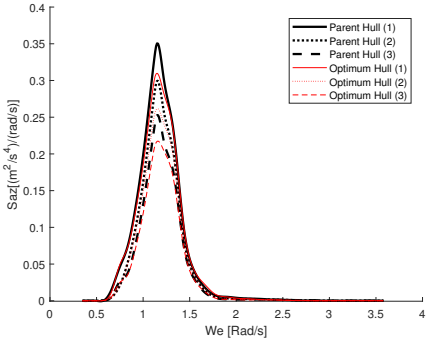

(b) β = 120°

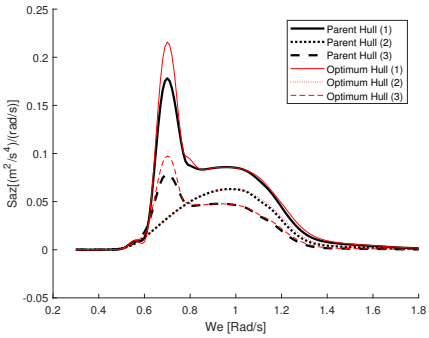

(c) β = 90°

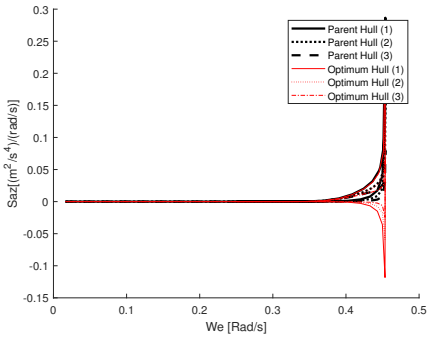

(d) β = 60°

Figure 6.23: Absolute vertical acceleration. Parent hull: SHIP2 (L_{WL} = 100%, LCB = 53%) Optimum hull: Set 5 (L_{WL} = 110%, LCB = 53%) , at points 1, 2 and 3.

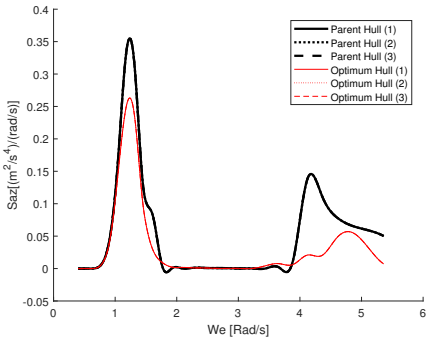

(a) β = 180°

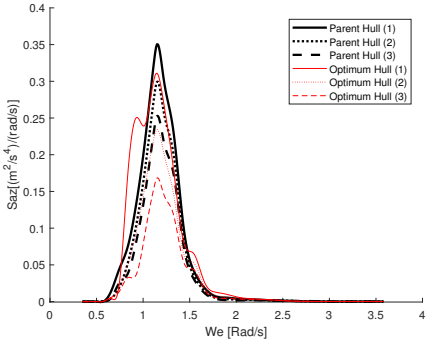

(b) β = 120°

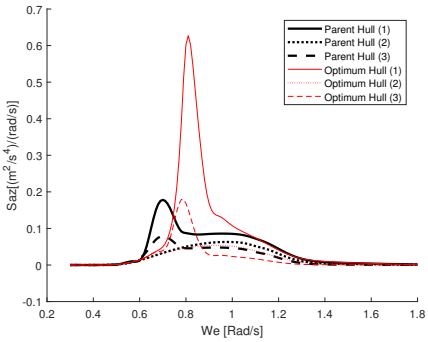

(c) β = 90°

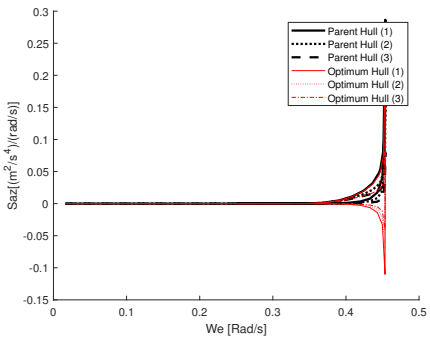

(d) β = 60°

Figure 6.24: Absolute vertical acceleration. Parent hull: SHIP2 (B_{WL}/T = 100%, LCB = 53%) Optimum hull: Set 6 (B_{WL}/T = 125%, LCB = 53%) , at points 1, 2 and 3.

6.4 Resistance analysis

As seen so far, the transformations on a ship hull can influence seakeeping both positively or negatively, depending on the transformation performed. These changes also affect other components on the performance of a ship, such as the case of resistance. The ship resistance is an important characteristic on a ship project, since it directly influences the power output required and therefore the project and operations costs. It is the job of a naval architect to find a balance between the comfort of the passengers and the cost associated with it. However, it is not the scope of this project to give an answer to which solution is best and a deeper analysis should be carried to understand how transformations that improve seakeeping may influence the ship resistance and its associated costs.

A preliminary analyses can be made using the generated ship hulls on *MAXSURF* Modeler [6] and test them on *MAXSURF* Resistance [8]. The method used to measure the ship's resistance was a slender body method, based on the work of Tuck et al. [48] and Couser et al. [13] available in *MAXSURF* Resistance. This method uses a Michell [32] based approach to compute the wave resistance of a port/starboard symmetrical mono-hull. This method may be applied to many hull forms including multi hulls. However, the individual hulls should be slender and should be symmetrical about their local centre line. Planing forces are neglected in the slender body method which limits speed range applicability. In general, sensible results can be obtained for a wide range of mono- and multi hull vessels operating at normal Froude numbers. This method predicts only the wave pattern resistance component. To calculate the total resistance, *MAXSURF* Resistance calculates and adds the viscous resistance component using the ITTC'57 friction coefficient calculation method and the specified form factor.

6.4.1 Resistance analysis for hull variations from SHIP1

The resistance analysis carried for the hull transformations based on SHIP1, are presented in the form of a table, that is consistent with how OMSI results were presented. The results in these table are the resistance in KN. These results were collected for a ship's maximum speed of 16 knots, which is the same used to calculate the OMSI.

Looking at Tables 6.13 - 6.15 it is clear that ship resistance is higher on hulls with larger C_B for the same LCB. Considering that the values of OMSI pointed for an increase in C_B to improve comfort. The best solutions will degrade the resistance performance. On the other hand, for the same C_B the shift of LCB closer to midship will contribute to reduce resistance, which for SHIP1 also contributes to reduce OMSI. For the hull variations at study on the combination of C_B = 0.72 and LCB = 50% would represent a reduction on OMSI while maintaining or reducing the original ship resistance. However, the improvements are not significant on either OMSI or resistance. From the three Sets *n* for changing C_B, using a variable displacement, Set 1, seems to be worse when compared to using a variable draft or variable draft combined with waterline beam at fixed ratio, Set 2 and Set 3 respectively. That is because the resistances are generally higher in the first method, Set 1.

The hull resistances of the hull variations based on C_M, Set 4 of hull variations, are presented on Tables 6.16. Once again, the variations that proved to reduce OMSI, also increased the resistance as it happened for C_B.

Regarding the geometrical transformations the resistance is affected differently. In the first type of transformation where L_{WL} was both increased and reduced, Set 5 of hull variations, the resistance will

be smaller in the cases of larger L_{WL}, as seen on Table 6.17. This is an important result, since increasing L_{WL} also reduced the values of OMSI. This means that if possible, this would be the ideal type of hull transformations, where comfort is being improved while requiring less power to do so. On the other hand the increase in B_{WL} ratio, Set 6 of hull variations, which reduced OMSI. This lead to higher ship resistances, as shown on Table 6.18, which like in the previous transformations is not the ideal situation.

Table 6.13: Resistance of different hull variations based Set 1 in [KN], SHIP1.

	C_B = 0.66	C_B = 0.68	C_B = 0.70	C_B = 0.71	C_B = 0.72	C_B = 0.74	C_B = 0.76
LCB = 50%	132	146	167	-	190	216	245
LCB = 52%	144	156	178	**190**	211	231	263
LCB = 54%	168	181	208	-	237	270	306

Table 6.14: Resistance of different hull variations based on Set 2 in [KN], SHIP1

	C_B = 0.66	C_B = 0.68	C_B = 0.70	C_B = 0.71	C_B = 0.72	C_B = 0.74	C_B = 0.76
LCB = 50%	139	155	172	-	189	207	227
LCB = 52%	147	164	181	**190**	199	220	242
LCB = 54%	168	186	208	-	230	254	279

Table 6.15: Resistance of different hull variations based on Set 3 in [KN], SHIP1.

	C_B = 0.66	C_B = 0.68	C_B = 0.70	C_B = 0.71	C_B = 0.72	C_B = 0.74	C_B = 0.76
LCB = 50%	140	154	170	-	186	204	222
LCB = 52%	149	165	181	**190**	199	218	238
LCB = 54%	173	191	211	-	233	254	277

Table 6.16: Resistance of different hull variations based on Set 4 in [KN], SHIP1.

	C_M = 0.99	C_M = 0.98	C_M = 0.97	C_M = 0.96	C_M = 0.95
LCB = 52%	**190**	186	194	201	211

Table 6.17: Resistance of different hull variations based on Set 5 in [KN], SHIP1.

	L_{WL} = 90 %	L_{WL} = 95%	L_{WL} = 100%	L_{WL} = 105%	L_{WL} = 110%
LCB = 52%	232	212	**190**	168	147

Table 6.18: Resistance of different hull variations based Set 6 in [KN], SHIP1.

	B_{WL}/T = 75%	B_{WL}/T = 85%	B_{WL}/T = 100%	B_{WL}/T = 115%	B_{WL}/T = 125%
LCB = 52%	178	184	**190**	196	200

6.4.2 Resistance analysis for hull variation from SHIP2

The same type of resistance analysis is carried on the hull variation applied to SHIP2 that connects Algarve to Madeira. The following tables contain the resistance in KN for the maximum ship speed of

21 Knots. It is immediately clear that the resistances are much higher on this second ship, however the same conclusions are taken.

Starting by looking at Table 6.19 it is confirmed that increasing C_B for the same LCB also increases the ships resistance and shifting LCB to the midship position reduces ship resistance. If SHIP2's point distribution was along the deck it would be expected to have both smaller values of OMSI and ship resistances. For this ship the shifting in LCB = 53% to LCB = 50% reduced resistance more than it was increased by increasing C_B. However, the improved hull to reduce OMSI was the combination with high C_B = 0.60 and a LCB = 56% and this will greatly increase resistance. Therefore, the reduction of OMSI and ship resistance become incompatible.

The transformations using C_M did not prove to be any better. Like in the previous case, the reduction on C_M increases the ship resistance as shown on Table 6.20. As seen in the same table increasing C_M also increased ship resistance, however it can not be directly attributed solely to the changes in this coefficient, since as stated before these hull transformations were heavily deformed compared to the parent hull.

Regarding the geometrical transformations, the same conclusion on the ship resistance are taken. Table 6.21 proves that increasing L_{WL} not only reduces OMSI but also reduced ship resistance. On Table 6.22 it is once again seen that improvements on OMSI, increasing B_{WL}/T ratio lead to slight increases in ship resistance. The geometrical transformations are therefore a better option in term of ship resistance compared to hull form transformations.

Table 6.19: Resistance of different hull variations based on Set 2 in [KN], SHIP2.

	C_B = 0.50	**C_B = 0.53**	**C_B = 0.56**	**C_B = 0.58**	**C_B = 0.60**
LCB = 50%	960	803	-	842	950
LCB = 53%	1275	1099	**1074**	1123	1226
LCB = 56%	1822	1662	-	1715	1861

Table 6.20: Resistance of different hull variations based Set 4 in [KN], SHIP2.

	C_M = 0.79	**C_M = 0.83**	**C_M = 0.87**	**C_M = 0.92**	**C_M = 0.96**
LCB = 53%	1337	1127	**1074**	1120	1444

Table 6.21: Resistance of different hull variations based on Set 5 in [KN], SHIP2.

	L_{WL} = 90 %	**L_{WL} = 95%**	**L_{WL} = 100%**	**L_{WL} = 105%**	**L_{WL} = 110%**
LCB = 53%	1274	1146	**1074**	991	948

Table 6.22: Resistance of different hull variations based on Set 6 in [KN], SHIP2.

	B_{WL}/T = 75%	**B_{WL}/T = 85%**	**B_{WL}/T = 100%**	**B_{WL}/T = 115%**	**B_{WL}/T = 125%**
LCB = 53%	1003	1036	**1074**	1116	1139

6.5 Operability assessment of various hull transformations with smallest OMSI

Complementary to the overall motion sickness analysis, an operability assessment is performed to the hull variations with greater reductions of OMSI. This way it is possible to assess how these transformations increase the ship operability on specific scenarios. It is done by analysing the ship operability based on common seakeeping criteria for passengers comfort and safety.

Two different criteria are selected namely, vertical accelerations and MSI. Since both of them were previously calculated, when obtaining OMSI at all points of the ship, for each sea state and heading waves. The criteria for vertical accelerations is that the maximum vertical acceleration during an exposure of 2 hours at any point should be smaller than **0.05*g** (g being the gravitational acceleration). The maximum MSI during an exposure of 2 hours at any point, should be less than **35%**. Both criteria are based on Tezdogan et al. [45]. The calculation was performed according to what was described in Section 3.9.

6.5.1 Operability of hull variations based on SHIP1

Looking at the transformations of C_B and LCB on SHIP1 it is clear that the operability is improved both on vertical accelerations and MSI, as shown in Tables 6.23-6.25. Vertical accelerations however are the limiting seakeeping criteria, as for the parent ship it could only operate around 65.7% of the time opposed to 94.1% of the time, if MSI is to be considered. For heading angles it seems that for bow and beam seas the ship presents smaller operability index's. These are reasonable values, since for smaller peak periods (T_P) the headings have generally higher accelerations and MSIs, compared to heading seas, as shown in Section 5.4. Also in the coast of Algarve, Operating Scenario 1, sea-states with small peak periods are particularly common, as shown in Table 5.3. However, these type of headings, have a smaller weight on the ship's operability as shown in Figure 5.9. For such reason the operability is more dependent on head seas than any other type of heading.

Using Set 1 of ship transformations it would increase only by 2.5% the ship operability based on vertical accelerations criteria and 3.1% considering the MSI criteria, see Table 6.23. On the other hand using the Set 2 of ship transformations, the ship operability would instead increase by 5.9% considering vertical accelerations, considerably more than in Set 1. The operability based on MSI criteria however would be around the same, improving 3.2%, see Table 6.24. Finally, similar results are obtained in Set 3 of hull transformations, where the operability improves by 5.5% using vertical accelerations criteria and 3.1% based on MSI criteria. Once again it is clear that transforming the ship hull using a variable draft and fixed beam, Set 2 of hull transformations, is a slightly better approach.

Regarding the hull transformations using C_M or Set 4 of hull transformations, similar results are obtained. The operability improves by 5% using vertical acceleration criteria and only 1.54% using MSI as seakeeping criteria, as shown in Table 6.26. Smaller improvements on operability based on an MSI criteria were to be expected, since the reductions of OMSI were also smaller on this particular hull transformation.

The results for the first geometric transformation, which is the variation of L_{WL} or Set 5 of hull transformations, are presented in Table 6.27. It shows an increase in operability of 9.4% if based on vertical accelerations criteria and 3.8% if based on MSI criteria. This hull variation presented the best improve-

Table 6.23: Operability of hull transformation based on Set 1. Parent Ship: SHIP1 (C_B = 0.71 and LCB = 52%) Optimum hull: (C_B = 0.76 and LCB = 50%).

Heading (deg)	Vertical Acceleration		MSI		All Criteria	
	Parent	Optimum Hull	Parent	Optimum Hull	Parent	Optimum Hull
180	0.554	0.587	0.946	0.978	0.554	0.587
150	0.422	0.432	0.938	0.946	0.422	0.432
120	0.275	0.275	0.824	0.939	0.275	0.275
90	0.319	0.401	0.773	0.932	0.319	0.401
60	1.000	1.000	1.000	1.000	1.000	1.000
30	1.000	1.000	1.000	1.000	1.000	1.000
Weighted Average	0.567	0.592	0.941	0.972	**0.567**	**0.592**

Table 6.24: Operability of hull transformation based on Set 2. Parent Ship: SHIP1 (C_B = 0.71 and LCB = 52%) Optimum hull: (C_B = 0.76 and LCB = 50%).

Heading (deg)	Vertical Acceleration		MSI		All Criteria	
	Parent	Optimum Hull	Parent	Optimum Hull	Parent	Optimum Hull
180	0.554	0.608	0.946	0.979	0.554	0.608
150	0.422	0.554	0.938	0.946	0.422	0.554
120	0.275	0.275	0.824	0.939	0.275	0.275
90	0.319	0.401	0.773	0.932	0.319	0.401
60	1.000	1.000	1.000	1.000	1.000	1.000
30	1.000	1.000	1.000	1.000	1.000	1.000
Weighted Average	0.567	0.626	0.941	0.973	**0.567**	**0.626**

Table 6.25: Operability of hull transformation based on Set 3. Parent Ship: SHIP1 (C_B = 0.71 and LCB = 52%) Optimum hull: (C_B = 0.76 and LCB = 50%).

Heading (deg)	Vertical Acceleration		MSI		All Criteria	
	Parent	Optimum Hull	Parent	Optimum Hull	Parent	Optimum Hull
180	0.554	0.631	0.946	0.978	0.554	0.631
150	0.422	0.456	0.938	0.946	0.422	0.456
120	0.275	0.275	0.824	0.939	0.275	0.275
90	0.319	0.352	0.773	0.919	0.319	0.352
60	1.000	1.000	1.000	1.000	1.000	1.000
30	1.000	1.000	1.000	1.000	1.000	1.000
Weighted Average	0.567	0.622	0.941	0.972	**0.567**	**0.622**

Table 6.26: Operability of hull transformation based on Set 4. Parent Ship: SHIP1 (C_M = 0.99 and LCB = 52%) Optimum hull: (C_M = 0.95 and LCB = 52%).

Heading (deg)	Vertical Acceleration		MSI		All Criteria	
	Parent	Optimum Hull	Parent	Optimum Hull	Parent	Optimum Hull
180	0.554	0.631	0.946	0.962	0.554	0.631
150	0.422	0.432	0.938	0.946	0.422	0.432
120	0.275	0.230	0.824	0.808	0.275	0.230
90	0.319	0.401	0.773	0.932	0.319	0.401
60	1.000	1.000	1.000	1.000	1.000	1.000
30	1.000	1.000	1.000	1.000	1.000	1.000
Weighted Average	0.567	0.617	0.941	0.9564	**0.567**	**0.617**

ments on ship operability consistent with the smallest results of OMSI. On the other hand the second type of geometrical transformation (Set 6) did not prove to be as successful. In fact the hull variation where the B_{WL}/T ratio was increased, led to a reduction of operability in the order of -8.8% when considering vertical accelerations criteria. Considering the MSI criteria, was registered an improvement of 1.2% in the ship's operability, as shown in Table 6.28. These operability results from Set 6 were expected

to be worse than the results from Set 5, since the reductions of OMSI in Set 6 were also considerably smaller than in Set 5, as shown in Tables 6.5 and 6.6.

Table 6.27: Operability of hull transformation based on Set 5. Parent Ship: SHIP1 (L_{WL} = 100% and LCB = 52%) Optimum hull: (L_{WL} = 110% and LCB = 52%).

Heading (deg)	Vertical Acceleration		MSI		All Criteria	
	Parent	Optimum Hull	Parent	Optimum Hull	Parent	Optimum Hull
180	0.554	0.643	0.946	0.983	0.554	0.643
150	0.422	0.612	0.938	0.965	0.422	0.612
120	0.275	0.334	0.824	0.946	0.275	0.334
90	0.319	0.402	0.773	0.949	0.319	0.402
60	1.000	1.000	1.000	1.000	1.000	1.000
30	1.000	1.000	1.000	1.000	1.000	1.000
Weighted Average	0.567	0.661	0.941	0.979	**0.567**	**0.661**

Table 6.28: Operability of hull transformation based on Set 6. Parent Ship: SHIP1 (B_{WL}/T = 100% and LCB = 52%) Optimum hull: (B_{WL}/T = 125% and LCB = 52%).

Heading (deg)	Vertical Acceleration		MSI		All Criteria	
	Parent	Optimum Hull	Parent	Optimum Hull	Parent	Optimum Hull
180	0.554	0.464	0.946	0.953	0.554	0.464
150	0.422	0.231	0.938	0.946	0.422	0.231
120	0.275	0.275	0.824	0.873	0.275	0.275
90	0.319	0.351	0.773	0.919	0.319	0.351
60	1.000	1.000	1.000	1.000	1.000	1.000
30	1.000	1.000	1.000	1.000	1.000	1.000
Weighted Average	0.567	0.479	0.941	0.953	**0.567**	**0.479**

6.5.2 Operability of hull variations based on SHIP2

It should be noticed when looking at the operability study of SHIP2 that the vertical accelerations criteria is too harsh for this ship and it's operations conditions. This way we can see the limitations when using the operability index. That is because the operability index is a pass/fail type of criteria and no information is given on an overall improvement at each sea state, unlike on a method using the OMSI. What is happening is that even though vertical accelerations are smaller on the hull variation, their reduction is not significant to pass the criteria. If a higher criterion for vertical accelerations were to be used it would present rates of operation more in line with what was obtained from the MSI criteria. Therefore, the operability analysis will be focused more on the later criteria since no significant improvements are to be taken on the vertical accelerations. By transforming the ship by increasing to C_B = 0.60 and LCB = 56%, the operability on the aft part increased from 77.04% to 87.72% and improved by 10.68% considering MSI seakeeping criteria, as shown on Table 6.29. The reduction in C_M also proved to be successful, increasing the operability by 7.86% for MSI seakeeping criteria, as shown on Table 6.30. These are significant results since only one factor was changed, maintaining well the original dimensions of the ship.

The operability assessment for the geometrical variations on SHIP2 is not exactly the same as on SHIP1. On both ships the hulls with smaller OMSI showed an increase in operability for MSI seakeeping criteria. However, the variation with increased L_{WL} the operability only improved by 7.66% no longer the best type of alternative tested, as shown Table 6.31 and confirming the results of OMSI. The ratio

Table 6.29: Operability of hull transformation based on Set 2. Parent Ship: SHIP2 (C_B = 0.56 and LCB = 53%) Optimum hull: (C_B = 0.60 and LCB = 53%).

Heading (deg)	Vertical Acceleration		MSI		All Criteria	
	Parent	Optimum Hull	Parent	Optimum Hull	Parent	Optimum Hull
180	0.001	0.020	0.631	0.880	0.001	0.020
150	0.002	0.006	0.693	0.825	0.002	0.006
120	0.021	0.021	0.847	0.871	0.021	0.021
90	0.443	0.443	1.000	1.000	0.443	0.443
60	1.000	1.000	1.000	1.000	1.000	1.000
30	1.000	1.000	1.000	1.000	1.000	1.000
Weighted Average	0.090	0.096	0.7704	0.8772	**0.090**	**0.096**

Table 6.30: Operability of hull transformation based on Set 4. Parent Ship: SHIP2 (C_M = 0.87 and LCB = 53%) Optimum hull: (C_M = 0.79 and LCB = 53%).

Heading (deg)	Vertical Acceleration		MSI		All Criteria	
	Parent	Optimum Hull	Parent	Optimum Hull	Parent	Optimum Hull
180	0.001	0.003	0.631	0.823	0.001	0.003
150	0.002	0.009	0.693	0.776	0.002	0.009
120	0.021	0.021	0.847	0.871	0.021	0.021
90	0.443	0.443	1.000	1.000	0.443	0.443
60	1.000	1.000	1.000	1.000	1.000	1.000
30	1.000	1.000	1.000	1.000	1.000	1.000
Weighted Average	0.090	0.093	0.7704	0.849	**0.090**	**0.093**

increase improved the operability by 8.9% considerably more than for SHIP1, see Table 6.32.

Table 6.31: Operability of hull transformation based on Set 5. Parent Ship: SHIP2 (L_{WL} = 100% and LCB = 53%) Optimum hull: (L_{WL} = 110% and LCB = 53%).

Heading (deg)	Vertical Acceleration		MSI		All Criteria	
	Parent	Optimum Hull	Parent	Optimum Hull	Parent	Optimum Hull
180	0.001	0.003	0.631	0.793	0.001	0.003
150	0.002	0.003	0.693	0.792	0.002	0.003
120	0.021	0.021	0.847	0.871	0.021	0.021
90	0.443	0.443	1.000	1.000	0.443	0.443
60	1.000	1.000	1.000	1.000	1.000	1.000
30	1.000	1.000	1.000	1.000	1.000	1.000
Weighted Average	0.090	0.091	0.7704	0.847	**0.090**	**0.091**

Table 6.32: Operability of hull transformation based on Set 6. Parent Ship: SHIP2 (B_{WL}/T = 100% and LCB = 53%) Optimum hull: (B_{WL}/T = 125% and LCB = 53%).

Heading (deg)	Vertical Acceleration		MSI		All Criteria	
	Parent	Optimum Hull	Parent	Optimum Hull	Parent	Optimum Hull
180	0.001	0.003	0.631	0.848	0.001	0.003
150	0.002	0.003	0.693	0.792	0.002	0.003
120	0.021	0.021	0.847	0.871	0.021	0.021
90	0.443	0.191	1.000	0.996	0.443	0.191
60	1.000	1.000	1.000	1.000	1.000	1.000
30	1.000	1.000	1.000	1.000	1.000	1.000
Weighted Average	0.090	0.0636	0.7704	0.8594	**0.090**	**0.0636**

6.6 Summary

In the present chapter the results of seakeeping analysis were presented. It started by comparing the Overall Motions Sickness Incidence for all hull variations. It is followed by a comparison of RAOs and absolute vertical accelerations on specific hulls and locations. Next, a simple resistance analysis on each type of hull variation was performed. Such analysis will give a preliminary idea of the effects from the hull transformations on the ship resistance. However, a more detailed study is required to understand the real impact of such transformations on the overall performance of the ship. Finally, an operability assessment was also performed to compare to the results obtained using OMSI.

Using OMSI as a parameter to be minimized in a comfort seakeeping analysis is clearly a good approach. Using this method multiple information is converted into one simple index, avoiding the exhausting work of comparing RAOs or vertical accelerations in detail. Also, it proved to be more efficient on accounting little improvements compared to using an operability index, as a pass/fail criteria, that discards any progress out of the criteria range.

From the different hull variations tested, it was shown that increasing C_B for a fixed C_M will improve comfort, since it reduces motions and seasickness overall. It is also shown that shifting LCB contributes for reducing seasickness depending on the intended location. If both forward and aft locations are being considered LCB should be shifted closer to the midship, which is the case of SHIP1. Also, RAOs are smaller on this condition. However, if the location to be improved is only focused on an aft region as the case of SHIP2, LCB should be closer to those locations obtaining improvements locally but not overall. Any increase C_B is associated with higher hull resistances. The same happens by shifting LCB further from to the midship, opposed to shifting LCB closer to the midship, that actually reduces ship hull resistance.

Regarding transformations of C_M for a fixed C_B, the results were not fully clear. However, it seemed to indicate that reducing C_M for a fixed C_B will reduce seasickness on the passengers. Also, it is the type of transformations that mostly maintains the general characteristics such as ships form, size and hull resistance.

Geometrical transformations showed significant improvements on passengers' comfort, with special regards to increasing L_{WL} while maintaining all other form factors. It was considered a good solution since it both reduced seasickness and ship hull resistance. Increasing B/T ratio also reduced seasickness however such transformations are associated with higher ship hull resistances.

The reductions on OMSI are associated with higher ship's operability, based on seakeeping comfort criteria. From the different types of hull transformations, it is confirmed that it is possible to improve the passenger's comfort on a specific type of operation. For a naval architect these hull variations become useful tools and they can be implemented on any type of passenger ship easily. It was also shown that OMSI is an useful parameter to check each the hull transformation regarding passenger's comfort at an early stage of design. However, the naval architect should also be critical when introducing a certain type of variation, since it may affect other aspects of the ship's performance.

Chapter 7

Conclusion

Passenger ships are a branch of vessels where the seakeeping performance is ever more demanding. Therefore, passenger's comfort places a central focus in the seakeeping analysis. For that reason, effects like seasickness have been widely studied on both its origin and methods of prediction. This dissertation focused on giving various solutions to help naval architects improving mono hull passenger ships right at an early stage of design. Such solutions were obtained by showing how a parameter like OMSI, originally presented by Scamardella and Piscopo [41], can be used to considered multiple information frequently neglected in an optimization process. It was possible to use a method that is easy to implement and without much effort for its analysis and interpretation. A strip theory based program was used to predict seakeeping behavior of multiple hull variations. These are great tools to be used at early stages of a design process, where fast results based on easy implementation are preferred. These are opposed to CFD solvers that require input files with greater detail and are considerably more difficult to implement on multiple variations. Two different passenger ships were used to perform various sets of hull transformations, for the purpose of improving passenger's comfort on a specific sea way, based on the reduction of OMSI. The hull variations, from each set of transformation considered as improved, were compared to their parent hulls. These included the comparison of RAOs plots (heave, roll and pitch) at different heading angles. The same hulls were compared regarding the absolute vertical acceleration at strategic locations of the deck. The hull resistance was predicted for all hull transformations, with the aim of establishing a relation between hull resistance and passenger's comfort. Finally, the improved ships of each set of transformations were compared to their parent ships regarding their operability on the specific operating scenario.

7.1 Achievements

The start of this dissertation was focused on the state of the art related to seasickness and how it could be framed into a seakeeping analyse. It was concluded that:

- Strip theory, would be the best method of assessing the seakeeping performance of a ship, within the available resources.
- The information collected from the study of seasickness helped to better understand how this effect has been handled and predicted throughout the years. Many valid methods of predicting seasickness emerged from this literature, from which the Motion Sickness Index (MSI) stood out. It was then selected as an ideal method of predicting seasickness for this dissertation.
- Based on previous researches on the ship hull's optimization using seakeeping analysis, it was

concluded that many of these methods could be adapted within this academic work. Various types of hull transformations, that proved to improve passengers comfort in the past, were selected to be used in this dissertation. Finally, the Overall Motion Sickness Index was chosen as the parameter to be minimized in the seakeeping analysis. This index not only uses MSI as a base of predicting seasickness, but also combines multiple locations on the deck, heading angles and sea-states.

Meaningful background theory for the results obtained in this dissertation was presented in Chapter 3. This included an overview on the strip theory by Salvensen et al. [39] with only the most important equations. It was also presented the formulation used to estimate the roll damping. This formulation was not directly included in the computer code *CENTEC-SK*, used to obtain the results from strip theory. The formulation for the JONSWAP spectrum was also presented, together with a study on spectrum transformations and the complications that come from account multiple headings particularly from quartering and following seas. The equations proposed to calculate the RMS avoided the mathematical errors that came from quartering and following seas. This was particularly useful since the formulation used to calculate MSI and OMSI directly depended on the values of RMS. Finally, the calculations of operability index were introduced, where it should be noticed that this formulation can be used directly together with the calculations of OMSI.

For this seakeeping analysis two different strip theory based programs, were available. Namely, *CENTEC-SK* an in house code developed by Fonseca and Guedes Soares [17] and *MAXSURF* Motions a commercial software from Bentley Systems [7]. Both heave, roll and pitch motions results from the two programs were compared to experimental results from the containership S-175, ITTC [24]. This comparison was performed for a Froude number equal to Fn = 0.275 and for six different headings: β=180º, β=150º, β=120º, β=90º, β=60º and β=30º. It was concluded that:

- *CENTEC-SK* is more flexible to work with *MATLAB* compared to *MAXSURF* Motions. However, the input files from *MAXSURF* Motions are easier to manipulate.
- The computational time from *MAXSURF* Motions is very high compared to *CENTEC-SK*.
- Both programs showed in general consistent results with the experimental results for heave and pitch motion. For roll motions the experimental results were generally inconclusive.
- *CENTEC-SK* was considered an adequate program to be used in this seakeeping analysis.

Two different passenger ships were used to study the comfort of passenger on the main deck. The first ship (SHIP1) was set to operate on calm waters near the coast of Algarve (Operating Scenario 1). SHIP1 had multiple points of interest along the deck. The second ship (SHIP2) was set to operate on the Atlantic Ocean (Operating Scenario 2), connecting Algarve to Madeira. SHIP2 only had a single area of interest. All the meaningful information regarding these ships and their operating scenarios was presented on Chapter 5. Six different sets of hull transformations were performed using *MAXSURF* Modeler [6]. Two types of hull transformations were performed: geometric and hull form transformations. The geometric transformations focused on main dimensions of the ship such as the length at waterline L_{WL} and the beam at waterline B_{WL}. The hull form transformations focused on the manipulation of form coefficients, more specifically the block coefficient C_B, the LCB and midship coefficient C_B. Before obtaining the results of OMSI on each hull transformations, it was studied the MSI distribution along the deck at various headings and sea-states. From this study it was concluded that each location is affected differently depending on both the type of heading or sea-state. Therefore, performing an optimization process based on just one location, sea-state or wave heading is not as accurate as considering a parameter like OMSI.

The main calculations and plots were performed using *MATLAB*. The first and most important results obtained in this dissertation were based on the OMSI of each hull variation. The hulls considered improved for passenger's comfort were the ones with the smallest OMSI, for each set of transformations. Based on this analysis the following steps may be taken to obtain an improved hull for passenger's comfort:

- Increase block coefficient (C_B) by reducing draft (T) for a fixed midship coefficient (C_M), displacement, breath and waterline length.
- Shift the longitudinal center of buoyancy (LCB), depending on locations of interest, equilibrium and trim considerations.
- Decrease midship coefficient (C_M), while increasing prismatic coefficient (C_P) and waterplane coefficient (C_{WP}.)
- Increase waterline length (L_{WL}) for fixed B_{WL}/T ratio, displacement and form coefficients.
- Increase B_{WL}/T ratio for fixed waterline length (L_{WL}), displacement and form coefficients.

It was also shown that reductions on OMSI were directly related to reductions on ship motions. This was done by comparing the plots of the heave, roll and pitch RAOs, of the improved hulls with their parent ships. In the end it became clear that it is a much harder process than just comparing the values of OMSI. Still, some conclusions were taken:

- Increasing C_B generally reduces heave, roll and pitch motions in all types of heading.
- Moving the LCB to the midship reduces pitch motions, however it has no influence on heave or roll.
- Reducing C_B may reduce heave and roll motion with no effect on pitch motions. However, his influence is very small.
- Increasing L_{WL} reduces heave and pitch motions.
- Increasing B_{WL} reduces heave and pitch motions. It also shifts the roll peak RAOs in the frequency range.

A similar analysis was performed by comparing the absolute vertical accelerations on strategic locations of the improved hulls with their parent ships. By comparing the plot of absolute vertical accelerations on various points along the deck, it was discovered that the hull variations do not improve at all the locations equally. That is, for some locations on the ship and at certain headings, these transformations proposed above may increase the vertical accelerations. Such side effect is obviously not desired. However, by using a parameter like OMSI where multiple locations and conditions are accounted, it was proved that these transformations are ultimately beneficial to improving comfort on an overall. In other words, these transformations improve the ship globally, even if some particular conditions are harmed.

The ship's hull resistance was assessed for every hull transformation. It was gathered that most reductions on OMSI are associated with higher ship hull resistances. The exceptions are for the cases of increasing the waterline length L_{WL} and shifting LCB to midship that may both reduce OMSI and ship hull resistance.

At last but not least, it was verified that the reduction in OMSI contribute for higher operability, based on criteria for passengers comfort and safety, of a ship in a certain operating scenario. However, the

isolated study of a ship's operability based on the operability index, may not account for subtle improvements in the seakeeping performance since it is a pass/fail criteria with much less accuracy. It is also important to refer that the performance of a ship may be affected by some of the transformations proposed, being up to the naval architect to account for their viability on a particular design project.

7.2 Future work

Regarding the improvement procedures the following suggestions for future work may be worth considering:

- Introducing a weight function for various points locations on the calculation of the Overall Motion Sickness Index (OMSI).
- Use the parameter Overall Motion Sickness Index (OMSI), to compare comfort levels of a passenger ship with different types of stabilizers (such as fins or rotors mounted beneath the waterline). The performance of these devices can be compared to the solutions proposed in this dissertation. It would be also interesting to compare the economic viability of these two types of solutions on improving passengers comfort.
- Develop a danger scale for ship operations based on the OMSI, like the ones available for MSI.

References

[1] ARRIBAS, F. L. P., AND PIÑEIRO, A. L. Seasickness prediction in passenger ships at the design stage. *Ocean Engineering 34, 2086-2092* (2007).

[2] ATTIAS, J., GORDON, C., RIBAK, J., BINAH, O., AND ROLNICK, A. Efficacy of transdermal scopolamine against seasickness: A 3-day study at sea. *Aviation, Space and Environmental Medicine, 58, 1, 60–62* (1987).

[3] BALES, N. K. Optimizing the seakeeping performance of destroyer-type hulls. *Thirteenth ONR Symposium on Naval Hydrodynamics, Tokyo* (1980).

[4] BELGA, F. *Seakeeping optimization of a fast displacement catamaran on the basis of strip-theory codes.* Técnico Lisboa, 2017.

[5] BELGA, F., VENTURA, M., AND SOARES, C. G. Seakeeping optimization of a catamaran to operate as fast crew supplier at the alentejo basin. *C. Guedes Soares and T. A. Santos(Eds). Progress in Maritime Engineering and Technology, London, UK:Taylor & Francis* (2018).

[6] BENTLEY SYSTEMS, I. *Maxsurf Modeler, Windows Version 21, User Manual*. Bentley Systems, Incorporated, 2017.

[7] BENTLEY SYSTEMS, I. *Maxsurf Motions, Windows Version 21, User Manual*. Bentley Systems, Incorporated, 2017.

[8] BENTLEY SYSTEMS, I. *Maxsurf Resistance, Windows Version 21, User Manual*. Bentley Systems, Incorporated, 2017.

[9] BRUNER, J. M. R. Seasickness in a destroyer escort squadron. *United States Armed Forces Medical Journal, 6, 4, 469–490* (1955).

[10] CEPOWSKI, T. Influence analysis of changes of design parameters of passenger-car ferries on their selected sea-keeping qualities. *POLISH MARITIME RESEARCH 1(64) Vol 17; pp. 25-32* (2010).

[11] CHINN, H. I. Motion sickness in the military service. 108, 20–29.

[12] COLWELL, J. L. Human factors in the naval environment: a review of motion sickness and biodynamic problems. *Technical Report DREA-TM-89-220, Defence Research Establishment Atlantic, Dartmouth, Nova Scotio, Canada* (1989).

[13] COURSER, P. An investigation into the performance of high-speed catamarans in calm water and waves. *PhD thesis, Department of Ship Science, University of Southampton* (1996).

[14] DENIS, M. S., AND PIERSON, W. J. On the motions of ships in confused seas. *Transactions of the Society of Naval Architects and Marine Engineers, Vol. 61, pp.280-354* (1953).

[15] DOBIE, T. G. The importance of the human element in ship design. *In: Proceedings of the Ship Structure Symposium, Arlington VA* (June, 2000).

[16] ESTEVES, R., AND GORDO, J. M. Vibration finite element analysis on a passenger vessel's self-service. *Twelfth International Congress on Sound and Vibration* (2005).

[17] FONSECA, N., AND SOARES, C. G. Time domain analysis of vertical ship motions. *Transaction on the Built Environment vol 5, WIT Press, ISSN 1743-3509* (1994).

[18] FONSECA, N., AND SOARES, C. G. Sensitivity of the expected ships availability to different sea-keeping criteria. *Proceedings of OMAE'02 21st International Conference on Offshore Mechanics and Artic Engineering June 23-28, Oslo, Norway, OMAE2002-28542* (2002).

[19] GRAHAM, R. Motion induced interruptions as ship operability criteria. *Naval Engineers Journal 102 (2). ISO. Evaluation of Human Exposure to Whole-body Vibration—Part 3: Evaluation of Whole-body z-axis Vertical Vibration in the Frequency Range 0.1 to 0.63 Hz.* (1985).

[20] GRIFFIN, M. G. *Motion Sickness. Handbook of Human Vibration*. Academic Press, New York, 1990.

[21] GRIGOROPOULOS, G. J., AND LOUKAKIS, T. A. A new method for developing hull forms with superior seakeeping qualities. *Department of Na val Architecture and Marine Engineering, National Technical University of Athens, 42 October 28th, Athens, Greece* (1988).

[22] HANDFORD, S. W., CONE, T. E., AND GOVER, S. C. A ship's motion and the incidence of seasickness. *The Military Surgeon, 113, 3, 157–167* (1953).

[23] HILL, J. The care of the sea-sick. *The British Medical Journal, 2,802–807* (1936).

[24] ITTC. Summary of results obtained with computer programs to predict ship motions in six degree of freedom and related responses: comparative study on ship motion program. *15th & 16th ITTC seakeeping committee, Japan* (1983).

[25] JACOBS, W. R. The analytical calculation of ship bending moments in regular waves. *Journal of Ship Research, vol.2, no.1* (1958).

[26] JOURNÉE, J., AND MASSIE, W. *OFFSHORE HYDROMECHANICS,First Edition*. Delft University of Technology, January 2011.

[27] KORVIN-KROUKOVSKY, B. V., AND JACOBS, W. R. Pitching and heaving motions of a ship in regular waves. *In Transactions of the Society of Naval Architects and Marine Engineers, SNAME, vol. 65, pp. 590-632.* (1957).

[28] KUKNER, A., AND SARIÖZ, K. High speed hull form optimization for seakeeping. *Advances in Engineering Software, 22(3):179-189* (1995).

[29] LACKENBY, H. On systematic geometrical variation of ship forms. *RINA Transactions, Vol.92* (1950).

[30] LAWTHER, A., AND GRIFFIN, M. J. Prediction of the incidence of motion frequency and duration of vertical oscillation. *The Journal of the Acoustical Society of America 82, 957-966* (1987).

[31] MCCAULEY, M. E., ROYAL, J. W., WYLIE, C. D., O'HANLON, J. F., AND MACKIE, R. R. Motion sickness incidence: Exploratory studies of habituation, pitch and roll, and the refinement of a mathematical model. *Technical Report 1733-2, Human Factors Research Inc., Goleta, California* (1976).

[32] MICHELL, J. H. The wave resistance of a ship. *Philosophical Magazine (5), vol 45, pp 106-123.* (1898).

[33] MILLER, E. R. Unknown title of a report on roll damping. *Technical Report 6136- 74-280, NAVSPEC* (1974).

[34] O'HANLON, J. F., AND MCCAULEY, M. E. Motion sickness incidence as a funtion of the frequancy and acceleration of vertical sinusoidal motion. *Aerospace Medicine, vol.45(4), pp. 366-369* (1974).

[35] ÖZÜM, S., SENER, B., AND YILMAZ, H. A parametric study on seakeeping assessment of fast ships in conceptual design stage. *Ocean Engineering 38 1439–1447* (2011).

[36] PETHYBRIDGE, J. R. Sea sickness incidence in royal navy ships. *INM Report 37/82, Institute of Naval Medicine, Gosport, England* (1982).

[37] PETHYBRIDGE, J. R., AND WALTERS, J. W. D. J. D. A pilot study on the incidence of sea sickness in rn personnel on 2 ships. *INM Report 55/78, Institute of Naval Medicine, Alverstoke, Hampshire, England* (1978).

[38] RAMOS, J., AND SOARES, C. G. On the assessment of hydrodynamic coefficients of cylinders in heaving. *Ocean Engineering, 24(8):743-763* (1997).

[39] SALVESEN, N., TUCK, E. O., AND FALTINSEN, O. Ship motions and sea loads. *In Transactions of the Society of Naval Architects and Marine Engineers, SNAME, vol. 78, pp. 250-287* (1970).

[40] SARIÖZ, K., AND NARLI, E. Effect of criteria on seakeeping performance assessment. *Ocean Engineering 32 1161–1173* (2005).

[41] SCAMARDELLA, A., AND PISCOPO, V. Passenger ship seakeeping optimization by the overall motion sickness incidence. *Ocean Engineering 76 (2014) 86-97* (2013).

[42] STEVENS, S. C., AND PARSONS, M. G. Effects of motion at sea on crew performance: A survey. *Marine Technology 39,29-47* (2002).

[43] SÖDING, H. Eine modifikation der streifenmethode. *Schiffstechnik Bd. 16, Heft 80* (1969).

[44] TASAI, F., AND TAKAKI, M. Theory and calculation of ship responses in regular waves. *Symposium on Seaworthiness of Ships, Japan Society of Naval Architects* (1969).

[45] TEZDOGAN, T., INCECIK, A., AND TURAN, O. Operability assessment of high speed passenger ships based on human comfort criteria. *Department of Naval Architecture, Ocean and Marine Engineering, University of Strathclyde, 100 Montrose Street, Glasgow, G4 0LZ, UK* (-).

[46] TIMMAN, R., AND NEWMAN, J. N. The coupled damping coefficients of symmetric ship. *Journal of Ship Research, vol.5, no.4* (1962).

[47] TRUMBULL, R., CHINN, H. I., MAAG, C. H., MILCH, L. J., HANDFORD, S. W., SEIBERT, R., SPERLING, P., AND SMITH, P. K. Effect of certain drugs on the incidence of seasickness. *Clinical Pharmacology and Therapeutics, 1, 3, 280–283* (1960).

[48] TUCK, E., LUZAUSKAS, L., AND SCULLEN, D. Sea wave pattern evaluation. part 1 report: Primary code and test results (surface vessels). *Applied Mathematics Department, The University of Adelaide. 30 April 1999* (1999).

[49] VOSSERS, G., SWAAN, W. A., AND RIJKEN, H. Experiments with series 60 models in waves. *Trans. SNAME, vol. 68* (1960).

[50] VOSSERS, G., SWAAN, W. A., AND RIJKEN, H. Vertical and lateral bending moment measurments on series 60 models. *International Shipbuilding Progress, vol.8, no. 83* (1961).

Appendix A

RAOs Plots

A.1 RAOs of SHIP1

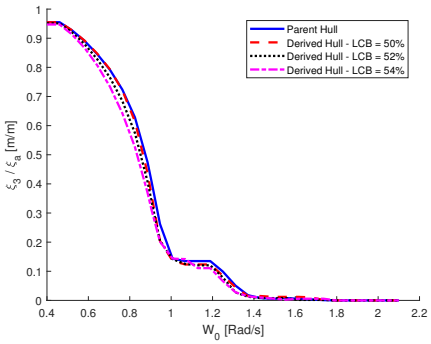

(a) β = 180°

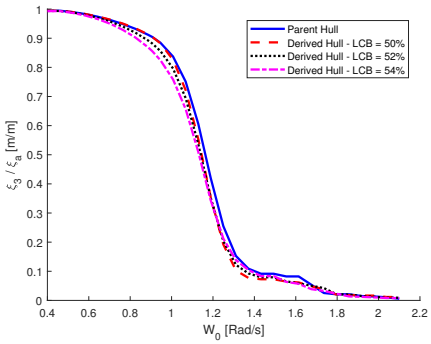

(b) β = 120°

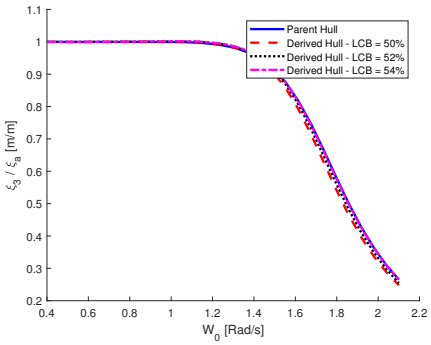

(c) β = 90°

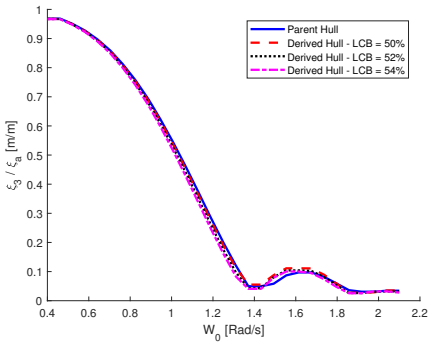

(d) β = 60°

Figure A.1: Heave RAOs. Parent Ship: SHIP1 with C_B = 0.71. Derived Hulls: Set 1 with C_B = 0.76.

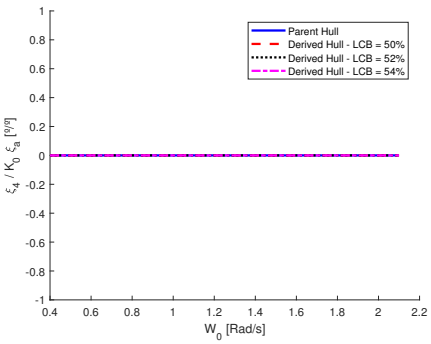

(a) β = 180º

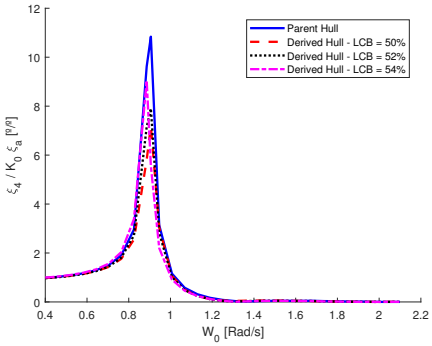

(b) β = 120º

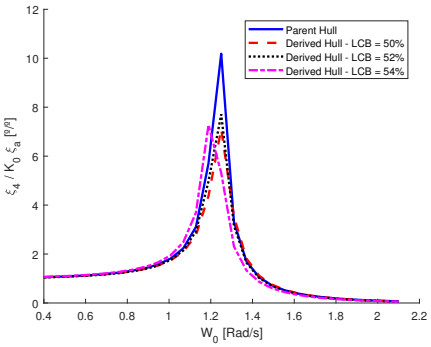

(c) β = 90º

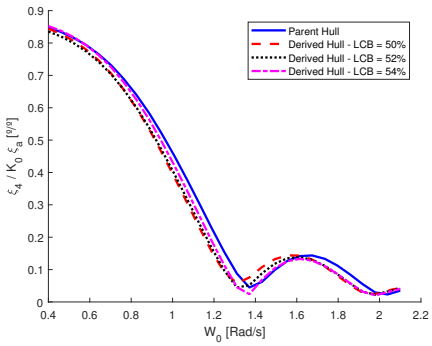

(d) β = 60º

Figure A.2: Roll RAOs. Parent Ship: SHIP1 with C_B = 0.71. Derived Hulls: Set 1 with C_B = 0.76.

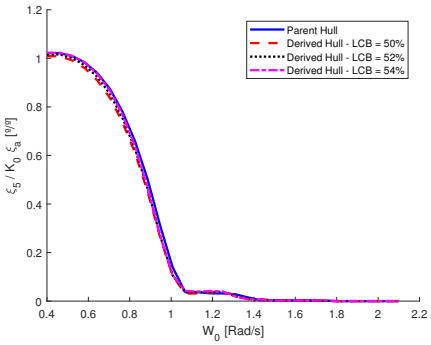

(a) β = 180º

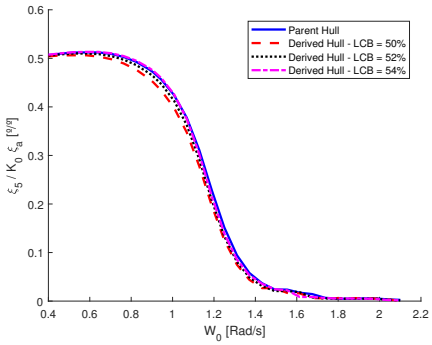

(b) β = 120º

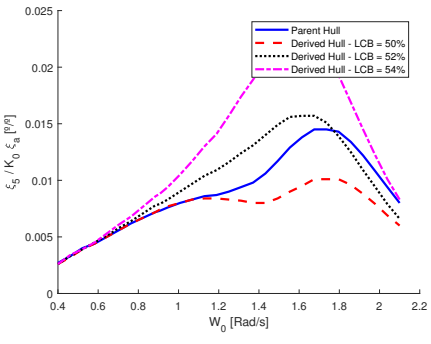

(c) β = 90º

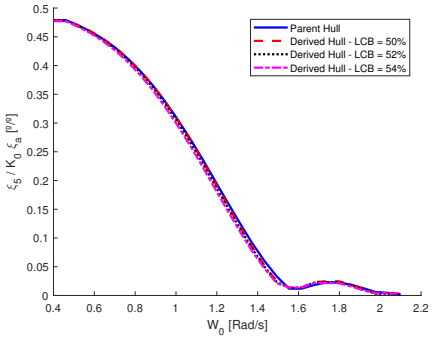

(d) β = 60º

Figure A.3: Pitch RAOs. Parent Ship: SHIP1 with C_B = 0.71. Derived Hulls: Set 1 with C_B = 0.76.

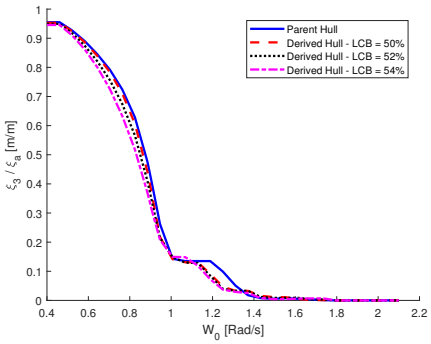

(a) β = 180°

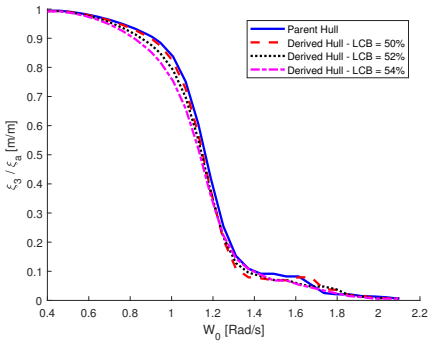

(b) β = 120°

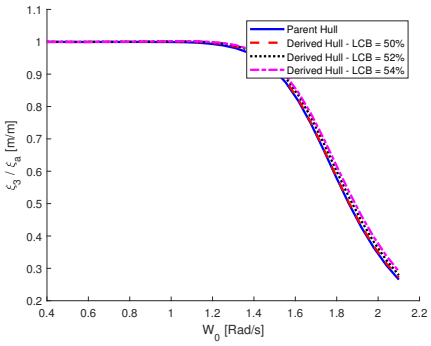

(c) β = 90°

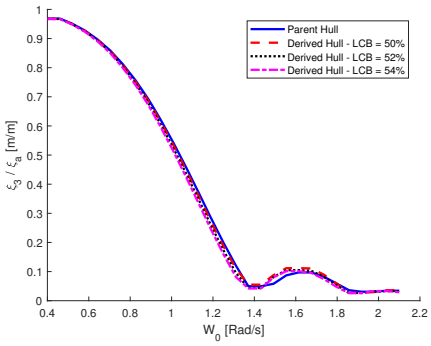

(d) β = 60°

Figure A.4: Heave RAOs. Parent Ship: SHIP1 with C_B = 0.71. Derived Hulls: Set 3 with C_B = 0.76.

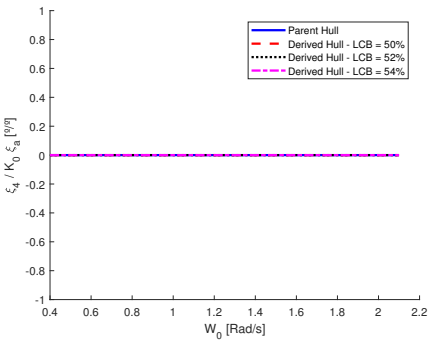

(a) β = 180°

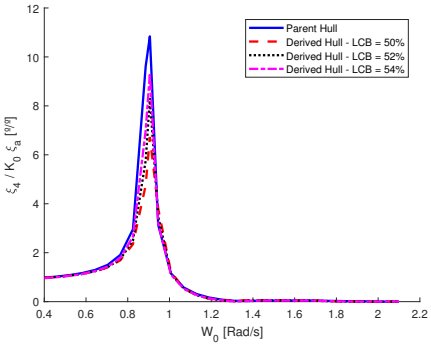

(b) β = 120°

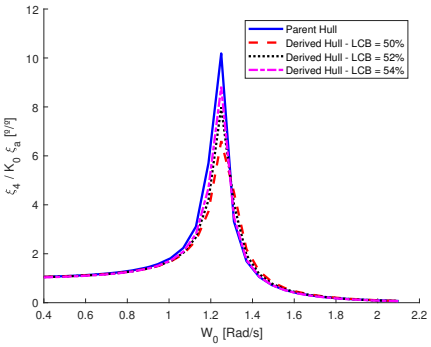

(c) β = 90°

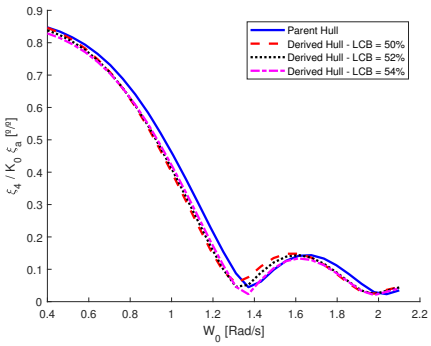

(d) β = 60°

Figure A.5: Roll RAOs. Parent Ship: SHIP1 with C_B = 0.71. Derived Hulls: Set 3 with C_B = 0.76.

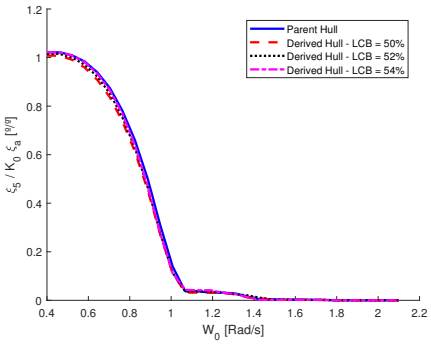

(a) β = 180º

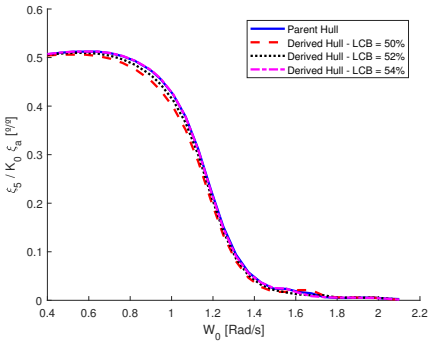

(b) β = 120º

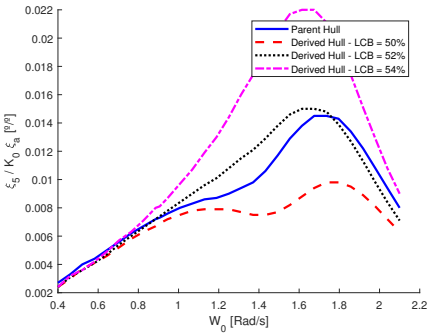

(c) β = 90º

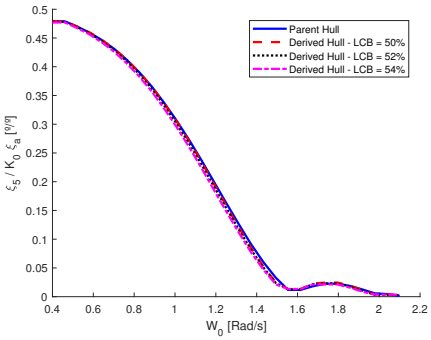

(d) β = 60º

Figure A.6: Pitch RAOs. Parent Ship: SHIP1 with C_B = 0.71. Derived Hulls: Set 3 with C_B = 0.76.

A.2 RAOs of SHIP2

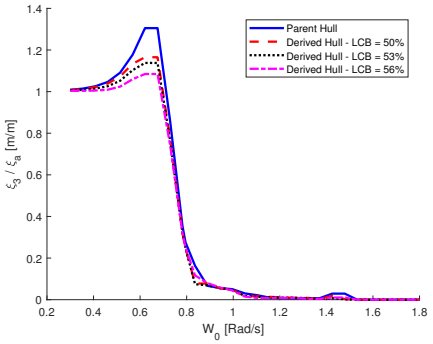

(a) β = 180°

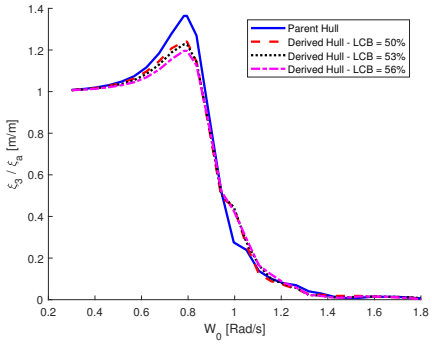

(b) β = 120°

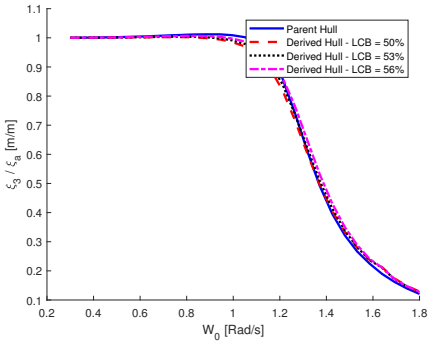

(c) β = 90°

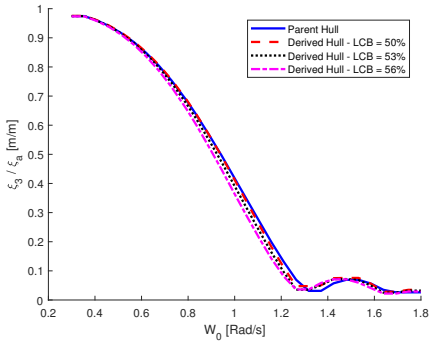

(d) β = 60°

Figure A.7: Heave RAOs. Parent Ship: SHIP2 with C_B = 0.56. Derived Hulls: Set 2 with C_B = 0.60.

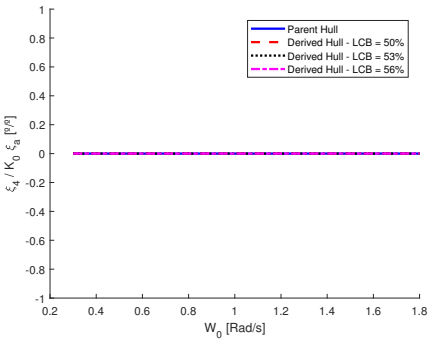

(a) β = 180°

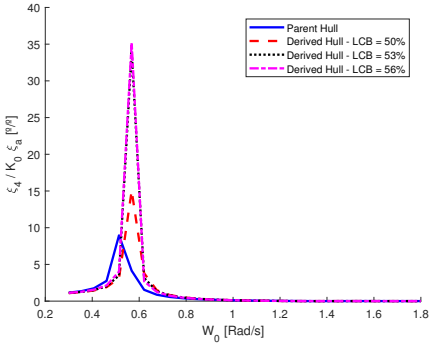

(b) β = 120°

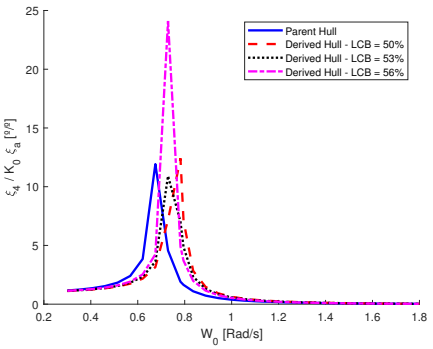

(c) β = 90°

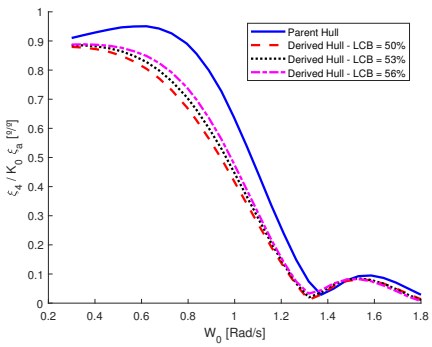

(d) β = 60°

Figure A.8: Roll RAOs. Parent Ship: SHIP2 with C_B = 0.56. Derived Hulls: Set 2 with C_B = 0.60.

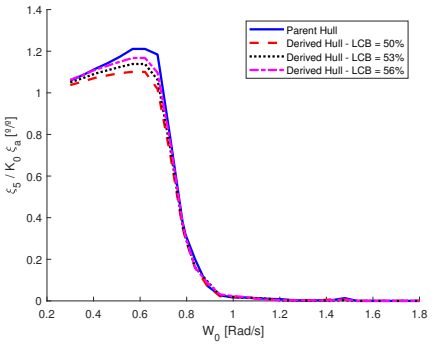

(a) β = 180º

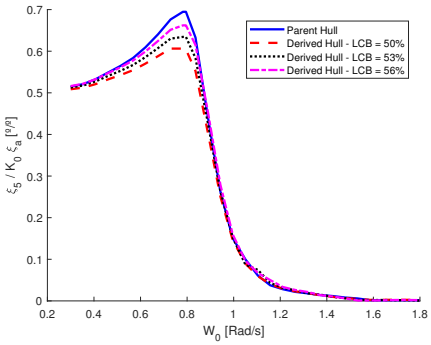

(b) β = 120º

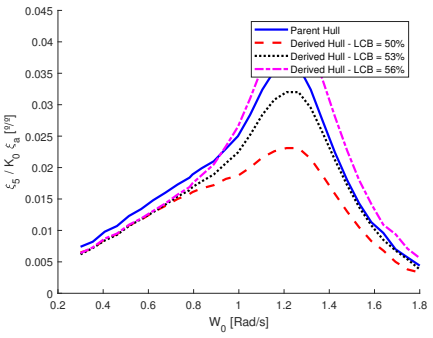

(c) β = 90º

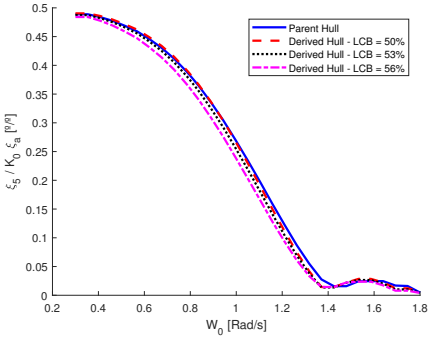

(d) β = 60º

Figure A.9: Pitch RAOs. Parent Ship: SHIP2 with C_B = 0.56. Derived Hulls: Set 2 with C_B = 0.60.

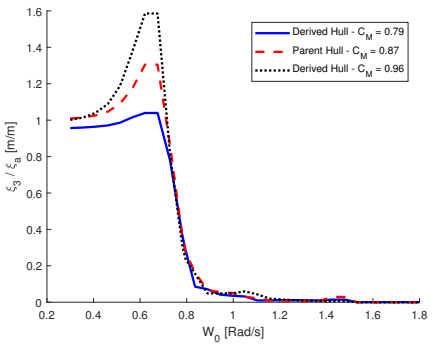

(a) β = 180º

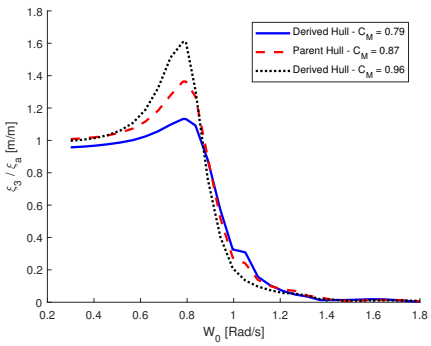

(b) β = 120º

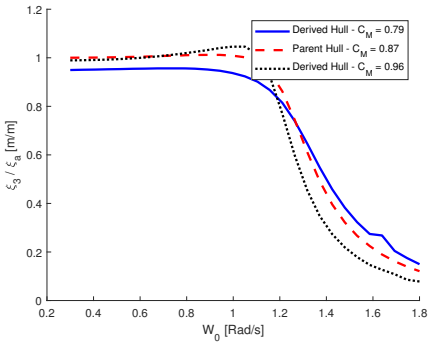

(c) β = 90º

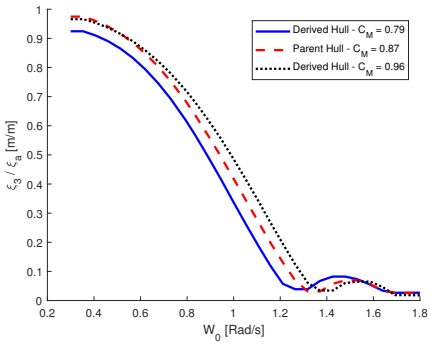

(d) β = 60º

Figure A.10: Heave RAOs. Parent Ship: SHIP2. Derived Hulls: Set 4.

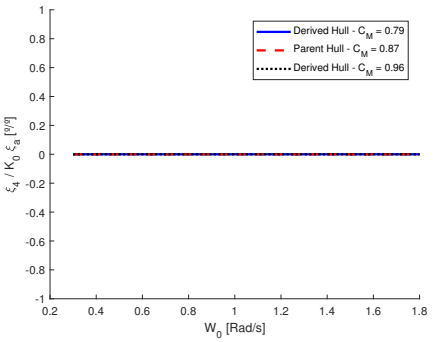

(a) β = 180º

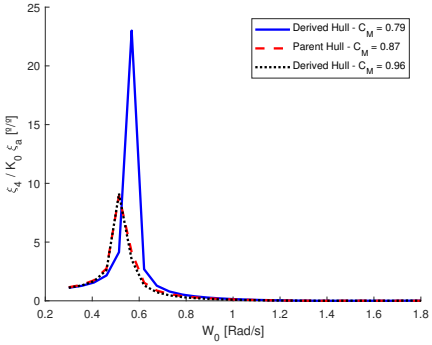

(b) β = 120º

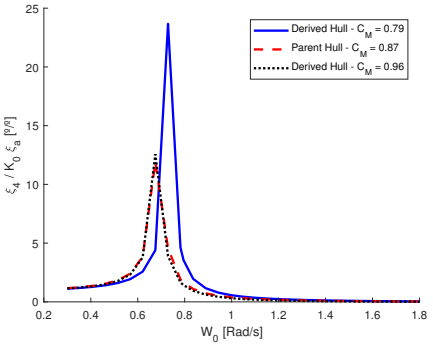

(c) β = 90º

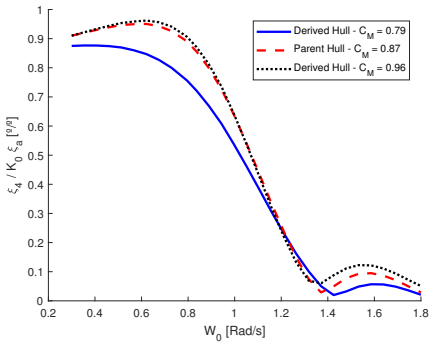

(d) β = 60º

Figure A.11: Roll RAOs. Parent Ship: SHIP2. Derived Hulls: Set 4.

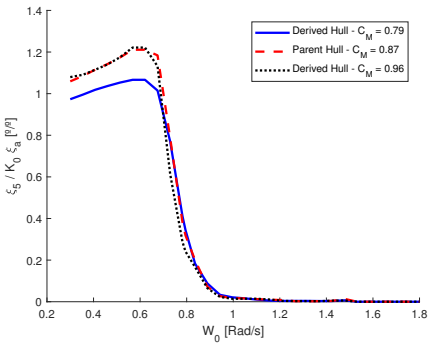

(a) β = 180º

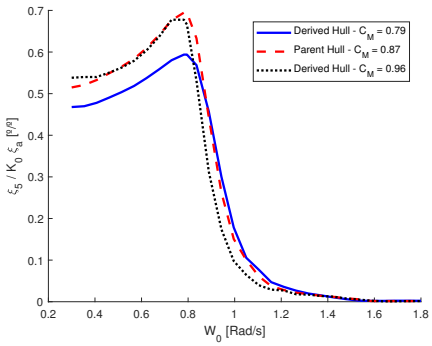

(b) β = 120º

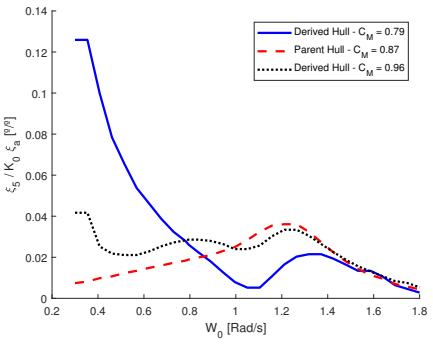

(c) β = 90º

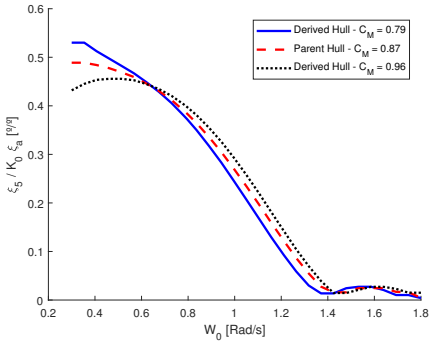

(d) β = 60º

Figure A.12: Pitch RAOs. Parent Ship: SHIP2. Derived Hulls: Set 4.

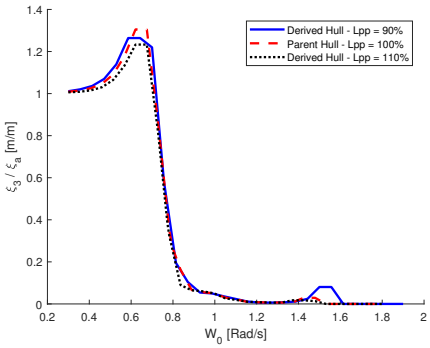

(a) β = 180°

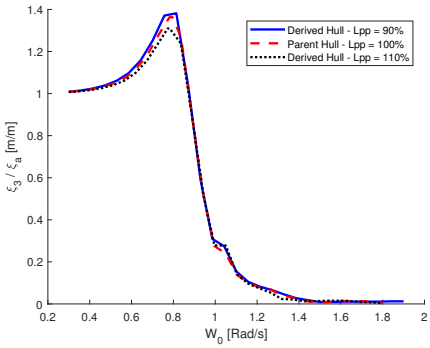

(b) β = 120°

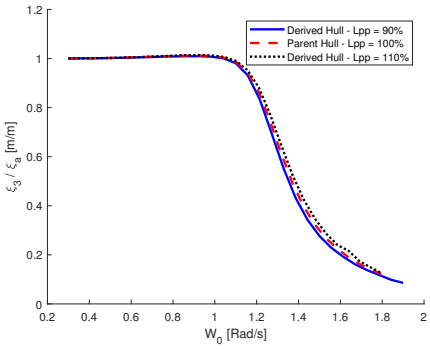

(c) β = 90°

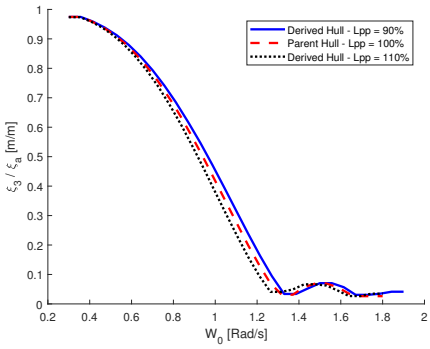

(d) β = 60°

Figure A.13: Heave RAOs. Parent Ship: SHIP2. Derived Hulls: Set 5.

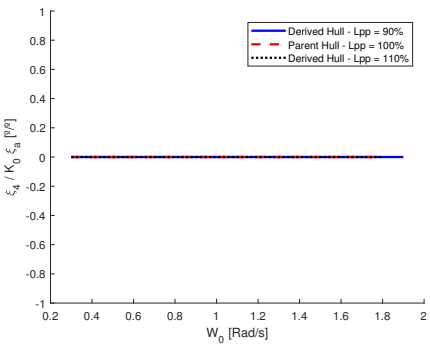

(a) β = 180°

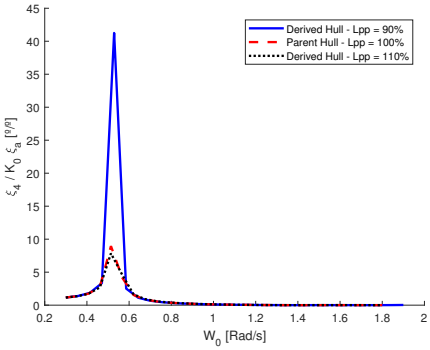

(b) β = 120°

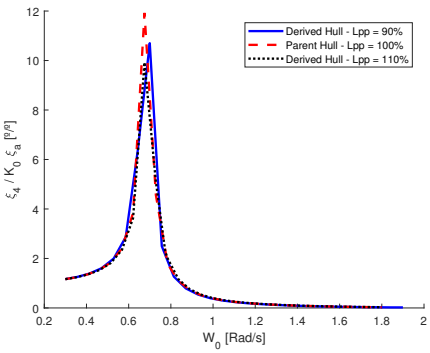

(c) β = 90°

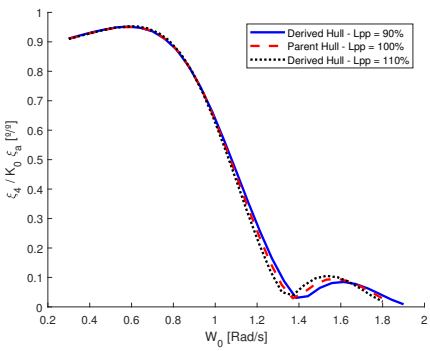

(d) β = 60°

Figure A.14: Roll RAOs. Parent Ship: SHIP2. Derived Hulls: Set 5.

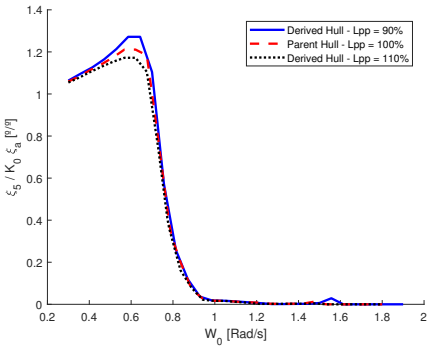

(a) β = 180º

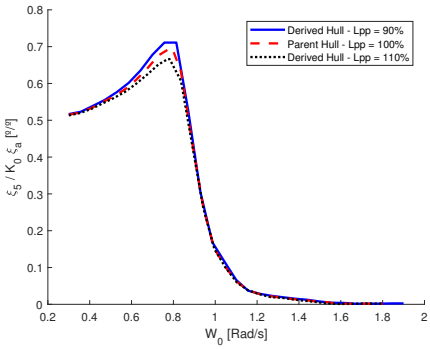

(b) β = 120º

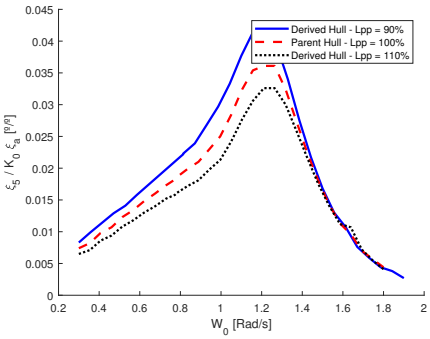

(c) β = 90º

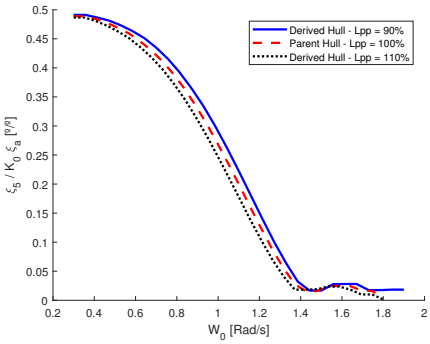

(d) β = 60º

Figure A.15: Pitch RAOs. Parent Ship: SHIP2. Derived Hulls: Set 5.

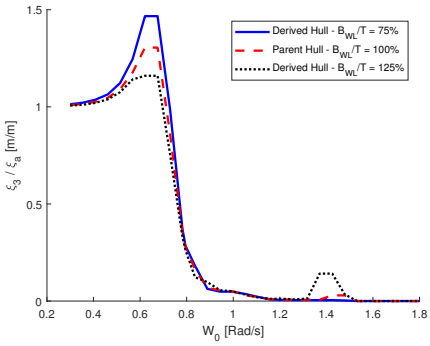

(a) β = 180º

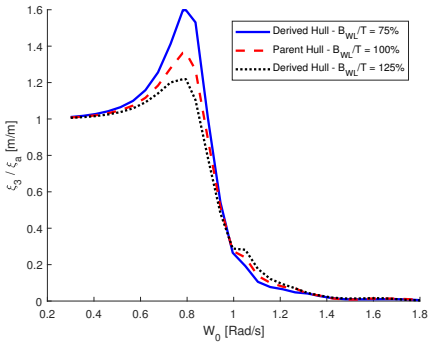

(b) β = 120º

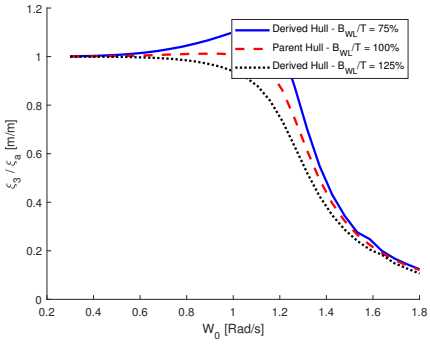

(c) β = 90º

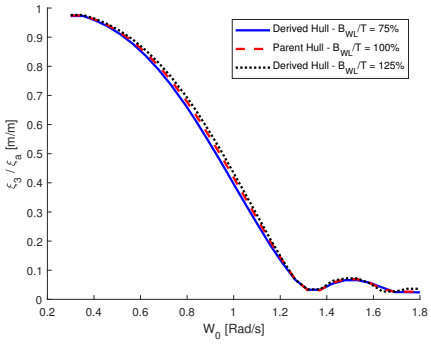

(d) β = 60º

Figure A.16: Heave RAOs. Parent Ship: SHIP2. Derived Hulls: Set 6.

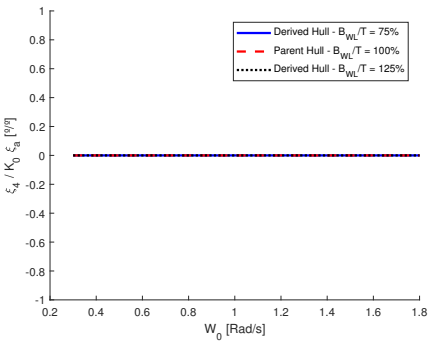

(a) β = 180º

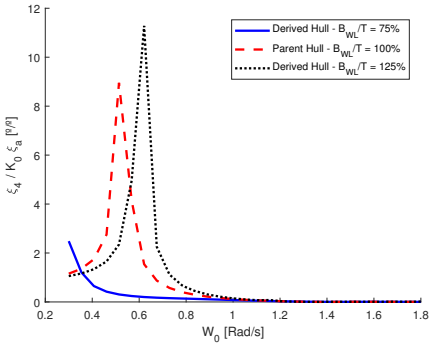

(b) β = 120º

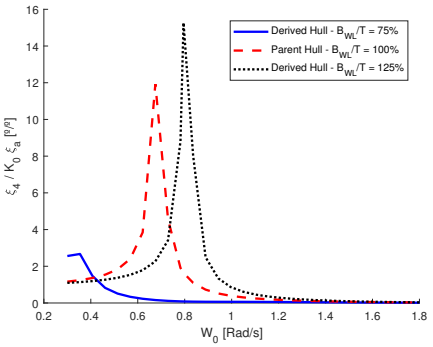

(c) β = 90º

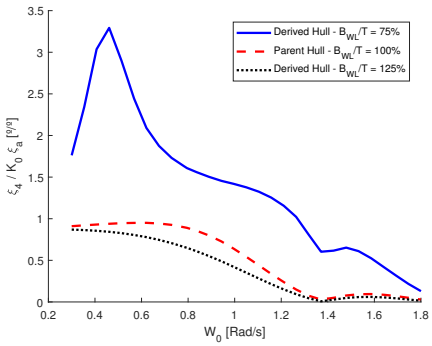

(d) β = 60º

Figure A.17: Roll RAOs. Parent Ship: SHIP2. Derived Hulls: Set 6.

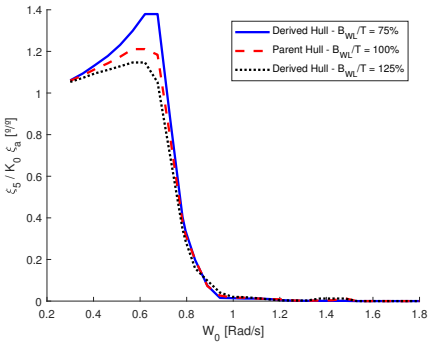

(a) β = 180º

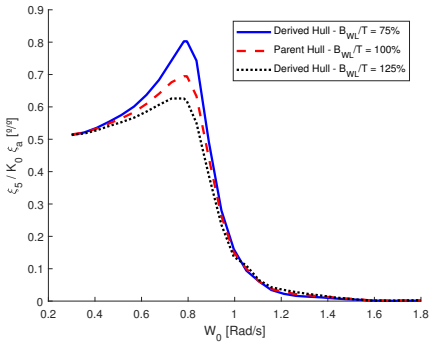

(b) β = 120º

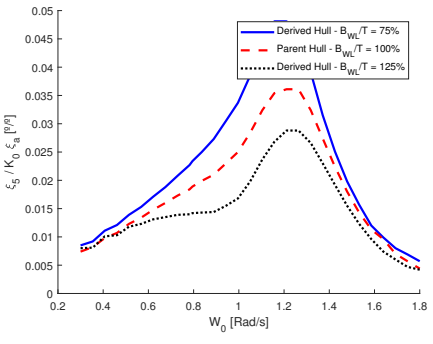

(c) β = 90º

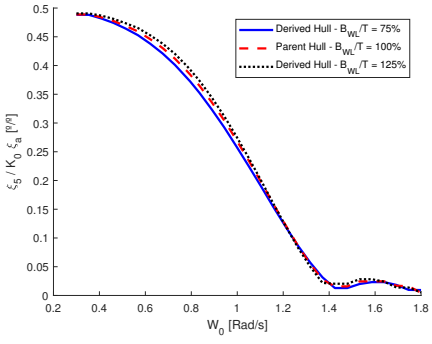

(d) β = 60º

Figure A.18: Pitch RAOs. Parent Ship: SHIP2. Derived Hulls: Set 6.

Appendix B

Absolute vertical Accelerations

B.1 Absolute vertical Accelerations of SHIP1

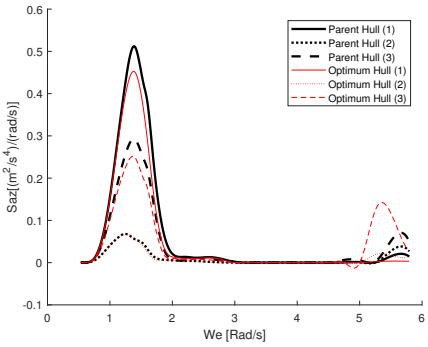

(a) β = 180°

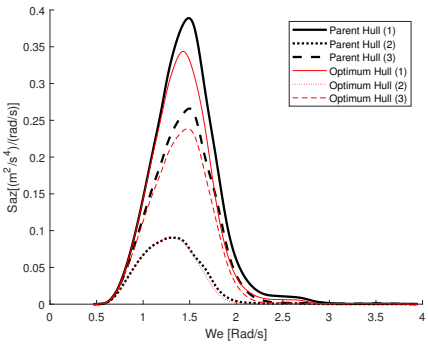

(b) β = 120°

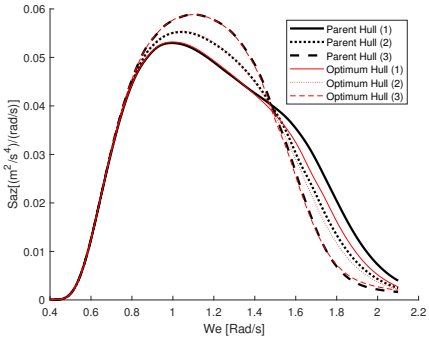

(c) β = 90°

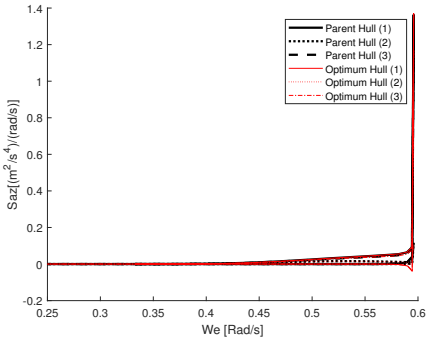

(d) β = 60°

Figure B.1: Absolute vertical acceleration. Parent hull: SHIP1 (C_B = 0.71, LCB = 52%) Optimum hull: Set 1 (C_B = 0.76, LCB = 50%) , at points 1, 2 and 3.

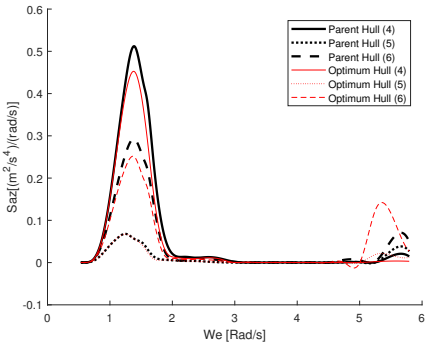

(a) β = 180°

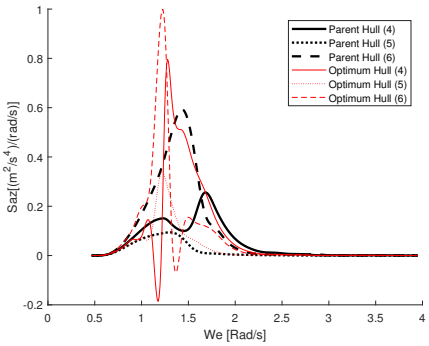

(b) β = 120°

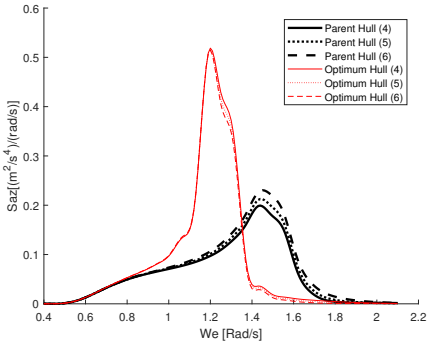

(c) β = 90°

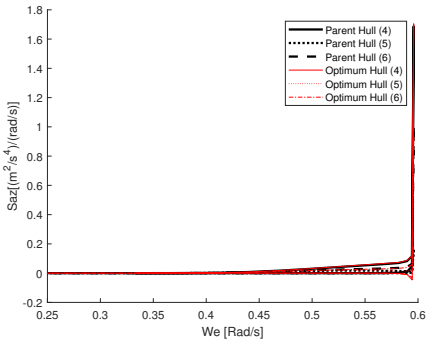

(d) β = 60°

Figure B.2: Absolute vertical acceleration. Parent hull: SHIP1 (C_B = 0.71, LCB = 52%) Optimum hull: Set 1 (C_B = 0.76, LCB = 50%) , at points 4, 5 and 6.

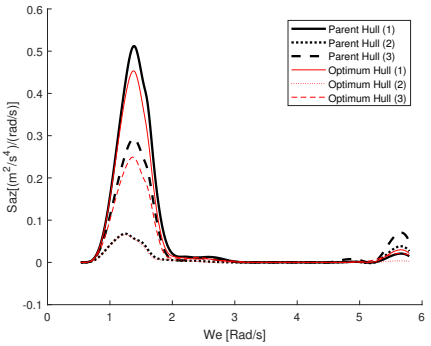

(a) β = 180°

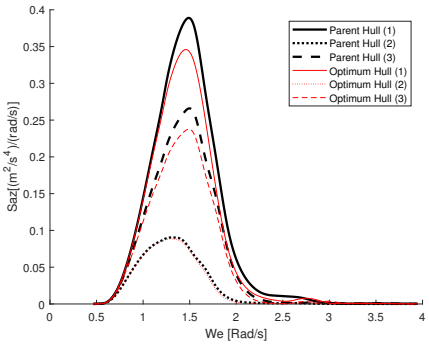

(b) β = 120°

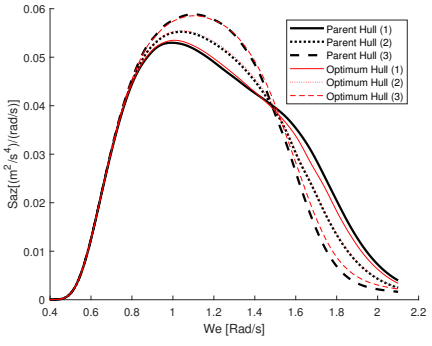

(c) β = 90°

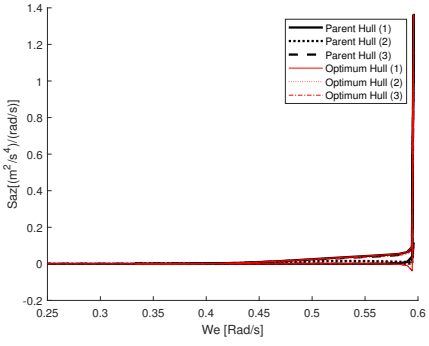

(d) β = 60°

Figure B.3: Absolute vertical acceleration. Parent hull: SHIP1 (C_B = 0.71, LCB = 52%) Optimum hull: Set 3 (C_B = 0.76, LCB = 50%) , at points 1, 2 and 3.

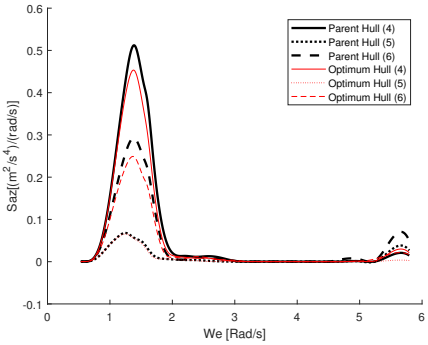

(a) β = 180^o

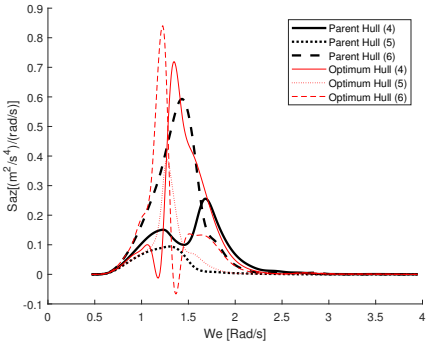

(b) β = 120^o

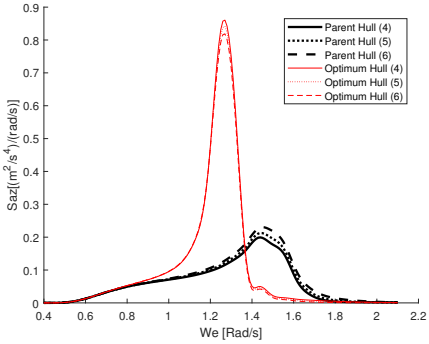

(c) β = 90^o

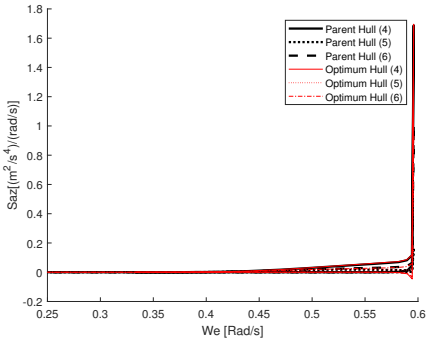

(d) β = 60^o

Figure B.4: Absolute vertical acceleration. Parent hull: SHIP1 (C_B = 0.71, LCB = 52%) Optimum hull: Set 3 (C_B = 0.76, LCB = 50%) , at points 4, 5 and 6.